Skolkovo Institute of Science and Technology

COMPARATIVE BIOLOGY OF AGING THROUGH THE LENS OF INDUCED PLURIPOTENT STEM CELLS

Doctoral Thesis

by

ALEKSEI MIKHALCHENKO

DOCTORAL PROGRAM IN LIFE SCIENCES

Supervisors
Professor Vadim Gladyshev
Professor Philipp Khaitovich

Moscow - 2018

Abstract

Many of the previous attempts to uncover mechanisms of aging focused on a few traditional model organisms, such as nematodes, yeast, fruit flies, and mice. However, considering the incredible diversity of lifespan across phylogeny, all these species are short-lived and therefore, by their nature, are less effective in resisting deleterious changes during aging. An alternative approach is to employ comparative biology of aging, taking advantage of exceptionally long-lived species and uncovering relevant molecular mechanisms underlying their longevity.

In this work, we initially focused on induced pluripotent stem cells (iPSCs) as a new tool for comparative aging studies. The use of iPSCs may address challenges associated with limited availability of biological samples from non-traditional species. We first used mouse and rat species to master our iPSC skills. We then developed a robust protocol for efficient generation of iPSCs from the longest-lived rodent, the naked mole rat (NMR). We generated and characterized these cells and performed comparative gene expression analyses involving mouse, human and NMR iPSCs. We also characterized the generated rat and NMR iPSCs for naïve pluripotency by examining their ability to contribute to embryonic interspecific chimeras via the injection of iPSCs to mouse blastocysts. To comparatively analyze interspecific chimeras involving long- and short-lived species, we developed full-term chimeras between rat and mouse. We further examined aging-related features using this rat-mouse model. Finally, as low body temperature is known to benefit lifespan, we examined the link between thermoregulation and aging by performing comparative studies on thermogenesis between homeothermic mouse and poikilothermic NMR.

We confirmed pluripotency of established mouse, rat, and NMR iPSCs and uncovered unique features of NMR iPSCs such as a propensity for a tetraploid karyotype and resistance to forming teratomas. Comparative gene expression analyses of NMR

iPSCs placed them close to human than mouse iPSCs. Remarkably, not only the rat, but also NMR iPSCs successfully contributed to embryonic interspecific chimeras indicating the potential to create paradigm-shifting chimeric models between long- and short-lived species. Analysis of age-associated changes in rat-mouse chimeras revealed a decrease of chimerism over the lifetime. We also uncovered active thermogenesis in the NMR, although heat loss appears to preclude homeothermy in these animals. The establishment of iPSCs from extremely long-lived animals, the development of relevant interspecific chimeric models, and advances in comparative analyses of thermogenesis open new opportunities for understanding the exceptional traits of longevity outliers.

Publications

1. Sang-Goo Lee#, **Aleksei Mikhalchenko#**, Sun Hee Yim, Alexei V. Lobanov, Jin-Kyu Park, Kwang-Hwan Choi, Roderick T. Bronson, Chang-Kyu Lee, Thomas J. Park, Vadim N. Gladyshev (2017) Naked mole rat induced pluripotent stem cells and their contribution to interspecific chimera. *Stem Cell Reports* 9, 1706-1720, # **Authors contributed equally to this work**

2. Sang-Goo Lee#, **Aleksei Mikhalchenko#**, Sun Hee Yim, Vadim N. Gladyshev (2018) A naked mole rat iPSC line expressing drug-inducible mouse pluripotency factors developed from embryonic fibroblasts. *Stem Cell Research* 31, 197-200. # **Authors contributed equally to this work**

Acknowledgements

This work was performed in 2015-2018 in the laboratory of Professor Vadim Gladyshev in the Division of Genetics, Department of Medicine, Brigham and Women's Hospital, Harvard Medical School.

I want to express my deepest gratitude to Professor Vadim Gladyshev for providing the opportunity to work in his lab and for his continuous support and guidance towards my PhD. I am forever grateful.

I also thank my Skoltech advisor, Professor Philipp Khaitovich, as well as the Skoltech Center of Life Sciences and the Department of Education for their financial support and the opportunity to carry out my research in the lab of Professor Gladyshev. There is no better place in Russia for innovative graduate research.

I would further like to express my very special thanks to Dr. Sang-Goo Lee for being my mentor and sharing his broad experience in the stem cell field, as well as for the numerous exciting discussions. It was a great pleasure working with and learn from him.

Next, I would like to thank Dr. Sun Hee Yim and Dr. Zalán Péterfi for their professional help and assistance with the experiments. Without their contribution, this dissertation would not be possible.

I am also grateful to all current and former members of the Gladyshev lab for their helpful comments and stimulating discussions during lab meetings.

I would also like to thank all the colleagues and collaborators at Brigham and Women's Hospital, Harvard, the Broad Institute of MIT and Harvard, University of

Rochester, Whitehead Institute for Biomedical Research, and University of Illinois at Chicago, with whom I had a pleasure to meet and collaborate. I also want to express my gratitude to Prof. Alexander Banks (Brigham and Women's Hospital, Harvard Medical School) for his help with and contribution to thermogenesis studies.

Finally, I am incredibly thankful to my family and friends, who have been supporting me all these years.

Table of Contents

List of Symbols, Abbreviations

2i – combinations of GSK3 and MEK/ERK inhibitors

AP – alkaline phosphatase

ATP – adenosine triphosphate

BAT – brown adipose tissue

BMP – bone morphogenic protein

DNA - deoxyribonucleic acid

Dox – doxycycline

EpiSCs – epiblast stem cells

ESCs – embryonic stem cells

FBS – fetal bovine serum

FGF – fibroblast growth factor

GFP – green fluorescent protein

GSK3 – glycogen synthase kinase-3

ICM – inner cell mass

IGF – insulin growth factor

iPSCs – induced pluripotent stem cells

LIF – leukemia inhibitory factor

MEF – mouse embryonic fibroblasts

MET - mesenchymal-to-epithelial transition

mTOR – mammalian target of rapamycin

NMR – naked mole rat

NST – non-shivering thermogenesis

OSKM – Oct4, Sox2, Klf4, c-Myc

T_a – ambient temperature

T_b – body temperature

TE – trophectoderm

UCP1 – uncoupling protein 1

List of Figures

List of Tables

Chapter 1

Review of the Literature

The Naked Mole Rat as a Model Organism for Comparative Studies on Aging and Longevity

For an extended period of time, attempts to uncover fundamental mechanisms of aging focused on a few traditional model species such as nematodes, yeast, fruit flies and mice (Dorman *et al.*, 1995; Lin, Hale and Schimmel, 1996; Lin, Defossez and Guarente, 2000; Kapahi *et al.*, 2004). Undoubtedly, all these species helped to gain significant insights into the biology of aging and shed light on the various aging-related signaling pathways such as insulin/insulin-like growth factor 1, mechanistic target of rapamycin, and nicotinamide adenine dinucleotide-dependent sirtuins (Kenyon, 2010; Pan and Finkel, 2017). However, initially, they have been chosen as model organisms not for their characteristics relevant to human aging, but because they are easy to breed, maintain and manipulate experimentally. Most importantly, even in an optimized laboratory environment, they do not live very long, which makes it easier to subject them to genetic manipulations or pharmacological interventions coupled with survival studies within a reasonable amount of time and at a reasonable cost (Austad, 2001). However, considering the remarkable diversity of maximum lifespans adjusted by evolution (Deweerdt, 2012), all these species are short-lived and therefore, by their nature, ineffective in resisting deleterious processes that accompany aging. Therefore, a more appropriate approach might be the use of some the exceptionally long-lived species and an analysis of relevant molecular mechanisms underlying their longevity. This approach might lead to the

discovery of more superior senescence-retarding mechanisms than those uncovered in the studies involving short-lived species (Austad, 2009). The naked mole rat (NMR) is one of most remarkable mammals, primarily due to its exceptionally long lifespan.

The NMR (*Heterocephalus glaber*) belongs to the class Mammalia, the order Rodentia, and the family Bathuergidae (Kock *et al.*, 2006). The order Rodentia covers more than 40% of all mammalian species (Gorbunova, Bozzella and Seluanov, 2008). It also includes species with profoundly different maximum lifespan. For example, mice and rats (*Mus musculus* and *Rattus norvegicus*) live no longer than ~3 and ~4 years, respectively; and guinea pigs (*Cavia porcellus*) live up to 12 years, whereas the maximum lifespan of eastern grey squirrels (*Sciurus carolinensis*) is reported to be 24 years (Tacutu *et al.*, 2013). Still, the most extended lifespan among rodent species is observed in NMRs, which are known to live up to 32 years in captivity (Lewis *et al.*, 2016). It is nearly ten times as long as the maximum lifespan of similar-sized laboratory mice. This is five times longer than lifespan predicted based on their body size (Magalhaes, Costa and Church, 2007; Edrey *et al.*, 2011). Thus, these extreme longevity outliers might play an important role in aging, and understanding the secrets behind their remarkably long lifespan could inform on candidate approaches to extend human lifespan.

Naked mole rat habitat and eusociality

In the wild, NMRs are endemic to the Horn of Africa where they live in deep subterranean burrows up to two and more meters below the ground with many layers of interconnected tunnels and chambers (Sherman *et al.*, 1991). Exhibiting a very high

degree of social and cooperative living, they are one of only two eusocial mammalian species known (Buffenstein *et al.*, 2012). Similar to eusocial insects, naked mole rats live in colonies, whose size varies from a few to almost 300 animals, with only one breeding female (queen) and from one to three breeding males, while the rest of colony mates may remain sterile over their whole lives (Jarvis, 1981). The queen regularly monitors the colony stimulating breeding males and physically intimidating other individuals to prevent their transition to a breeding status. Inhibition of reproductive capacity of the non-breeding females is thought to be sustained by the behavior of the queen or her skin odor rather than by urine pheromones (Faulkes and Abbott, 1993; Smith, Faulkes and Abbott, 1997; Holmes *et al.*, 2009). Non-breeding males and females are sexually monomorphic having a similar external appearance, body weight, anogenital distance, perineal muscles and perineal motor neurons, brain, spinal cord, and femoral bone morphology and micro-architecture (Peroulakis, Goldman and Forger, 2002; Holmes *et al.*, 2007; Pinto *et al.*, 2010). Non-breeding males have low testosterone levels, small internal testes, and abnormal predominantly non-motile sperm while non-breeding females have low estrogen levels, small functionally quiescent ovaries and uteri without corpora lutea, and exhibit no signs of ovarian cyclicity or ovulation (Faulkes, Abbott and Jarvis, 1990; Faulkes and Abbott, 1991; Endo *et al.*, 2002; Holmes *et al.*, 2009). However, if the queen dies, any individual within the colony has a competence to ascend into a breeder (Buffenstein *et al.*, 2012). The unique eusocial lifestyle of naked mole rats also represents a strict division of labor. Individual roles include protection of the colony, maintenance of burrow system, searching for and gathering food, and rearing of young

(Jarvis, 1981; Judd and Sherman, 1996). Being housed in laboratory conditions, these eusocial animals preserve many features of their social behavior (Buffenstein *et al.*, 2012).

Unique traits of naked mole rats

In addition to extremely long lifespan, naked mole rats exhibit a minimal decline in physiological and biochemical functions (Edrey et al., 2011). Moreover, it was recently reported that these remarkable animals, unlike any other mammals, show no signs of an age-related increase in mortality (Ruby, Smith and Buffenstein, 2018). Also, unlike most mammals, naked mole rats show no age-related decline in fertility in both males and females breeders (Buffenstein, 2005).

Many unique features of delayed aging phenotype have been reported. Compared to mice, naked mole rats demonstrate higher levels of oxidative damage, which they can successfully tolerate (Andziak, Connor and Buffenstein, 2005). Examination of naked mole rat cardiovascular systems revealed enhanced cardiac reserve (Grimes et al., 2014) and altered cardiac myofilament composition (Grimes et al., 2017). Transcriptome studies showed reduced expression of genes associated with aging relevant to insulin/IGF-1 and mTOR pathways (Kim *et al.*, 2011). Enhanced cytoprotection through high levels of Nrf2 protein and constitutive Nrf2-signaling activity (Lewis *et al.*, 2012), as well as exceptional protein homeostasis through the elevation of autophagy, proteasome activity, and heat shock proteins (Pride *et al.*, 2015; Rodriguez *et al.*, 2016) were suggested to contribute considerably to the healthy aging of naked mole rats.

Naked mole rats are also highly resistant to both spontaneous and experimentally induced cancer (Buffenstein, 2005; Liang *et al.*, 2010). Protective mechanisms underlying such resistance are interpreted differently among research groups. According to one report, naked mole rat anticancer capacity is mediated by the extreme sensitivity of their cells to early contact inhibition associated with the induction of tumor suppressor $p16^{INK4A}$ (Seluanov *et al.*, 2009). High-molecular-mass hyaluronan binding to CD44, which causes arrest of the cell cycle, was suggested as a trigger for such contact inhibition and thereby a mediator of naked mole rat cancer resistance (Tian *et al.*, 2013). In addition, it was shown that the INK4a/b locus of the naked mole rat genome encodes an additional product consisting of the first exon of $p15^{INK4b}$ together with the second and third exons of $p16^{INK4a}$ (Kim *et al.*, 2011; Tian *et al.*, 2015). This product $pALT^{INK4a/b}$ was shown to have a stronger ability to induce cell-cycle arrest than $p15^{INK4}$ or $p16^{INK4a}$ (Tian *et al.*, 2015). Another study showed that cells expressing a combination of oncogenes, SV40 large T antigen, and Ras, rapidly entered crisis when transplanted into immunodeficient mice proposing rapid crisis as a tumor suppressor mechanism, which can be abolished by ectopic expression of human telomerase reverse transcriptase (hTERT) (Liang *et al.*, 2010). High constitutive levels of p53 may play a key role in such rapid crisis thus preventing mutation accumulation and cancer (Lewis *et al.*, 2012).

Subterranean lifestyle in sealed underground tunnels where the air is low in oxygen and high in carbon dioxide, exposure to heavy metals and other chemicals in soil, as well as other challenges of living in large colonies and sharing limited resources, have also undoubtedly resulted in many anatomical and physiological adaptations of naked

mole rats. In addition to hairless skin, the visual capacity of *Heterocephalus glaber* is very poor, animals are only able to distinguish the light from the dark, but cannot clearly see objects (Hetling *et al.*, 2005). These animals have a metabolic rate twice lower than that of other rodents of their weight, which helps them to decrease oxygen consumption (McNab, 1979). Additionally, their hemoglobin has higher oxygen affinity, promoting effective oxygen extraction (Johansen *et al.*, 1976). Gene expression analysis of several naked mole rat tissues subjected to 8% O_2 for one week revealed many changes associated with redox control and energy metabolism (Kim *et al.*, 2011).

Additionally, genome sequencing revealed unique amino acid changes in hypoxia-induced factor 1a (HIF1a) and its ubiquitin-dependent degradation mediator von Hippel-Lindau (VHL), which is compatible with adaptations to low oxygen conditions (Kim *et al.*, 2011). Interestingly, in addition to a highly prolonged period of brain maturation (Penz *et al.*, 2015; Orr *et al.*, 2016), naked mole rats were shown to preserve neotenous brain characteristics by retaining hypoxia-protective GluN2D subunit of membrane calcium channel N-methyl-D-aspartate (NMDA) receptor, which closes in hypoxia conditions preventing the calcium intake and cell death (Peterson et al., 2012). Remarkably, the brain of naked mole rats can tolerate anoxia for up to 30 min (Larson and Park, 2009) and animals can be recovered from 18 min of anoxia exposure with no apparent physiological complications by switching to fructose metabolism (Park *et al.*, 2017).

Due to abnormalities in the trigeminal pain pathway and hypofunctional TRKA receptor, naked mole rats are selectively insensitive to chemical pain and entirely lack

behavioral hyperalgesia in response to painful thermal stimuli (T. J. Park *et al.*, 2008; LaVinka and Park, 2012; Omerbašić *et al.*, 2016). Perhaps, the inhibition of acid-induced pain signaling in naked mole rats may be due to species-specific variant of nociceptor sodium channel $Na_V1.7$ protein (Smith *et al.*, 2011). Most recently, cortical neurons of these animals were shown to exhibit enhanced cellular resistance to acid-induced cell death (Husson and Smith, 2018). These adaptations allow *Heterocephalus glaber* to survive in acidic environment of poorly ventilated burrows with high carbon dioxide and ammonia.

Naked mole rat thermoregulation

Life in equatorial Africa in sealed subterranean burrows protects naked mole rats not only from predators but also from climate fluctuations. While soil surface temperature may become extremely hot (up to 63 °C), the temperature in naked mole rat underground tunnels (29-32 °C) is very stable with seasonal differences no more than 1-1.5 °C (Bennett, Jarvis and Davies, 1988) or even lower (0.6 °C) (McNab, 1966). Such thermally buffered conditions have provided little demand for facultative thermogenesis of *Heterocephalus glaber*.

It is known that in their natural habitat naked mole rats huddle together in groups frequently lying on the top of each other (Yahav and Buffenstein, 1991). It seems that such huddling behavior plays a substantial role in their thermoregulation by minimizing heat loss and consequently reducing the metabolic cost of maintaining body temperature and thus supporting the maintenance of homeothermy over the narrow range of ambient temperatures observed in their natural subterranean environment (Yahav and Buffenstein,

1991). Moreover, it was demonstrated that when isolated from the colony, naked mole rats exhibited a complete dependence of their body temperature (T_b) on the ambient temperature (T_a) ($T_b = 0.568 + 1.016T_a$) over the whole range tested (12–37 °C) and are thus acknowledged as the only poikilothermic mammals (Buffenstein and Yahav, 1991). Interestingly, on the ambient temperature interval from 29 °C to 34 °C, animals' oxygen consumption reflected the typical endothermic pattern decreasing with increasing T_a. Within this range, level of oxygen consumption reached its minimum rate at 31 °C and barely changed till 34 °C, representing the thermoneutral zone (31–34 °C) of these animals (Buffenstein and Yahav, 1991). Outside of this "endothermic" range (from 12 to 29 °C and from 34 to 37 °C) naked mole rats abandoned endothermy and exhibited a typical poikilothermic pattern increasing their oxygen consumption with increasing T_a.

Furthermore, as soon as ambient temperature drops below thermoneutrality (31–34 °C) metabolic rate was shown to increase harshly in a way that a drop in T_a from 32 °C to 29 °C induced 120% rise above basal levels, which is an equivalent to that observed in mice housed within their thermoneutral zone and being exposed to severe cold of around 5 °C (Woodley, 2000; Woodley and Buffenstein, 2002). Overall, this pioneering study (Buffenstein and Yahav, 1991) was the first to propose that naked mole rats are in fact endothermic poikilotherms revealing thermoregulatory potential only within a narrow range of ambient temperatures observed in their natural subterranean environment. In later studies, the ability to employ non-shivering thermogenesis (NST) when subjected to noradrenaline stimulation at temperatures above 29 °C fully confirmed the presence of endothermic thermoregulation in *Heterocephalus glaber* (Hislop and

Buffenstein, 1994; Woodley and Buffenstein, 2002). However, one cannot help but point out an interesting observation that in the previously mentioned work (Buffenstein and Yahav, 1991) there was a statement referring to unpublished data that naked mole rats did not employ NST following noradrenaline stimulation, both under normal and cold conditions. Although it was highly likely a preliminary misinterpretation, it would be interesting to check if these animals exhibit a pharmacologically induced NST at the temperature range below 29 °C.

While during initial incidents of cold exposure mammals utilize shivering in order to boost heat generation (Griggio, 1982), the central role of heat production in small eutherian mammals is driven by more efficient non-shivering thermogenesis, which is managed by the sympathetic nervous system via noradrenergic innervation of brown adipose tissue (BAT) in response to cold exposure (Smith *et al.*, 1969; Carneheim, Nedergaard and Cannon, 1984; Cannon and Nedergaard, 2011). The ratio between the implementation of shivering and non-shivering thermogenesis depends heavily on an animal's experience of cold exposure. Thus, while animals exposed to the cold for the first time may respond mainly by shivering, in those with previous experience of cold stress the response would be facultative and adaptive NST in the BAT (Carneheim, Nedergaard and Cannon, 1984; Cannon and Nedergaard, 2011; Speakman, 2013). As already demonstrated in naked mole rats, the evaluation of the potential for endogenous heat generation via the induction of NST response can be performed by administration of pharmacological doses of noradrenaline (Hislop and Buffenstein, 1994; Woodley and

Buffenstein, 2002) or specific β3-adrenergic agonist CL-316,243 (Cannon and Nedergaard, 2011).

In addition to experimentally confirmed capability to employ non-shivering thermogenesis via pharmacological noradrenaline stimulation, inspection of the ultrastructure of naked mole rat interscapular brown adipose tissue and associated sympathetic innervation revealed anatomical characteristics required for thermogenesis, therefore also promoting NMR thermogenic potential (Daly, Williams and Buffenstein, 1997).

Overall, these studies illustrate that, in the NMR natural environment, behavioral thermoregulation such as huddling and choosing warmer sectors within the burrows, together with non-shivering thermogenesis within 29-32 °C temperature range, contribute to homeothermy. Taking into consideration that for animals separated from their colony the ambient temperature of two degrees below thermoneutrality (31 °C → 29 °C) already represents an extreme cold and that bellow 29 °C they entirely abandon endothermy and exhibit a typical poikilothermic pattern, it seems that their BAT may function at its full capacity already at 29 °C. Nonetheless, the molecular mechanisms explaining why single-housed naked mole rats cannot or choose not to employ endothermy at ambient temperatures below 29°C remains unclear.

The principal mechanism driving the production of heat in the brown adipose tissue is mediated through uncoupling protein 1 (UCP1), which resides in the inner mitochondrial membrane and dissipates the mitochondrial proton gradient in the form of heat rather than adenosine triphosphate (ATP) (Cannon, 2004). UCP1 was found in all

studied placental mammals except pigs and dolphins (McGaugh and Schwartz, 2017) and is thought to be the only true thermogenic uncoupling protein (Cannon and Nedergaard, 2011). However, the specific molecular mechanism of its uncoupling remains unclear, and the mechanism of UCP1 activation in response to noradrenaline stimulation continues to be a subject of debate (Cannon and Nedergaard, 2017; Crichton, Lee and Kunji, 2017; Schreiber *et al.*, 2017; Shin *et al.*, 2017). Analysis of the naked mole rat genome revealed that its UCP1, despite being highly conserved across mammals, harbors unique amino acid changes (His146Gln, Gly263Arg, Pro264Trp) that occur within the site that supports regulation of the protein by fatty acids and nucleotides. It was proposed that these changes may affect the function of UCP1 through the loss of tight regulation by purine nucleotides as inhibitors and fatty acids as activators, in turn leading to inefficient thermogenesis (Kim *et al.*, 2011; Gorbunova *et al.*, 2014). A direct test of this hypothesis is needed to understand the role of UCP1 in NMR thermogenesis.

Induced pluripotent stem cells as a source for comparative aging studies

Cell resources from non-traditional long-lived species may provide a valuable contribution to a novel comparative approach in aging research. Induced pluripotent stem cells may be particularly useful as they do not require utilization of embryos, can be generated from adult somatic cells such as fibroblasts and are able to differentiate into multiple cell types of interest. Additionally, they may alleviate many of the difficulties related to the limited availability of biological samples from extreme and rare species.

Since extreme longevity and cancer resistance of the NMR was first determined, more and more research groups worldwide developed their interest in this remarkable

mammal as a model for biogerontology (Lewis and Buffenstein, 2015). Sequencing and annotation of the NMR genome pushed this interest even further (Kim *et al.*, 2011). However, the endemic origin of these animals, their social lifestyle, and strict housing conditions impose apparent difficulties resulting in their limited availability for research community. The successful generation of iPSCs from the naked mole rat and other extremely long-lived animals could bring a much-needed resource for characterizing their unique phenotypes.

Pluripotency, Pluripotent Stem Cells, and Interspesific Chimeras

Embryonic origin of pluripotency

In eutherian mammals, pluripotency is a temporal developmental plasticity of embryonic epiblast during early embryogenesis. It signifies the capacity to give rise to all somatic cells and germ line cells of the developing embryo. As embryo evolves from the morula to the blastocyst, the first cell-fate determination of embryogenesis is a formation of two distinct cell lineages: the inner cell mass (ICM) and the trophectoderm (TE). The trophectoderm eventually leads to the formation of placenta. The ICM, in turn, starts to segregate into the hypoblast (extraembryonic primitive endoderm), which ultimately forms the yolk sac, and the pluripotent epiblast (primitive ectoderm), which forms the fetus. Soon after, blastocyst undergoes implantation into the maternal uterine wall, which results in a rapid proliferation and reorganization of epiblast cells. Multiple signaling events between maternal tissues, extra-embryonic tissues, and the epiblast provide the foundation for its further somatic lineages specification (Bedzhov *et al.*, 2014; Wu, Yamauchi and Izpisua Belmonte, 2016). Pluripotency in the epiblast decreases with its development during early gastrulation and is lost by the beginning of somitogenesis (Osorno *et al.*, 2012).

When morula develops to blastocyst, newly formed ICM maintains the expression of POU-domain transcription factor Oct4 (Pou5f1), opposite to the trophectoderm, in which Oct4 becomes downregulated. Thereby, Oct4 appeared to be essential for

establishing the distinct cell lineage identity of the ICM as it was shown that Oct4-negative ICM cells underwent differentiation to the trophectoderm (Nichols *et al.*, 1998). Cooperative expression of Oct4 and SRY-box-2 (Sox2) transcription factors regulates the expression of multiple target genes including Nanog transcription factor (Boyer *et al.*, 2005). Without Sox2, blastocysts still can be formed but promptly fail their development before progressing to the gastrulation stage (Avilion *et al.*, 2003). When ICM, in which Nanog is expressed stochastically in different cells (Dietrich and Hiiragi, 2007), finishes its segregation into hypoblast and epiblast, Nanog expression becomes limited to the epiblast (Messerschmidt and Kemler, 2010). Nanog deficient ICM fails to form epiblast and eventually degenerates (Mitsui *et al.*, 2003; Silva *et al.*, 2009). Thus, Oct4, Sox2, and Nanog transcription factors were shown to be essential for the establishment of the epiblast. Nowadays, these three transcription factors are known as critical drivers of pluripotency.

Captured or induced pluripotency in vitro

Pluripotency of the epiblast persists for about 4-5 days within mouse embryo development (from embryonic day 3.5 (E3.5) till approximately E8.0) and about two weeks in human embryo (Smith, 2017). During this period of time, by isolating epiblast cells from the embryo, it can be captured in *in vitro* culture, and the established cells are known as pluripotent stem cells (PSCs). In addition to embryonic tissues, PSCs can be obtained from some tumor tissues, for example, teratocarcinomas (Stevens and Little, 1954; Stevens, 1970). Most amazingly, pluripotency can also be artificially acquired in differentiated adult cells via cell fusion (Tada *et al.*, 2001; Ying *et al.*, 2002), somatic

cell nuclear transfer (Gurdon, 1962; Wakayama *et al.*, 1998), or can be "induced" using specific pluripotency-associated transcription factors and chemicals. Pioneering work on reprogramming mouse somatic cells to PSCs using transcription factors was published in 2006 by Kazutoshi Takahashi and Shinya Yamanaka (Takahashi and Yamanaka, 2006) and since that time it has become the most commonly used method of obtaining PSCs. Only six years since this revolutionary discovery, Yamanaka has been awarded the Nobel Prize in Physiology or Medicine in 2012. His original method is based on the forced expression of four transcription factors (Oct4, Sox2, Klf4, c-Myc; OSKM) in target somatic cells. The resulting pluripotent cells are known as induced pluripotent stem cells (iPSCs). Combining culture conditions of mouse embryonic stem cells (ESCs), which have been known since 1981 (Evans and Kaufman, 1981) with the induction of exogenous OSKM expression appeared to be efficient for reprogramming of mouse somatic cells to iPSCs (Takahashi and Yamanaka, 2006), and nowadays this successful experiment may seem pretty straightforward. However, after all, it became clear that not all PSCs are equal. Depending on the timing of isolation from the embryo (for embryonic PSCs), the species, and extrinsic culture environment (for all PSCs including iPSCs), pluripotent stem cells can exist in discrete pluripotent states, each with recognizable functional and molecular characteristics (Tesar *et al.*, 2007; Nichols and Smith, 2009; Wu, Yamauchi and Izpisua Belmonte, 2016; Ying and Smith, 2017). This is reflected in the complexity of iPSC generation from different mammalian species.

Overall, PSCs and especially iPSCs are of enormous interest in developmental biology research, genome engineering, regenerative medicine, disease modeling,

rejuvenation, and aging. They are "trapped" *in vitro* and thus can self-renew indefinitely producing an unlimited amount of cells while maintaining their pluripotent status. iPSCs can be generated without embryo utilization, which allows to avoid ethical issues in case of human studies and promotes the research on wild and endangered animals. Also, patient-specific iPSCs can be established from any individual thereby eliminating the problem of immune rejection after transplantation. Independent of origin, the hallmark of pluripotent capacity of PSCs is their ability to self-renew and to produce the derivatives of all three germ layers by forming teratomas (multilineage tumors) upon injection into immunocompromised mice, and to contribute to normal development of chimeras when introduced into the blastocysts (Martí *et al.*, 2013).

Characteristics of PSCs from different species

Mouse embryonic stem cells (ESCs) were first PSCs established from a mammalian species. They were derived in 1981 from blastocysts or ICMs of the mouse strain 129 by explanting them on a feeder cells layer of mitotically inactivated mouse embryonic fibroblasts (MEF) in medium with of fetal bovine serum (FBS) (Evans and Kaufman, 1981; Martin, 1981). Cultures without feeder layer showed that pluripotent cells could proliferate but rapidly undergo differentiation while the culture in conditioned by feeder cells medium could cause a temporal delay of differentiation (Smith and Hooper, 1983; Koopman and Cotton, 1984). Thereby, it was shown that differentiation was inhibited by a secreted protein. This observation led to the identification of leukemia inhibitory factor (LIF) cytokine (Smith *et al.*, 1988). LIF provides the main self-renewal signal via receptor-mediated stimulation of Janus-associated kinase (JAK) and activation

of the signal transducer and activator of transcription 3 (Stat3) pathway (Niwa *et al.*, 1998). Still, LIF/Stat3 alone, without FBS, is not sufficient to prevent differentiation of mouse ESCs. However, bone morphogenetic proteins (BMPs) together with LIF but not alone were shown to be able to replace FBS and provide self-renewal as well as suppress differentiation of mouse ESCs via the induction of Id genes (Ying *et al.*, 2003). Thus, the combination of LIF and BMP is known as a first defined culture condition for mouse ESCs. In this condition, mouse somatic cells were reprogrammed to iPSCs using forced expression of OSKM transcription factors (Takahashi and Yamanaka, 2006). Mouse ESCs resemble and can be derived from the pre-implantation stage ICM (E3.5–E4.5) (Evans and Kaufman, 1981; Boroviak *et al.*, 2014). They display dome-shaped colony morphology, express canonical pluripotency factors Oct4, Sox2 and Nanog as well as express alkaline phosphatase (AP) and Ssea1. Additionally, like their *in vivo* equivalents, mouse ESCs from female individuals show two active X chromosomes. The ability of mouse ESCs and iPSCs to form germline-competent chimeras have been widely used to create genetically engineered lines of mice and revolutionized developmental, genetic, and biomedical research (Capecchi, 2005).

After first mouse ESCs were established, human ESCs were expected to be their equivalents because of the blastocyst origin. However, all attempts to derive them using mouse ESCs serum/LIF culture conditions gained no success (Bongso *et al.*, 1994). It took seventeen years after the derivation of mouse ESCs to establish first human ESCs from human blastocysts (Thomson, 1998). Unlike those of mouse, they appeared to be depend not on LIF/Stat3 and BMP for maintaining pluripotency and self-renewal but

rather on fibroblasts growth factor (FGF2) and activin (INHBA)/nodal signaling; exhibit flat colony morphology, poor clonogenicity, pronounced levels of DNA methylation, and show propensity for X chromosome inactivation (Vallier, 2005; Ludwig *et al.*, 2006; De Los Angeles *et al.*, 2015). Human iPSCs were successfully generated using OSKM pluripotency factors (Takahashi *et al.*, 2007), as well as using Oct4, Sox2, Nanog and Lin28 (Yu *et al.*, 2007). Human PSCs express AP, Oct4, Sox2, Nanog as well as several cell surface markers, which appeared to be representative for human and nonhuman primate PSCs (SSEA3, SSEA4, TRAl-60, TRA1-81) (Martí *et al.*, 2013). Importantly, they are able to form derivatives of all three somatic lineages (Thomson, 1998).

Although nowadays it is known that pluripotency in mouse epiblast lasts for about five days during early embryogenesis, for many years mouse PSCs could be derived only from pre-implantation blastocysts (E3.5 – E4.5). When post-implantation epiblast cells (E5.5 – E7.5) were attempted to be maintained in conventional serum/LIF containing mouse ESCs medium, they differentiated or died. The discovery of alternative pluripotency maintaining capacity of FGF2 and activin resulted in the establishment of an alternative pluripotent state of mouse epiblast stem cells (EpiSCs) isolated from a post-implantation embryo (Brons *et al.*, 2007; Tesar *et al.*, 2007). Originated from post-implantation epiblast, mouse EpiSCs were shown to reflect changes during maturation of pre-implantation epiblast to post-implantation epiblast exhibiting specific gene expression profile of later one with downregulated expression of pluripotency-associated Nanog, Klf4 and Rex2 and elevated expression of some lineage-specific markers like Fgf5, as well as exhibiting X chromosome inactivation in female cells (Tesar *et al.*, 2007;

Boroviak *et al.*, 2014; Kojima *et al.*, 2014; De Los Angeles *et al.*, 2015). Like conventional human ESCs, mouse EpiSCs in their self-renewal rely on FGF2 and activin/nodal, as well as on transforming growth factor-β (Tgf-β) and Erk1/2, display flat-shaped colony morphology with limited clonogenicity, and are able to form teratomas but not blastocyst chimeras (Tesar *et al.*, 2007; Ying and Smith, 2017). Due to these similarities, it was proposed that human ESCs were in fact the counterpart of mouse EpiSCs rather than mouse ESCs (Tesar *et al.*, 2007) and that the main explanation of differences between mouse ESCs and human ESCs was developmental stage rather than species origin (Rossant, 2015). Nevertheless, some differences in gene expression profiles of human ESCs and mouse EpiSCs were noted. Human ESCs express cell-surface markers SSEA3 and SSEA4 and are AP positive, while mouse EpiSCs express SSEA1 and lack AP (Schnerch, Cerdan and Bhatia, 2010). Additionally, human ESCs exhibit the expression of Dppa3 and Klf4, as do mouse ESCs but EpiSCs do not (Davidson, Mason and Pera, 2015). Both Dppa3 and Klf4 were shown to be critical for transformation of mouse EpiSCs into ESCs (Hayashi *et al.*, 2008; Guo *et al.*, 2009).

Attempts to eliminate the dependency of mouse ESCs on external stimuli of LIF/Stat3 and BMP pathways resulted in the discovery of a new intrinsic program for ESC self-renewal and the first articulation of the concept of "ground state" pluripotency (Ying *et al.*, 2008). It was shown that self-renewal of ESCs could be enabled without LIF/BMP by inhibition of glycogen synthase kinase-3 (GSK3) and mitogen-activated protein kinase (Mek/Erk). Independence from these pathways can be achieved by combining their selective inhibitors, PD0325901 (Mek/Erk) and CH99021 (GSK3).

Utilization of these two small-molecule inhibitors (2i) were shown to be sufficient for establishment and self-renewal of homogenous PSCs from different strains of mice and, most importantly, in combination with LIF resulted in the derivation of first rat ESCs (Buehr *et al.*, 2008; Li *et al.*, 2008) and iPSCs (Liao *et al.*, 2009), which has been unsuccessful until 2008. Thus, the theory of two pluripotency states has been formed, the so-called naïve pluripotency, and primed pluripotency. According to this theory, naïve pluripotency, or ground state of pluripotency, reflects universal characteristics of pre-implantation epiblast, which is believed to exhibit an unbiased capacity to give rise to all somatic cell lineages as well as to germ cells (Ying *et al.*, 2008; Nichols and Smith, 2009). Utilization of the 2i system plus LIF is sufficient for maintenance of mouse and rat ESCs and iPSCs, and thus they are considered to be naïve PSCs (Nichols and Smith, 2009; Smith, 2017). Employment of 2i/LIF is not sufficient for human ESC and iPSCs derivation. Human ESCs and iPSCs (Takahashi *et al.*, 2007; Yu *et al.*, 2007), are conventionally maintained in similar culture conditions with mouse EpiSCs (Fgf2/activin) and do not tolerate 2i/LIF, hence are considered to represent a primed pluripotent state, which reflects features of the post-implantation epiblast. Both types are pluripotent and are able to differentiate into the derivatives of all three germ layers and form teratomas when injected into immuno-compromised mice (Nichols and Smith, 2009). The inability of conventional human ESCs/iPSCs and mouse EpiSCs to contribute to chimera formation when injected to the blastocyst (Rossant, 2008), as well as the inability to differentiate to germ cells are considered to be the main functional differences between mouse ESCs and mouse EpiSCs (Smith, 2017). However, primed ESCs/iPSCs

readily form chimeras when implanted to post-implantation epiblast (Huang *et al.*, 2012). Nevertheless, some manipulations like the forced expression of E-cadherin (Ohtsuka, Nishikawa-Torikai and Niwa, 2012) or Bcl2 (Masaki *et al.*, 2016) were reported to enable primed PSCs contribution to somatic lineages and even to primordial germ cells (Zhang *et al.*, 2016) after the injection into pre-implantation blastocysts. In the latter study, inhibition of histone H3K4 methyltransferase MLL1 activity were claimed to reprogram mouse EpiSCs to ESCs, while in two former studies genetic manipulations did not change the identity of EpiSCs but rather increased cell-cell adhesion (E-cadherin) or cell survival (Bcl2) therefore enabling chimeric contribution.

The primed pluripotency of conventional human ESCs/iPSCs is considered to be a key contributing factor to the heterogeneity of different lines of ESCs/iPSCs, which is also common in mouse EpiSCs. Recently, efforts have been made to establish human naive ESCs/iPSCs using 2i/LIF with additional pathways inhibitors (Takashima *et al.*, 2014; Theunissen *et al.*, 2014, 2016; Yang *et al.*, 2017). Insufficiency of 2i/LIF alone might be explained by the absence of Esrrb expression in naive human epiblast (Blakeley *et al.*, 2015), in consideration of that Esrrb is known as a critical factor downstream of GSK3 inhibition in naïve mouse ESCs/iPSCs. Even if so, the rapid development of the field may soon lead to the discovery of novel regulators establishing human equivalents of rodent naïve PSCs with a capability to contribute to blastocyst chimeras.

Reprogramming to iPSCs

After the groundbreaking discovery of Takahashi and Yamanaka in 2006, when they reported the successful reprogramming of mouse adult fibroblasts to iPSCs using

overexpression of OSKM transcriptional factors (Takahashi and Yamanaka, 2006), it has become the most commonly used reprogramming cocktail for generating iPSCs. The same four Yamanaka factors were shown to successfully reprogram differentiated cells from human (Takahashi *et al.*, 2007; I. H. Park *et al.*, 2008), rhesus monkey (Liu *et al.*, 2008), rat (Li *et al.*, 2009; Liao *et al.*, 2009), pig (Esteban *et al.*, 2009) and other species suggesting the evolutionary conserved nature of pluripotency-driven transcriptional network.

The expression of these exogenous factors triggers epigenetic and transcriptional changes in differentiated cells eventually leading to reactivation of the endogenous Oct4, Sox2, and Nanog and relevant feed-forward auto-regulatory loops that sustain pluripotent cell identity independently of the transgenes (Boyer *et al.*, 2005). However, the process of reprogramming is highly inefficient and the molecular events accompanying it are not completely uncovered. Given that only small and unpredictable fraction of OSKM transduced differentiated cells eventually becomes iPSCs and that the time required for successful transition from differentiated cell to one with activated pluripotency markers varies within the starting cell population, transcription factors-based reprogramming was assumed to be consistent with a stochastic rather than a deterministic model of reprogramming (Meissner, Wernig and Jaenisch, 2007; Hanna *et al.*, 2009; Yamanaka, 2009). Over time, however, it was shown that some stages of reprogramming correspond to a stochastic nature while other seem to follow deterministic patterns (Buganim *et al.*, 2012; Polo *et al.*, 2012).

A transcriptomic study on OSKM induction in mouse embryonic fibroblast populations suggested the separation of three reprogramming phases: initiation, maturation, and stabilization (Samavarchi-Tehrani *et al.*, 2010). According to this study, the maturation phase was characterized by endogenous activation of Nanog, Sall4, Esrrb, Rex1, Tcl1, Cripto, and Nodal expression, while the expression of Dnmt3l, Lin28, Utf1, Pecam, Stella, and Dppa4 was characteristic of the stabilization phase. In agreement with another study focused on morphological changes induced by ectopic OSKM expression, the initial phase of reprogramming was marked by destabilization of mesenchymal phenotype of MEF through the induction of BMP signaling and a mesenchymal-to-epithelial transition (MET), which is the opposite to the epithelial-to-mesenchymal transition (EMT) during embryo development (Li *et al.*, 2010; Samavarchi-Tehrani *et al.*, 2010). The induction of epithelial features was related to the suppression of EMT mediator Snail by Oct4 and Sox2, suppression of TGF-βR1 and TGF- βR2 by c-Myc, as well as to the induction of E-cadherin expression by Klf4. Thus, Snail, TGF-βR1, TGF-βR2, and E-cadherin may serve as markers of MET as initial stage of reprogramming. Moreover, the manipulation of genes and extrinsic factors related to MET can effect both efficiency and speed of reprogramming (Li *et al.*, 2010; Polo and Hochedlinger, 2010). In consistence with this, TGF-β receptor inhibitor ALK5 was shown to enhance the reprogramming efficiency in the absence of c-Myc (Maherali and Hochedlinger, 2009).

Other studies utilizing doxycycline-inducible OSKM transgenes revealed that mesenchymal marker Thy1 is lost before SSEA1 becomes activated while endogenous Oct4-GFP reporter starts to be expressed even later (Brambrink *et al.*, 2008; Stadtfeld *et*

al., 2008). This established roadmap was used in dynamic studies of intermediate cell populations isolated based on Thy1/SSEA1/Oct4 markers enrichment allowing to gain additional insights on the transcriptional, epigenetic (Polo *et al.*, 2012) as well as on proteomic (Hansson *et al.*, 2012) changes during reprogramming. Both works detected two highly coordinated waves of transcriptome and proteome transformations underlying the induction of pluripotency. According to Polo *et al*., first wave was driven by c-Myc and Klf4 and corresponded to upregulation of genes related to cell division, DNA replication, metabolism, and cytoskeleton organization and downregulation of developmental genes. Early stage was also characterized by histone modifications. Second wave was shown to be associated with the induction of pluripotency factors such as Oct4, Sox2, Nanog, Esrrb, Lin28, Dnmt3L, Tcl1, and Nr5a2 driven by Oct4, Sox2, and Klf4 transgenes. Interestingly, DNA methylation changes were reported to be exclusive to the very end of the second wave when stable pluripotency is established (Polo *et al.*, 2012).

Limitations of cell population-based studies caused by cell heterogeneity and asynchronous nature of reprogramming process were partially overcome in the work of Buganim *et al*., in which the analysis of gene expression changes during various stages of transition from MEFs to fully reprogrammed iPSCs was performed on the single-cell level (Buganim *et al.*, 2012). Analyzed 48 genes were related to cell cycle regulation, ESC-associated chromatin remodeling, signal transduction, and pluripotency markers. Obtained data revealed that expression levels of these genes were highly variable among different sister cells at early phase of reprogramming, which is consistent with a

stochastic model, while afterwards more hierarchical pattern of endogenous pluripotency establishment was evident thus proposing deterministic nature of late reprogramming period. Among the most valuable observations emerged from this study were those related to the predictive power of various genes to ensure the reprogramming outcome. It was shown that the expression of MET marker E-cadherin and pluripotency marker Sall4 is necessary but not sufficient for pluripotency induction as MET was observed in both iPSC-producing and non-iPSC-producing cells as well as Sall4 was detected in E-cadherin-negative cells. Most importantly, early expression of Oct4 was shown to be non-predictive for eventual reprogramming, in contrast to Esrrb and Utf1, which appeared to be more reliable early predictive markers. In regard to the later stage of reprogramming, the activation of endogenous Sox2 was identified as a key event initiating the subsequent gradual progression towards pluripotency thereby proposing that following steps are not stochastic anymore (Buganim *et al.*, 2012).

Overall, upon reprogramming of differentiated cells to iPSCs, several mechanistic and molecular events have been described: rapid increase of cell proliferation rate, upregulation of DNA replication genes (Knoepfler, 2008; Smith *et al.*, 2010), apoptosis and senescence (Banito *et al.*, 2009; Plath and Lowry, 2011), acquisition of ESC-like cell cycle (Sridharan *et al.*, 2009), suppression of differentiated cell-specific genes (Stadtfeld *et al.*, 2008), chromatin remodeling (Maherali *et al.*, 2007; Knoepfler, 2008; Mansour *et al.*, 2012), MET (Li *et al.*, 2010; Samavarchi-Tehrani *et al.*, 2010), activation of DNA repair (Hansson *et al.*, 2012; Buganim, Faddah and Jaenisch, 2013), activation of glycolysis (Zhang *et al.*, 2012), upregulation of early embryonic markers AP, SSEA-1

(mouse iPSCs), SSEA-3, SSEA-4, TRA-1-60 and TRA-1-81 (human and nonhuman primate iPSCs) (Brambrink *et al.*, 2008; Stadtfeld *et al.*, 2008; Martí *et al.*, 2013), ultimate activation of core pluripotency markers Sox2, Sall4, Lin28, Esrrb, Oct4, Nanog, Dppa2, Utf1, Fgf4, Fbxo15, Cdc20, and Dnmt3b, silencing of transgenes and transgene-independent self-renewal (Samavarchi-Tehrani *et al.*, 2010; Buganim *et al.*, 2012; Golipour *et al.*, 2012), loss of epigenetic memory and DNA demethylation (Polo *et al.*, 2010), reactivation of X-chromosome in female cells via Xist silencing (Maherali *et al.*, 2007; Plath and Lowry, 2011) and telomere elongation via Tert activation (Marion *et al.*, 2009).

Interspecific mammalian chimeras

An interspecific chimera is typically determined as an organism that consists of a mixture of different cell populations derived from zygotes of different species. They can be created by mixing of early embryos or by tissue transplantation. They also can be formed via injection of naive PSCs into pre-implantation blastocysts (Suchy and Nakauchi, 2017; Wu *et al.*, 2017). Nowadays, research on chimeras is of increased interest for both basic and translational science. Evolutionary divergence and developing matching of various species, pluripotency potential of PSCs, humanized mice and rats as human disease models, and production of human organs for drug testing or for transplantation are some possible applications of interspecific chimera research (Wu *et al.*, 2016).

The first studies on interspecific mammalian chimera formation were reported in 1970s, when rat ICM cells were introduced into mouse blastocysts, which were

transferred to the uteri of pseudopregnant mice. Several days later, the chimeric contribution was confirmed in all three germ layers (Gardner and Johnson, 1973). Later, first full-term chimeras were reported between two different mouse species – *Mus caroli* and *Mus musculus* – using ICM of former one and blastocysts of later (Rossant and Frels, 1980). This and the follow-up study (Rossant *et al.*, 1983), when *Mus caroli* pups were born using blastocysts composed of *Mus musculus* trophectoderm and *Mus caroli* ICM, concluded that the trophectoderm and the uterus must be from the same species for embryo implantation and development. Consistent with this conclusion, there was a report on goat-sheep chimeras formed by blastocyst complementation, (Fehilly, Willadsen and Tucker, 1984). Although these pioneer studies revealed the ability of interspecific chimera formation and gained first insights in this process, the authentic interest in generating interspecific chimeras has been reborn with the establishment of naïve pluripotency culture environment and recent rapid progress in iPSCs and gene editing techniques. Recent studies revealed several interesting insights. It was shown that utilization of genetically modified pancreogenesis-disabled mouse blastocysts and donor rat PSCs resulted in the formation of mouse-sized pancreas entirely derived from rat cells (Kobayashi *et al.*, 2010; Wu *et al.*, 2017). Moreover, chimeras born upon injection of rat PSCs into mouse blastocysts were generally mouse-sized and *vice versa*. Finally, the fact that mice have a gallbladder, but rats do not have one, revealed that PSC-derivatives are subject to regulation by the host programs that drive organogenesis (Kobayashi *et al.*, 2010; Wu *et al.*, 2016, 2017).

Unlike rodents, germline-competent iPSCs have yet to be isolated from other species. Human iPSCs grown in different primed culture conditions were shown to integrate into mouse gastrula-stage embryos and form ex vivo interspecific chimeras (Wu *et al.*, 2015; Mascetti and Pedersen, 2016). Humans and mice vary considerably in numerous aspects, including post-implantation epiblast development, embryo size, the speed of development and the gestational period. Interspecific chimera research using large animal hosts that are more similar to humans in anatomy, physiology and organ size could result in an improved chimeric research models. It was recently shown that several types of human iPSCs could contributed into both cattle and pig preimplantation blastocysts and even showed some chimeric contribution to post-implantation pig embryos (Wu *et al.*, 2017).

Growing human organs *in vitro* or in animal hosts, as well as attenuating aging and extending lifespan have been distant dreams of many stem cell and aging biologists. These dreams may come true with the lessons learned from interspecific mammalian chimeras.

Chapter 2

Naked Mole Rat Induced Pluripotent Stem Cells and Their Contribution to Interspecific Chimera

Abstract

Naked mole rats (NMRs) are exceptionally long-lived, cancer-resistant rodents. Identifying the defining characteristics of these traits may shed light on aging and cancer mechanisms. Here, we report generation of induced pluripotent stem cells (iPSCs) from NMR fibroblasts and their contribution to mouse-NMR chimeric embryos. Efficient reprogramming could be observed under N2B27+2i conditions. The iPSCs displayed a characteristic morphology, expressed pluripotent markers, formed embryoid bodies and showed typical differentiation patterns. Interestingly, NMR embryonic fibroblasts and the derived iPSCs had propensity for a tetraploid karyotype and were resistant to forming teratomas, but within mouse blastocysts they contributed to both interspecific placenta and fetus. Gene expression patterns of NMR iPSCs were more similar to those of human than mouse iPSCs. Overall, we uncovered unique features of NMR iPSCs and report the first mouse-NMR chimeric model. The iPSCs and associated cell culture systems can be used for a variety of biological and biomedical applications.

Introduction

The naked mole rat (NMR; *Heterocephalus glaber*) (Figure 1; top) is an emerging model organism for studies on aging and cancer. While NMRs and mice have a similar body size, the former live 10 times longer than the latter (~30 years vs. ~3 years) (Edrey et al., 2011). NMRs are also highly resistant to both spontaneous and experimentally induced cancer (Liang et al., 2010; Seluanov et al., 2009). Moreover, NMR exhibits the absence of pain sensitization due to hypofunctional TRKA receptor (Omerbasic et al., 2016) and extreme resistance to hypoxia through fructose metabolism to avoid tissue damage (Park et al., 2017). In addition, these animals do not maintain stable body temperature, can live at low oxygen and high carbon dioxide concentrations in the atmosphere, and show other features that are useful for biomedical research (Edrey et al., 2011; Kim et al., 2011).

Until now, tissue samples have been the main source for comparative studies involving NMRs. However, phenotypes of these animals have been difficult to assess, mainly due to the limited access to embryonic material and cell culture models. Live cell models are preferred over tissue samples in assessing and manipulating the unique features of these animals. Pluripotent stem cells could be an important biological resource for such studies. Embryonic stem cells exhibit pluripotency and can form any cell type (Evans and Kufman, 1981; Martin, 1981; Brook and Gardner, 1997). However, NMRs

are eusocial rodents that live in large colonies with only one breeding female. Such reproductive behavior is a major limitation for generating ESCs from blastocysts.

Induced pluripotent stem cells have similar biological characteristics to ESCs, including morphology, capacity for infinite proliferation, gene expression profiles, the ability to form the derivatives of all three germ layers, and the utility for germline transmission (Takahashi and Yamanaka, 2006; Chin et al., 2009). iPSCs also offer several advantages over ESCs because they can be generated without using embryos, e.g. by manipulating adult cells. The first iPSCs were generated 12 years ago using four pluripotency factors, OCT4, SOX2, KLF4 and C-MYC (OSKM), reprogramming mouse fibroblasts (Takahashi and Yamanaka, 2006). Since then, iPSCs were generated from several mammals, including humans (Takahashi et al., 2007; Yu et al., 2007), rats (Liao et al., 2009), pigs (Esteban et al., 2009; Ezashi et al., 2009), cows (Huang et al., 2011), dogs (Luo et al., 2011), rabbits (Honda et al., 2010), horses (Nagy et al., 2011), buffalos (Deng et al., 2012), sheep (Bao et al., 2011) and bats (Mo et al., 2014). In many studies, iPSCs have served as a substitute for ESCs and a source of somatic cells. The successful generation of NMR iPSCs could bring a much-needed resource for characterizing relevant phenotypes.

Recently, Miyawaki et al., 2016, reported the generation of NMR iPSCs and found resistance to teratoma formation and attributed this feature to elevated Arf expression and mutation in the Eras oncogene. They used a conventional human culture condition to derive NMR iPSCs and found that they could be generated at high oxygen

and with a low efficiency of reprogramming in case of adult fibroblasts. Moreover, chimeric contribution of NMR iPSCs has not been reported for proving their pluripotency and applying to appropriate genetic manipulation.

Here, we report the development of NMR iPSCs from embryonic and adult fibroblasts using drug-inducible expression of OSKM with high efficiency. The iPSCs displayed the pluripotency and some non-canonical features such as a propensity for a tetraploid karyotype and resistance to forming teratomas. Interestingly, these iPSCs contributed to interspecific chimeras despite differences of physiological temperature and phylogenetic distance in rodents. Moreover, the transcriptomes of NMR iPSCs were more similar to those of human than mouse iPSCs even they have genetic diversification or evolutionary distance with human. These cells and the associated protocols should pave the way for generation of gene-targeted NMR models for biomedical research and provide much needed cell culture systems to facilitate aging and cancer-related research at the cellular and molecular levels.

Results

Conventional protocols that support preparation of mouse iPSCs do not favor NMR cell reprogramming

To reprogram NMR cells, we employed a doxycycline-inducible lentiviral system, in which mouse or human OSKM were inserted downstream of a tetracycline operator (Hockemeyer *et al.*, 2008; Carey *et al.*, 2009). We first used NMR embryonic fibroblasts (~45 days post-coitum) (Figure 1; top) and maintained them in a conventional mouse ESC medium following transduction (Figure 1; bottom, blue letters). Reprogramming of somatic cells towards iPSCs is thought to proceed through three phases: initiation, maturation and stabilization (Samavarchi-Tehrani *et al.*, 2010; Plath and Lowry, 2011). The initiation phase is marked by the mesenchymal-to-epithelial transition (MET) and bone morphogenic protein (BMP) signaling (Li *et al.*, 2010; Samavarchi-Tehrani *et al.*, 2010), and E-cadherin impeding reprogramming (Chen et al., 2010). Esrrb and Utf1 represent early markers that predict an eventual reprogramming event, whereas endogenous Sox2 is a late phase reprogramming factor (Buganim *et al.*, 2012).

To gain insights into MET and NMR cell reprogramming, we quantified NMR-specific E-cadherin (Ecad), Esrrb, Utf1 and Sox2 transcripts on day 6 following transduction (Figure 1; bottom). Mouse OSKM-transduced NMR cells showed higher

expression of these transcripts compared to cells transduced with human OSKM, although both approaches induced expression of the marker genes.

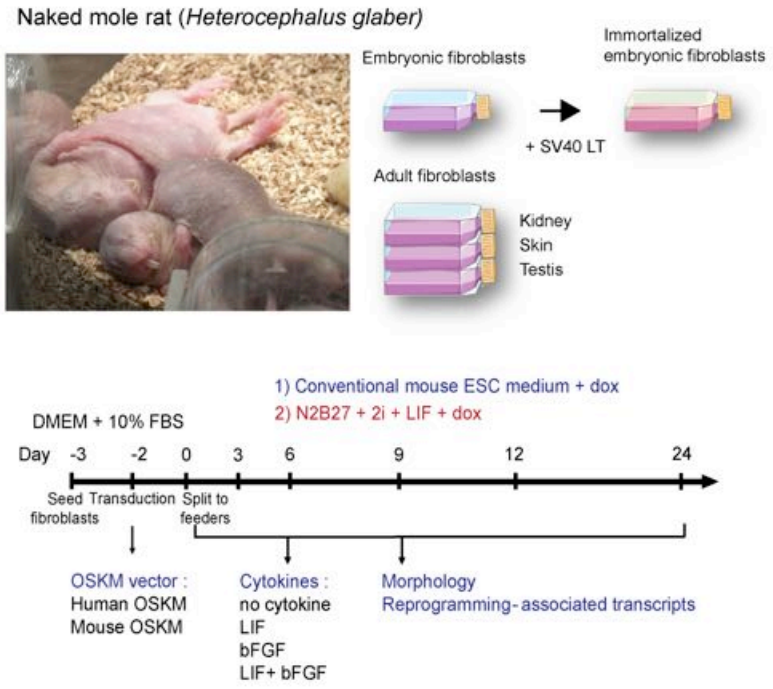

Figure 1. Naked mole rat (*Heterocephalus glaber*) and fibroblasts used in this study (top). Schematic diagram of the conventional (blue) and NMR (red) reprogramming protocols (bottom).

In particular, the Ecad levels were 30 fold higher than in control fibroblasts (Figure 2A). We further found that cytokine treatment increased the expression of reprogramming-related genes, with LIF (Leukemia inhibitory factor) being a stronger inducer than bFGF (basic fibroblast growth factor) (Figure 2B). Hence, mOSKM and LIF were chosen for further experiments. We screened for changes in marker gene expression until day 24 and also analyzed the initial reprogramming genes Snail and Tgfb1 (Figure 2C). Snail expression increased starting from day 3 and was maximal at day 24. Tgfb1 increased at

day 6 and gradually decreased until day 24. Ecad, Esrrb and Utf1 were dramatically increased from days 3-6 and gradually decreased to day 24. Sox2 was gradually increased to day 24. Thus, transcription factors and cytokines could alter reprogramming-associated gene expression in NMRs. With the same method, we generated mouse iPSCs from embryonic and adult fibroblasts (Figure 3A and B). However, NMR cells showed no visible morphological changes until day 24 (Figure 2D), when we detected OCT4-expressed cells (Figure 2E). Nevertheless, this approach did not result in viable ESC-like NMR colonies, suggesting that the conventional protocols, which readily support preparation of mouse iPSCs, are unsatisfactory for deriving NMR iPSCs.

Development of optimal protocols to support generation of NMR iPSCs

SV40 large T antigen has been reported to improve the efficiency of iPSC generation (Park et al., 2008). Reducing p53 expression can also improve this process (Mali et al., 2008; Utikal et al., 2009; Hong et al., 2009; Hanna et al., 2009a). In fact, SV40 large T antigen may support iPSC generation by inhibiting p53 expression (Bao et al., 2011). Also, unlike mouse cells, rat ESCs and iPSCs require specific culture conditions, such as serum-free defined culture medium (N2B27) with inhibition of the MEK (mitogen activated protein kinase)/ERK (extracellular signal regulated kinases 1 and 2) pathway and glycogen synthase kinase-3 (GSK3) by small synthetic drugs PD0325901 (PD) and CHIR99021 (CHIR), respectively. These culture conditions (N2B27+2i) were also beneficial for establishing and maintaining ground state

pluripotent cells from other species, including mouse and human (Ying et al., 2008; Hanna et al. 2009b; Buehr et al., 2008).

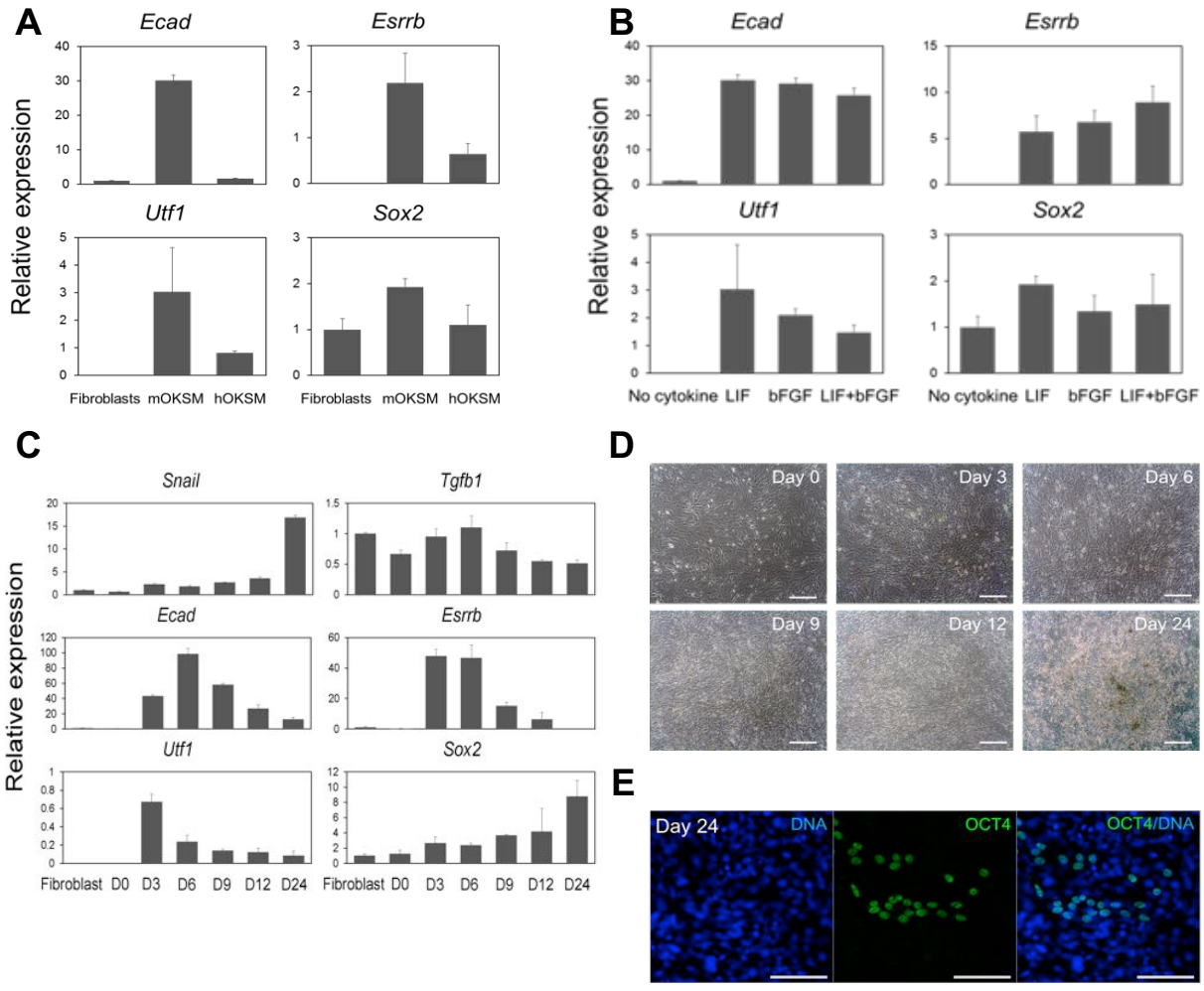

Figure 2. Conventional iPSC conditions do not favor NMR cell reprogramming.
(**A**) Real-time PCR analyses of endogenous Ecad, Esrrb, Utf1 and Sox2 expression in NMR cells expressing mouse or human OSKM. All values are mean ± SEM from three independent experiments. (**B**) Real-time PCR analyses of endogenous Ecad, Esrrb, Utf1 and Sox2 expression in NMR cells subjected to mouse OSKM in combination with cytokines. All values are mean ± SEM from three independent experiments. Relative expression was normalized to the expression of GAPDH. (**C**) Real-time PCR analyses of

reprogramming-associated gene expression up to day 24 (e.g. D1=day 1, D3= day 3, etc.). All values are mean ± SEM from three independent experiments. Relative expression was normalized to the expression of GAPDH. (**D**) No changes in morphology of NMR cells were detected during the 24-day procedure. Scale bars, 100 μm. (**E**) Immunocytochemical analyses of Oct4 in NMR cells at day 24. Scale bars, 100 μm.

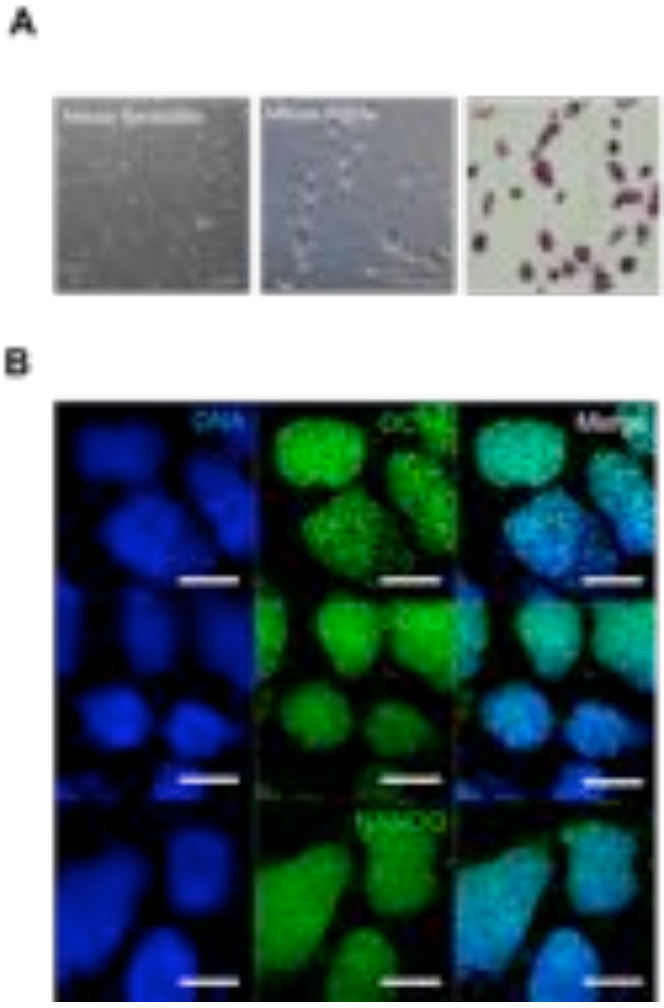

Figure 3. Generation of mouse iPSCs from embryonic fibroblasts.
(**A**) Mouse fibroblasts, morphology of iPSC cells and AP staining, respectively. Scale bars, 100 μm. (**B**) Representative images of mouse iPSC colonies following immunostaining for OCT4, SOX2 and Nanog. Scale bars, 100 μm.

We applied the N2B27+2i culture model to NMR embryonic fibroblasts and immortalized embryonic fibroblasts by inserted SV40 large T antigen in combination

with the lentiviral system (Figure 1; bottom). Remarkably, 16 days after transduction, typical ES colony-like cells were observed in immortalized embryonic fibroblasts (Figure 4A). These colonies showed strong alkaline phosphatase (AP) activity, suggesting pluripotency (Figure 4A). Interestingly, in the case of normal embryonic fibroblasts, the first colonies were visible at day 30 (Figure 4B). NMR iPSCs could be routinely passaged on feeder systems every five days. These colonies exhibited round, tightly packed morphology characterized by a high ratio of nucleus to cytoplasm and prominent nucleoli (Figures 2A and 2B), similar to rat iPSCs. To optimize the protocol, we cultured OSKM-transduced cells in various culture conditions and performed AP staining. These analyses confirmed the difference between conventional ES and N2B27 +2i media (Figure 5A). Clearly, N2B27 +2i media dramatically induced AP-positive colonies with typical ES-like morphology, suggesting that this culture condition is particularly effective for reprogramming NMR cells.

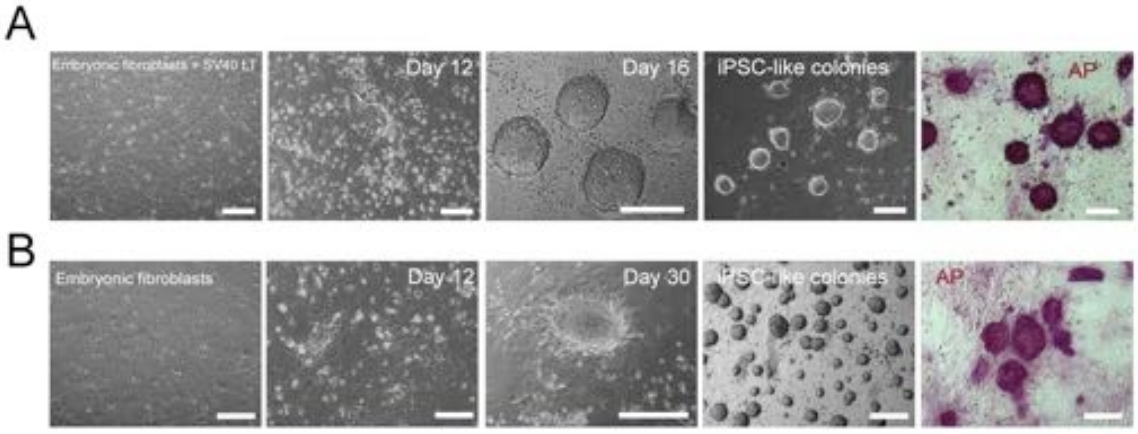

Figure 4. Generation of NMR iPSCs from embryonic fibroblasts.
(**A**) Generation of NMR iPSCs from embryonic fibroblasts transfected with SV40 LT. Immortalized cells, cells at day 12 after transduction, cells day 16 after transduction, showing iPSC-like morphology and AP staining. (**B**) Generation of NMR iPSCs from embryonic fibroblasts. Embryonic fibroblasts, cells at day 12 after transduction, cells at

day 30 after transduction, showing iPSC-like morphology and AP staining. Scale bars, 100 μm.

We next examined the effect of inhibitors on AP-positive colony formation using N2B27+LIF with or without PD or CHIR. The number of AP-positive colonies in the presence of CHIR and 2i was much higher than under other conditions, supporting a role of CHIR in reprogramming (Figure 5B). We also examined the effect of cytokines, with LIF representing the most effective factor (Figure 5C). On the other hand, the reprogramming efficiency was influenced by neither feeder/feeder-free monolayer culture (Figure 5D) nor ascorbic acid (Figure 5E). After serial passaging of ES-like colonies, extensive spontaneous differentiation was observed. An inhibitor of type 1 transforming growth factor beta receptor ALK5 (A83-01) can help maintain rat iPSCs (Li et al., 2009), and we found that it supported homogeneous population and prevented spontaneous differentiation of NMR iPSCs (Figure 5F). We also observed that the expression of SV40 Large T accelerated reprogramming of NMR iPSCs, e.g. the reprogramming time was reduced in immortalized fibroblasts compared to normal fibroblasts (16 and 30 days, respectively).

We further applied these culture conditions to reprogram adult somatic fibroblasts isolated from the kidney of a 1-year old male NMR. In this case, the first colony was visible on day 43, suggesting that the reprogramming period was extended compared to embryonic fibroblasts (Figure 6A). The reprogramming efficiency was 0.17±0.001% for immortalized embryonic fibroblasts, 0.24± 0.001% for normal embryonic fibroblasts (embryonic), and 0.085±0.0132% for adult somatic fibroblasts.

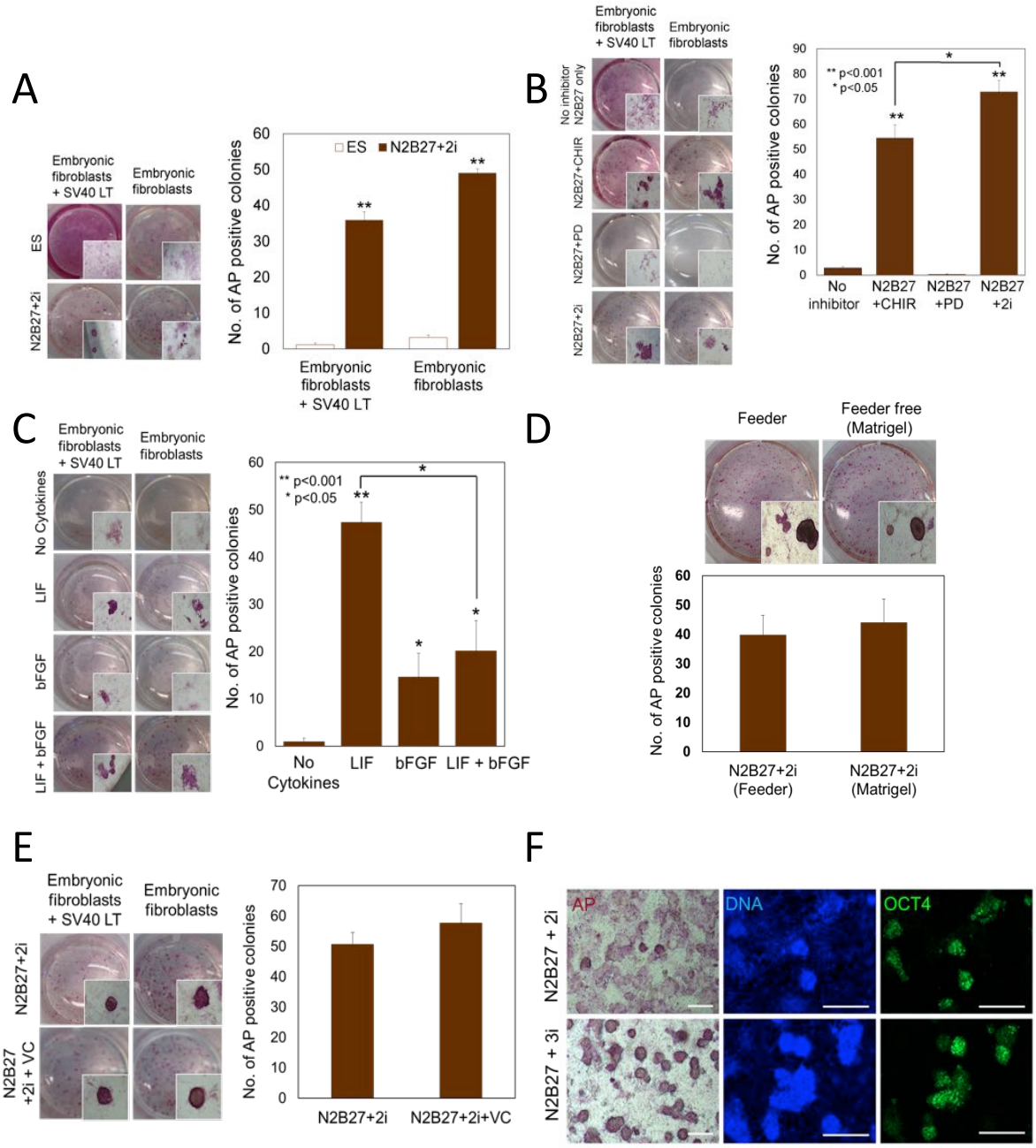

Figure 5. Reprogramming efficiency of NMR embryonic fibroblasts in various culture conditions.

(**A**) AP-positive colonies derived from NMR embryonic fibroblasts maintained in ES and N2B27 media (left panel). Quantification is in the right panel. Values represent means ± standard deviations for three independent experiments. **p<0.001. (**B**) AP-positive

colonies derived from NMR embryonic fibroblasts maintained in the indicated medium in combination with inhibitors (left panel). Quantification is in the right panel. Values represent means ± standard deviations for three independent experiments. *<0.05, **p<0.001. (**C**) AP-positive colonies derived from NMR embryonic fibroblasts in different combination of cytokines. (**D**) AP staining under feeder or feeder-free (Matrigel) conditions (upper panel). Number of AP-positive colonies are shown in the lower panel. (**E**) Role of vitamin C (VC) in generation of iPSCs from immortalized or primary embryonic fibroblasts. AP staining in the presence of vitamin C is shown in the left panel, and the numbers of AP-positive colonies in the right. (**F**) AP-staining and Oct4 immunocytochemical analyses of iPSCs generated under N2B27+2i and N2B27+3i conditions. Scale bars, 100 μm.

We also succeeded in generating iPSCs from adult skin and testis cells (Figures 6B), suggesting that the procedure we developed represents a robust protocol for derivation of stable NMR iPSCs. Real-time PCR analysis using primers specific for OSKM transgenes showed no expression of exogenous OCT4 and C-MYC after removal of doxycycline (dox) from culture medium (Figure 6C). Taken together, we established effective conditions for cell reprogramming and for maintaining NMR iPSCs.

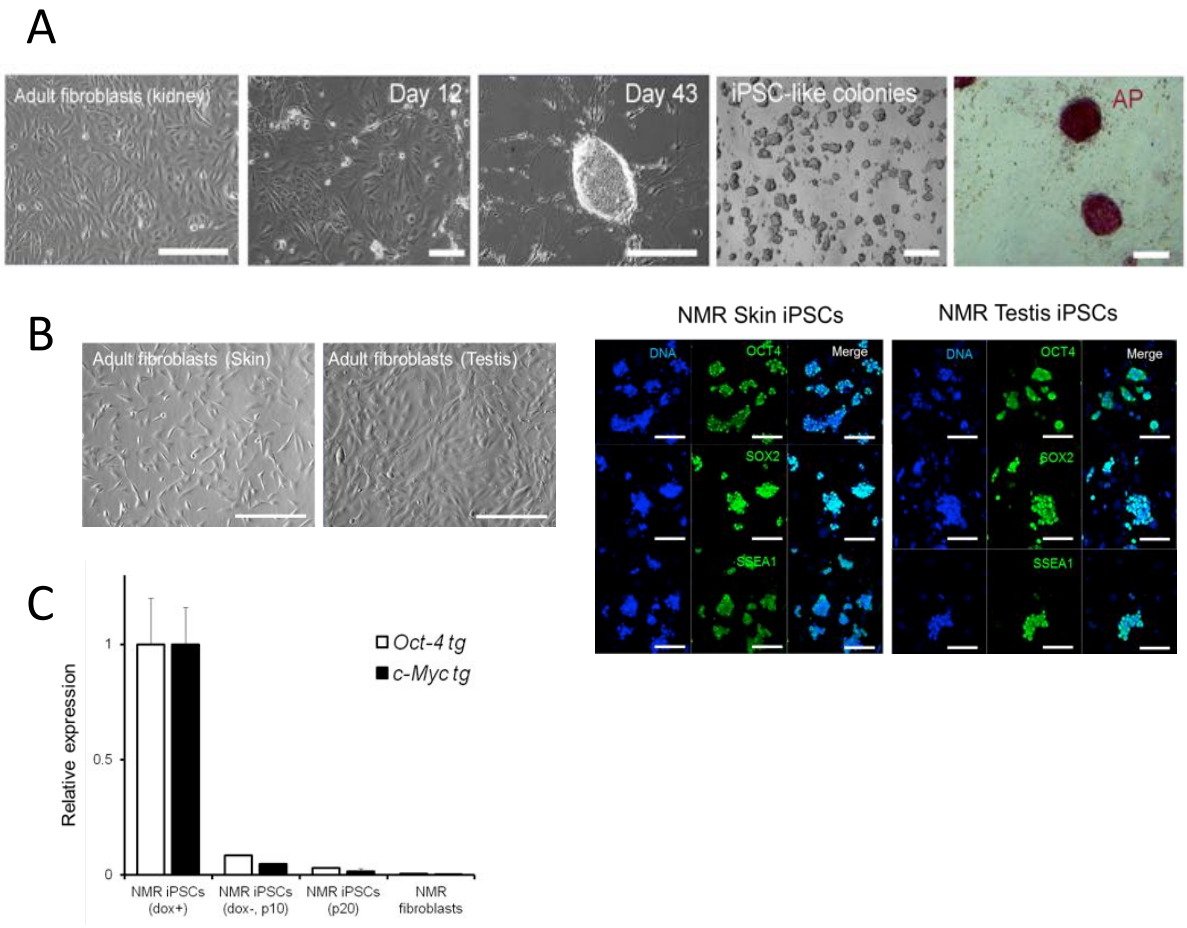

Figure 6. Generation of NMR iPSCs from adult fibroblasts.
(**A**) Generation of NMR iPSCs from adult fibroblasts. Adult fibroblasts, cells at day 12 after transduction, cells at day 43 after transduction, showing iPSC-like morphology and AP staining. All Scale bars, 100 μm. (**B**) Representative images of NMR skin and testis fibroblasts. Representative images of NMR skin and testis iPSC colonies from skin and testis fibroblasts following immunostaining for OCT4, SOX2 and SSEA-1. Scale bars, 100 μm. (**C**) Real-time PCR analysis of transgene (Oct-4 tg and c-Myc tg) expression in NMR iPSCs following removal of doxycycline (dox). dox+: culture with dox, dox-: culture without dox, p10: passage 10. All values are mean ± SEM from three independent experiments. Relative expression was normalized to the expression of GAPDH.

Pluripotent characteristics of NMR iPSCs

The generated NMR iPSCs could be stably passaged for more than 30 generations. They exhibited pluripotent cell markers, including OCT4, SOX2, and SSEA1 (Figure 7A). RT-PCR analysis revealed upregulation of several endogenous pluripotency-associated genes (Sox2, Nanog, Fgf4, Utf1, Zfp42 and Tert) in NMR iPSCs (Figure 7B). To test for differentiation of NMR iPSCs in vitro, we allowed them to form embryoid bodies (EB) and undergo differentiation for 7 days, and then analyzed for the presence of markers characterizing each germ layer. NMR iPSCs were able to differentiate into all three germ layers, as evidenced by high expression of Sox17 (endoderm), Gata4 (endoderm), Pdx1 (endoderm), Acta2 (mesoderm), Actc1 (mesoderm), Kdr (ectoderm), Sox1 (ectoderm), Pax6 (ectoderm) and Nestin (ectoderm) (Figure 8A).

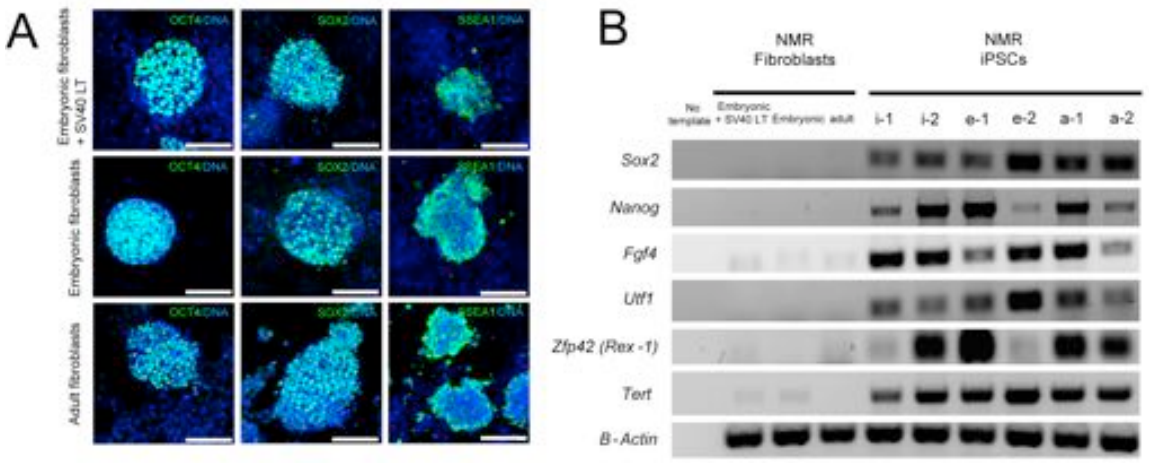

Figure 7. Characterization of NMR iPSCs: pluripotency associated genes.
(A) Representative images of NMR iPSC colonies from cells of indicated origin following immunostaining for OCT4, SOX2 and SSEA-1. Scale bars, 100 μm. **(B)** RT-PCR analysis of endogenous pluripotency genes expressed in NMR iPSCs. (i), iPSCs from immortalized fibroblasts; (e), iPSCs from embryonic fibroblasts; (a), iPSCs from adult fibroblasts; origin, two independently established clones.

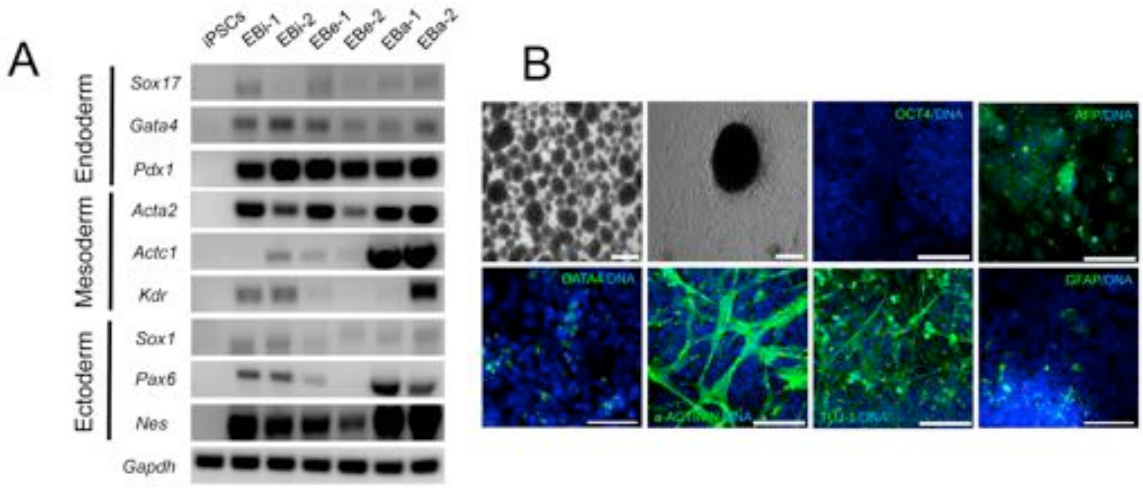

Figure 8. Characterization of NMR iPSCs: *in vitro* differentiation.
(A) RT-PCR analysis of genes expressed in EBs derived from NMR iPSCs. (Immortalized, EBi; embryonic, EBe; adult, EBa origin: two independently established NMR iPSC lines; iPSCs: undifferentiated iPSC line). **(B)** *In vitro* differentiation of NMR iPSCs. EB formation. Immunocytochemical analyses of EB expression: pluripotency marker (Oct4; negative control), endoderm (AFP and GATA4), mesoderm (a-actinin) and ectoderm (TUJ-1 and GFAP) markers. Scale bars, 100 μm.

We further examined in vitro differentiation of NMR iPSCs by immunocytochemistry. NMR EBs were transferred onto gelatin-coated plates for continued cultivation, and the attached cells exhibited different morphologies. Immunocytochemistry analyses detected cells positive for alpha fetoprotein (AFP; endoderm), GATA4 (endoderm), alpha actinin (a-actinin; mesoderm), βIII-tubulin (TUJ-1; ectoderm) and glial fibrillary acidic protein (GFAP; ectoderm) (Figure 8B).

NMRs exhibit an unusual mode of thermoregulation in that they are endothermic poikilotherms (Buffenstein and Yahav, 1991). NMR fibroblasts grow poorly at the standard 37 °C conditions, perhaps because the animals have a body temperature several degrees lower in their natural environment (Lewis et al., 2012). Prior to teratoma assays

and chimera production, we examined the effect of high temperature on maintenance of NMR iPSCs and the process of differentiation in vitro. The number of viable NMR iPSCs significantly decreased at 37 °C after culturing them for 10 or 20 days (Figure 9A). When we cultured NMR iPSCs in a normal fibroblast medium without pluripotent environment (LIF and 2i), the number of viable cells decreased at day 30, but no significant differences were observed in comparison with the 32 °C environment (Figure 9B). We also compared the formation of embryonic bodies (EBs) between 32 °C and 37 °C, but there was no difference in morphology (Figure 9C) and the number of EBs (Figure 8D). These EBs were differentiated to three germ layers as revealed by immunocytochemistry (Figure 9E). Together, we found that elevated temperature (37 °C) led to a reduced number of NMR iPSCs and their derivatives during differentiation in vitro. Nevertheless, some surviving cells could differentiate into all three germ layers even at elevated temperature.

To determine whether NMR iPSCs displayed *in vivo* pluripotency, 6 lines of NMR iPSCs were injected into renal capsules of 6 SCID mice. No teratomas were detected 12 weeks following injection. However, nerves were found on the cortex in a half of the injected kidneys as revealed by histological examination and NMR-specific sequences (Figure 10A; left panel). We also used EGFP-expressed iPSCs (Figure 10B) for teratoma assay and found that these cells were positive for a neuronal marker (TUJ-1) by immunocytochemistry (Figure 10C). Thus, these nerve cells were derived from the NMR iPSCs rather than from mouse cells, and this happened without tumor formation.

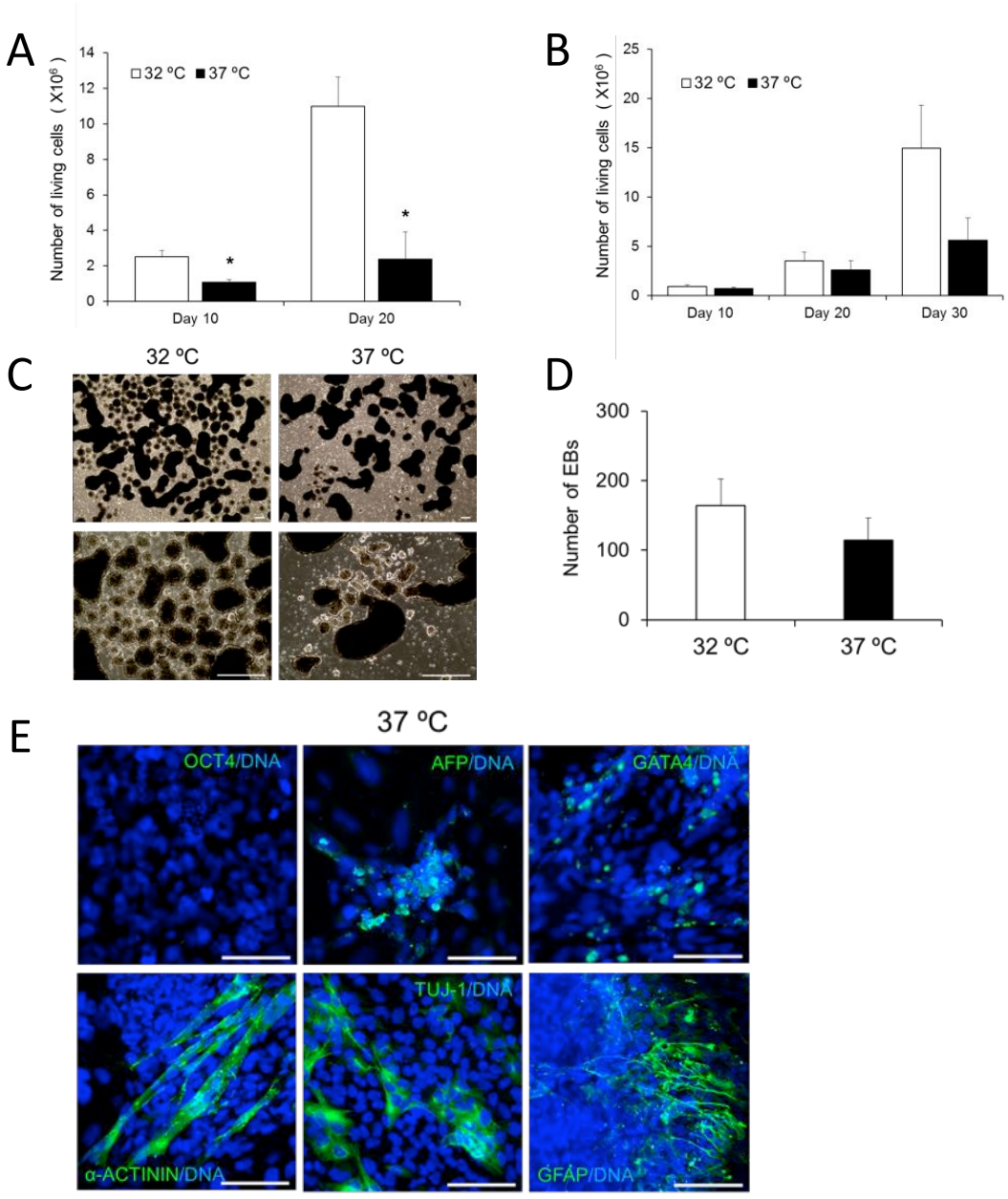

Figure 9. Characterization of NMR iPSCs in 32 °C vs. 37 °C.
(**A**) Number of viable iPSCs at normal (32 °C) and elevated (37 °C) temperature. NMR iPSCs were cultured at 32 °C or 37 °C for 20 days. Viable cells were detected by trypan blue staining. All values are mean ± SEM from three independent experiments. Asterisk indicates P=0.05 by t-test. (**B**) Number of viable cells during differentiation. NMR iPSCs cultured at 32 °C or 37 °C without pluripotent enviroment. Viable cells were detected by trypan blue staining. All values are mean ± SEM from three independent experiments. (**C**) Morphology of EBs at indicated temperature. NMR iPSCs were grown as a suspension culture on low adherent plates using normal medium for one week. The same

number of cells used for EB formation. The experiment was repeated 3 times, with similar morphology. Scale bars, 100 μm. (**D**) Number of EBs at indicated temperature. EBs were counted following one week in culture. The same number of cells were used for EB formation. All values are mean ± SEM from three independent experiments. (**E**) In vitro differentiation of NMR iPSCs at 37 °C. Immunocytochemical analyses of EB expression: pluripotency marker (Oct4; negative control), endoderm (AFP and GATA4), mesoderm (alpha-actinin) and ectoderm (TUJ-1 and GFAP) markers. Scale bars, 100 μm.

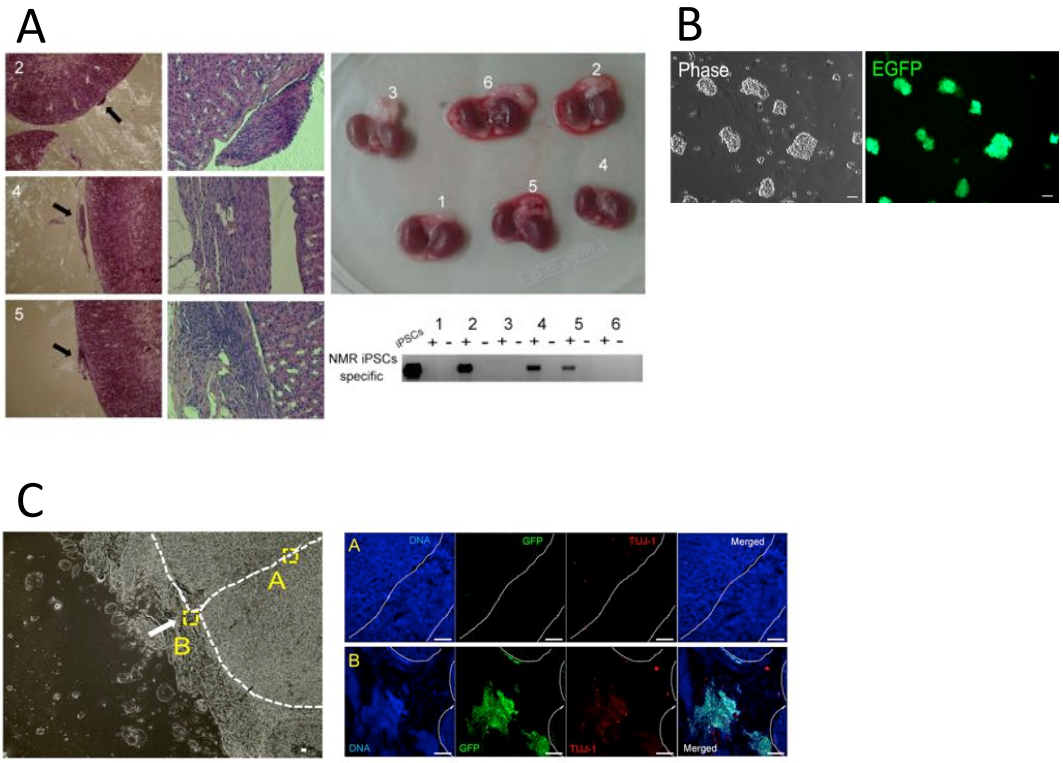

Figure 10. Characterization of NMR iPSCs: teratoma formation assay.
(A) Teratoma assay involving NMR iPSCs. Sections of kidney capsules of mice transplanted with NMR iPSCs (5 tetraploid and one diploid iPSCs; #2 kidney was injected with the diploid iPSCs) after 10 weeks (upper right). Some nerve-like cells were observed on the cortex (left panels, shown by arrows; magnified in the middle panels). Hematoxylin and eosin staining is also shown. Numbers represent individual kidney samples. Genomic PCR analyses showed that the nerve-like cells were of the NMR origin (lower right panel). (+) injected kidney capsule, (-) non-injected kidney capsule in this panel. (**B**) Morphology of the generated EGFP-expressing NMR iPSCs. Scale bars, 100 μm. **(C)** Teratoma assay involving EGFP-expressed NMR iPSCs. Arrow indicates injection site of NMR iPSCs into kidney capsules. A: regions of inner cortex; B: regions of injection site on the cortex. Immunocytochemical analyses of EGFP cell expression: neuronal marker (TUJ-1). Scale bars, 100 μm.

Propensity for a tetraploid karyotype in naked mole rat fibroblasts and iPSCs

Karyotype abnormality is often associated with quality of iPSCs. We karyotyped 12 NMR iPSCs lines, which were derived from 3 different fibroblast lines, at passage 10. Except for one line (2N=60 chromosomes) derived from immortalized fibroblasts, NMR iPSCs lines showed a sign of tetraploidy (2N=120 chromosomes) (Figure 11A). We also karyotyped the 7 fibroblast lines that were used for generation of NMR iPSCs. Interestingly, embryonic fibroblasts also showed the tetraploid karyotype, while adult fibroblasts exhibited primarily normal karyotype (Figure 11A and B). To clarify these characteristics of NMR cells, we performed DNA content analysis in fibroblasts and their respective iPSCs by fluorescence-activated cell sorting (FACS). Embryonic fibroblasts exhibited diploid (2N), tetraploid (4N) and mixed diploid/tetraploid DNA, while adult fibroblasts were primarily diploid (2N) (Figure 11C). These findings support the idea that NMRs may rely on the increased use of tetraploid cells. We noted that iPSCs derived from embryonic fibroblasts did not change DNA content, whereas iPSCs from adult fibroblasts increased their tetraploidy (4N). The DNA content of each iPSC line did not change during differentiation (Figure 11D). We also found that 4N cells increased during long-term culture of fibroblasts (Figure 11E). We did not observe differences between NMR tetraploid and diploid iPSCs when they were grown at 32 °C and 37 °C (Figure 9A and B) or subjected to the teratoma assay (Figure 10A). Overall, NMR embryonic fibroblasts and iPSCs showed high a propensity for the tetraploid karyotype. Nevertheless, in addition to tetraploid NMR iPSC lines mentioned above, we successfully developed and characterized diploid iPSC line, which may be more appropriate for the

development of NMR cell culture systems and should be of interest to researchers in various fields (Figure 12).

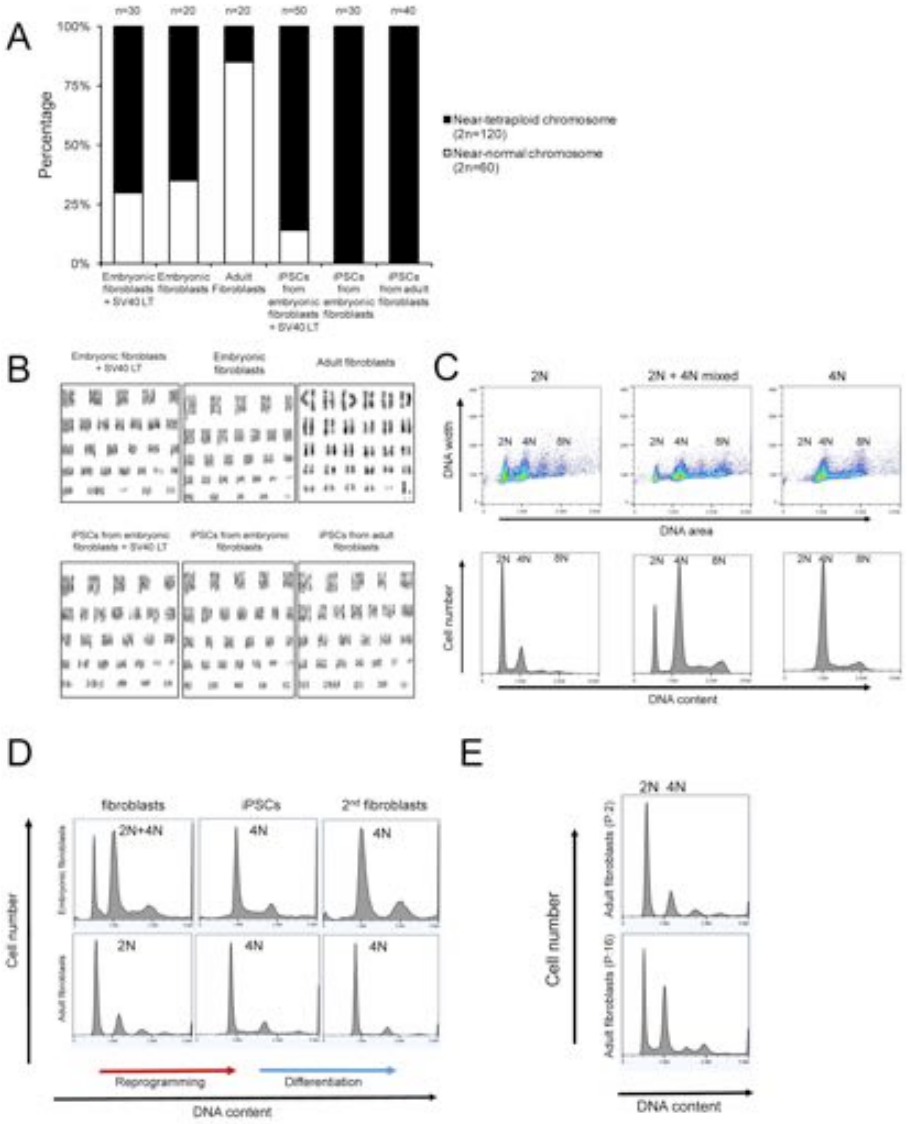

Figure 11. Propensity of NMR fibroblasts and iPSCs for a tetraploid karyotype.
(A) Percentage of diploid and tetraploid NMR fibroblasts and iPSCs based on karyotype analyses. n= number of cells with chromosome counts. 7 NMR fibroblast and 12 NMR iPSC lines were analyzed. **(B)** Karyotype analysis showing tetraploid karyotypes of NMR embryonic fibroblasts and iPSCs. Adult fibroblasts show a mostly diploid karyotype. **(C)** DNA content of NMR embryonic fibroblasts and iPSCs as analyzed by FACS. **(D)** Changes in the DNA content during reprogramming and differentiation in embryonic and adult cells. **(E)** Changes in the DNA content of NMR adult fibroblasts during long-term culture.

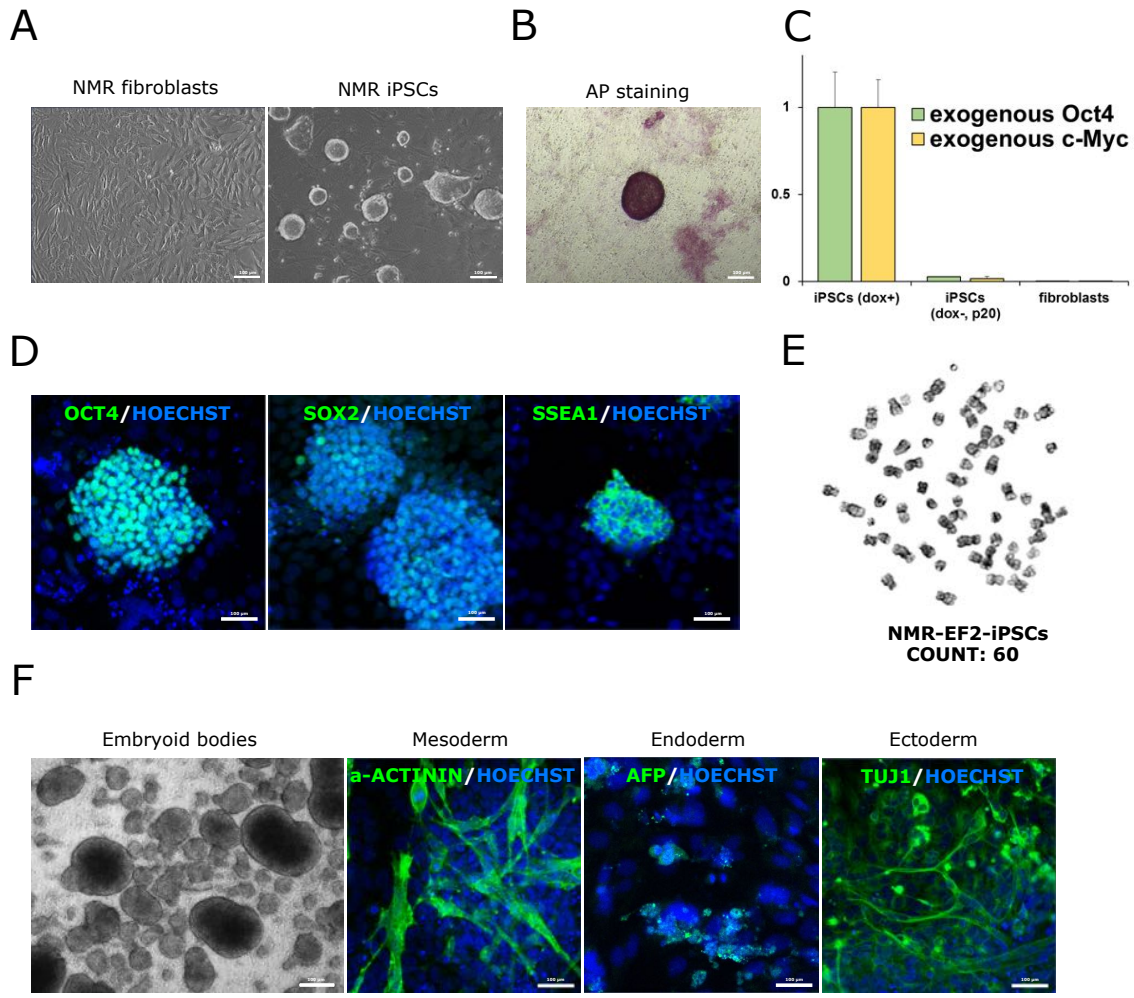

Figure 12. Generation and characterization of diploid NMR iPSCs.

(**A**) Immortalized embryonic fibroblasts (left) and derived iPSCs (right). (**B**) AP staining of primary iPS-like colonies. (**C**) Real-time PCR analysis of exogenous Oct4 and c-Myc transcripts expression in NMR iPSCs following removal of doxycycline (dox). dox+: culture with dox, dox-: culture without dox, p20: passage 20. All values are mean ± SEM from three independent experiments. Relative expression was normalized to the expression of GAPDH. **(D)** Representative images of NMR iPSCs following immunostaining for pluripotency associated transcription factors: OCT4, SOX2 and SSEA-1. (**E**) Standard G-banding karyotype analysis of diploid (2N=60) NMR iPSCs. (**F**) *In vitro* differentiation of NMR iPSCs. EB formation. Immunocytochemical analyses of EB expression: mesoderm (alpha-actinin), endoderm (AFP), and ectoderm (TUJ-1) markers. All Scale bars, 100 μm.

Contribution to chimera embryogenesis

To test for the ability of NMR iPSCs to generate interspecific chimeras in vivo, we prepared NMR iPSCs that expressed EGFP (Figure 10B) and exhibited pluripotent cell makers (Figure 13A). These cells were microinjected into embryonic day 3.5 (E3.5) blastocysts of C57BL/6 mice and allowed to develop to the E13.5 (Figure 13B). After dissection, a total 28 embryos were obtained from 2 surrogate mothers, with an equal

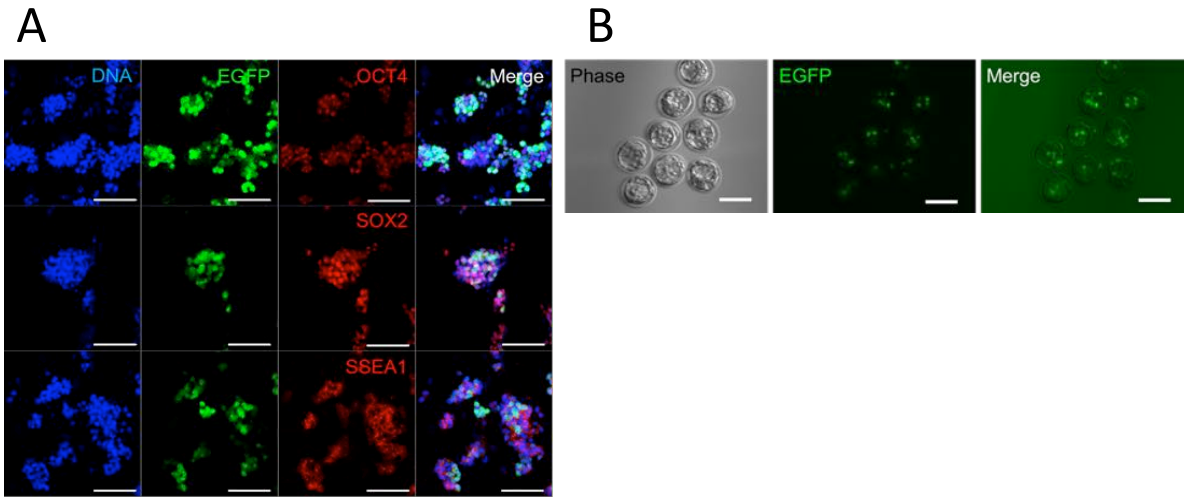

Figure 13. NMR iPSCs and blastocysts injection.
(A) Representative images of EGFP-expressing NMR iPSC colonies after immunostaining for OCT4, SOX2 and SSEA-1. Scale bars, 100 μm. **(B)** Mouse blastocyst stage embryos soon after injection of EGFP-expressing NMR iPSCs. Injected iPSCs lie in the subzonal space. Scale bars, 100 μm.

number of normal and aborted embryos (Figure 14A; upper). To confirm the interspecific chimerism of NMR iPSCs, genomic DNA extracted from normal and aborted embryos was PCR-amplified using NMR iPSCs–specific primers (Figure 14B). About a quarter of normal embryos from two surrogated mothers were confirmed to be interspecific chimera by genomic PCR (Figure 14A; bottom). Compared to a previous data in rat-mouse

interspecific chimera production (Kobayashi et al., 2010), the percentage of NMR iPSCs chimerism in mouse fetus was similar, even though there are species-specific developmental patterns of NMRs, rats and mice. Whole-mount immunostaining with anti-GFP antibodies revealed the presence of NMR iPSC-derived cells in chimeric embryos (Figure 15A and B).

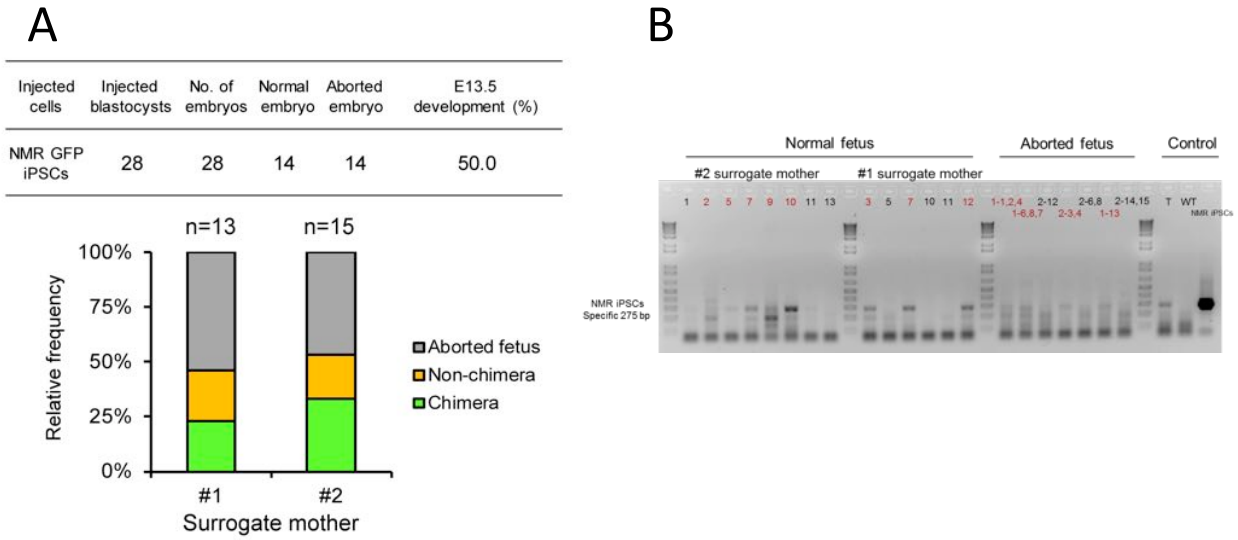

Figure 14. NMR iPSC contribution to interspecific chimera.
(A) Summary of interspecific chimera production (E13.5). Relative frequencies of aborted, non-chimeras, and chimera during embryonic development from 2 surrogated mothers (bottom panel). Data from genotyping results. **(B)** NMR contribution to the embryos (E13.5). Genomic PCR analyses of mouse embryos derived from blastocyst injection of NMR iPSC. NMR-specific primers were used for the detection of chimeric contribution from NMR iPSCs. Numbers: fetus ID; 1-2,3: No 2 and 3 abnormal embryo from #1 surrogate mother, etc.; T: kidney capsules of mice transplanted with NMR iPSCs; WT: wild type fetus. Confirmed chimera are labeled in red, and non-chimeric fetuses in black.

Aborted embryos generally showed higher integration of GFP-expressing cells (Figure 16A). Intriguingly, we found that NMR iPSC-derived cells could integrate into both placenta and normal fetus (Figure 15B), suggesting their contribution in embryonic

and extra embryonic tissues. We further examined the identity of these GFP-positive cells by immunostaining with different lineage markers such as TUJ-1 (ectoderm) and a-actinin (mesoderm) (Figure 16A). In several chimeric embryos, we found that GFP-positive cells co-expressed appropriate lineage-specific markers in aborted embryo and normal fetuses (Figure 16B and C). Together, these data suggest that NMR iPSC-derived cells could repopulate into the mouse early embryos with further differentiation and contribute to interspecific chimera.

Comparative gene expression analyses involving mouse, human and NMR iPSCs

To gain insights into similarities and differences in gene expression among mouse, human and NMR iPSCs, we performed RNA sequencing (RNA-seq) analyses on six lines of fibroblasts and their respective iPSC lines in NMR. Principle component analysis (PCA) revealed tight clustering of all iPSCs and their split from the cells of origin (Figure 17A). Next, we performed RNA-seq analyses on 4 mouse fibroblast lines and the respective iPSCs, which were generated in parallel with the NMR iPSCs. We also used published human fibroblast/iPSC dataset (Choi et al., 2015). First, we identified differentially expressed genes (DEGs) between fibroblasts and iPSCs for each species (Figure 17B), revealing elevated expression of 2,799 mouse, 1,027 NMR and 3,852 human genes in iPSCs.

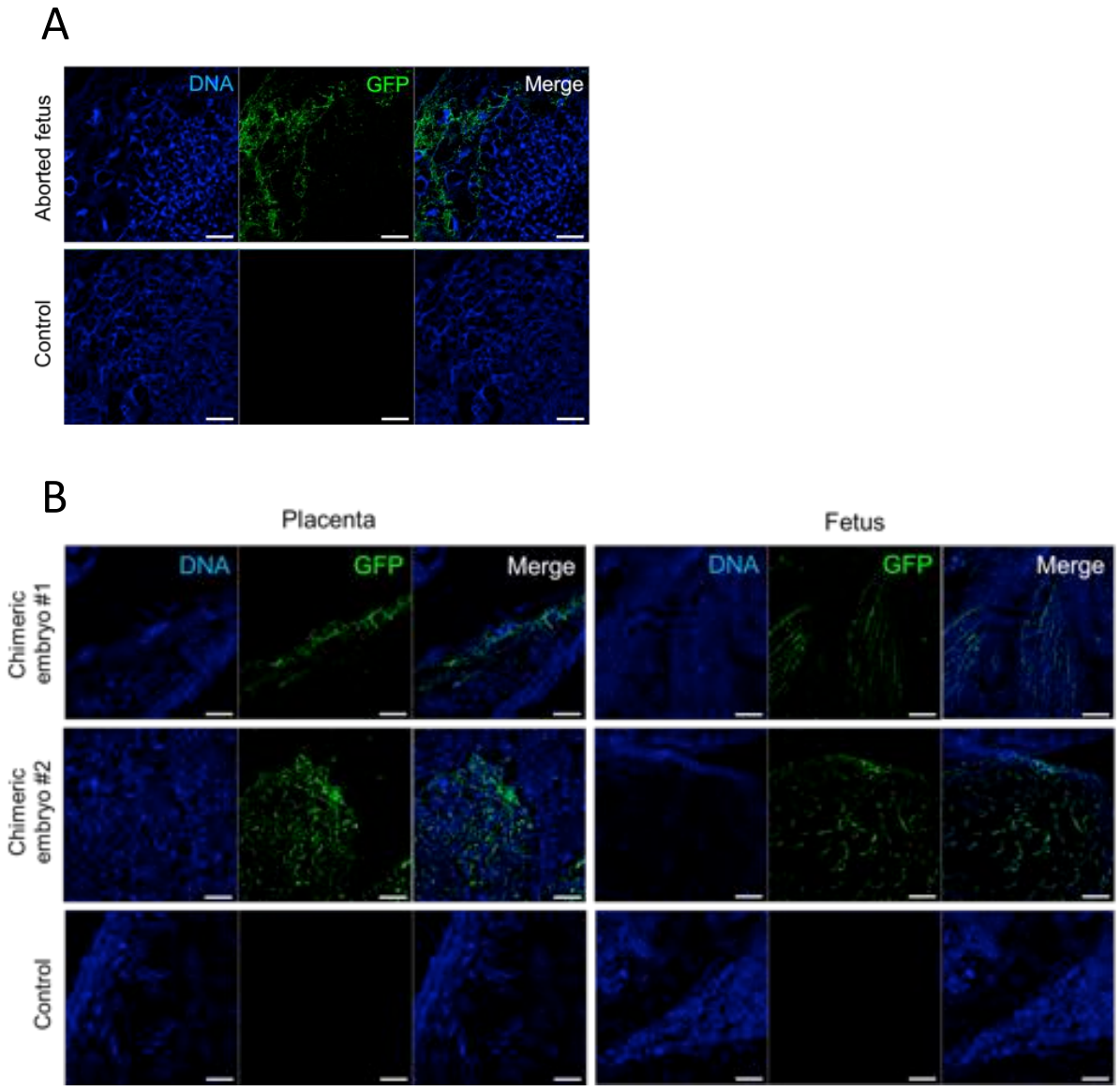

Figure 15. Detection of NMR iPSC-derived cells in E13.5 embryos.
(A) Aborted fetus was analyzed 11 days after embryo transfer into uteri of 2.5 dpc pseudopregnant mice (E13.5). Representative images show integration of NMR iPSCs into different locations in the aborted fetus body after whole-mount immunostaining with anti-GFP antibodies and confocal analysis. Controls are the samples treated only with secondary antibodies. Scale bars, 100 μm. (**B**) Representative images showing integration of NMR iPSCs into different locations in the placenta and fetus following whole-mount immunostaining with anti-GFP antibodies and confocal analysis. Controls show samples treated only with secondary antibodies. Scale bars, 100 μm.

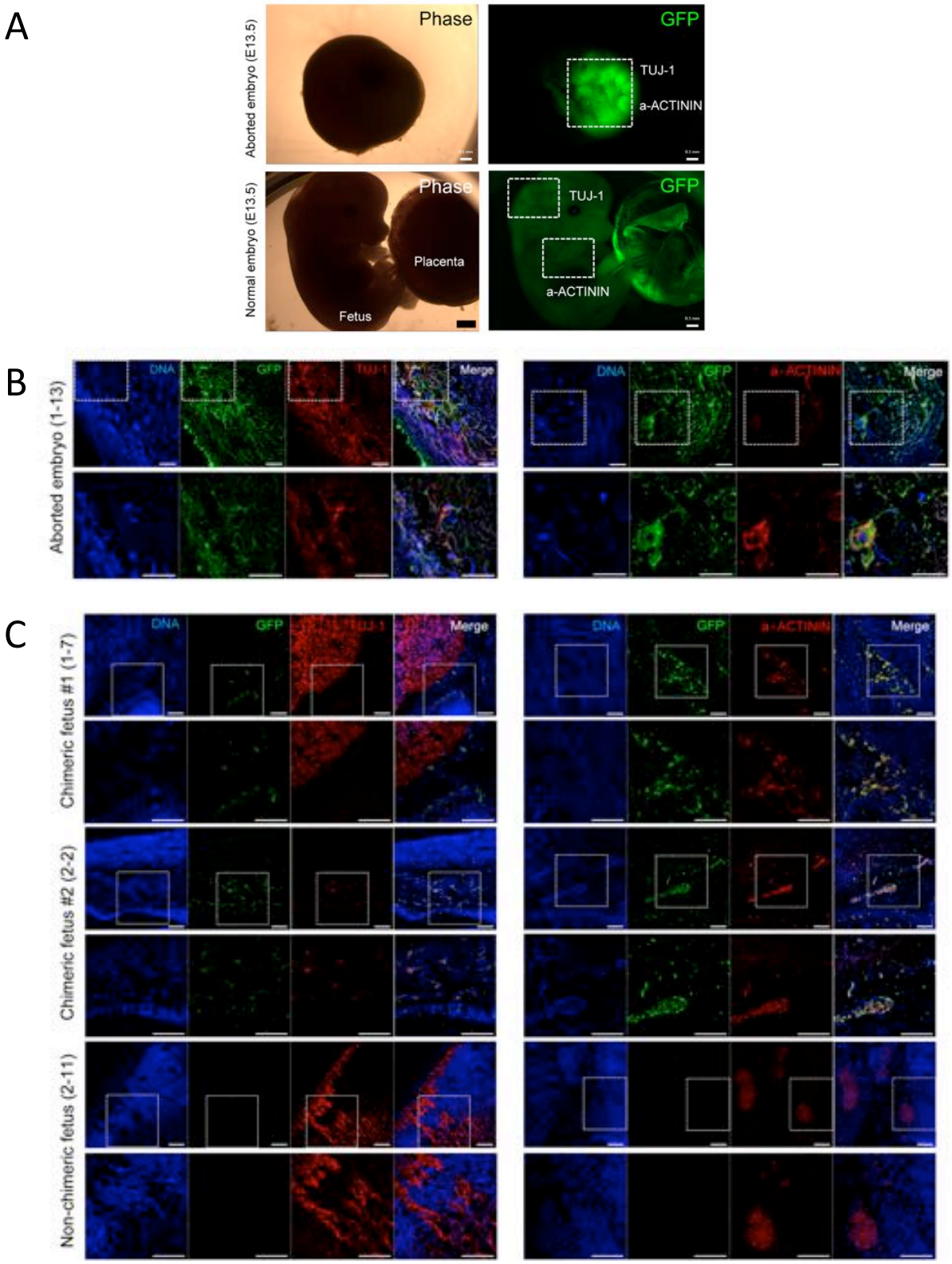
A
Aborted embryo (E13.5)
Phase
GFP
TUJ-1
a-ACTININ
Normal embryo (E13.5)
Phase
Placenta
Fetus
TUJ-1
GFP
a-ACTININ
B
Aborted embryo (1-13)
DNA
GFP
TUJ-1
Merge
DNA
GFP
a-ACTININ
Merge
C
Chimeric fetus #1 (1-7)
Chimeric fetus #2 (2-2)
Non-chimeric fetus (2-11)
DNA
GFP
Merge
DNA
GFP
a-ACTININ
Merge

Figure 16. Lineage specific development of NMR iPSC cells in E13.5 embryos.
(A) Representative images showing aborted embryo and normal embryo (E13.5). White boxes indicate the sagittal section of brain and heart regions in normal fetus (bottom panel). Scale bars, 100 μm. (**B**) Representative images showing the integration of NMR iPSCs-derived cells into mouse E13.5 aborted embryos (embryo number; 1-13 from Figure 12B). Anti-GFP antibody was co-stained with anti-TUJ1 (left panels) and anti-a-actinin (right panels) antibodies. The bottom panels are enlargements of the white boxes. Scale bars, 100 μm. (**C**) Representative images showing the integration of NMR iPSCs-derived cells into mouse E13.5 normal fetuses (embryo number; 1-7 and 2-2 from Figure 12B). Non-chimera as control (embryo number; 2-11 from Figure 12B) Anti-GFP antibody was co-stained with anti-TUJ1 (left panels) and anti-a-actinin (right panels) antibodies. The bottom panels are enlargements of the white boxes. Scale bars, 100 μm.

These corresponded to 42 GO terms in mouse, 43 in NMR and 61 in human (Figures 18-20). Interestingly, 23 GO terms overlapped between NMR and human iPSCs, which were related to cell morphogenesis, ion transport and neuronal function, whereas only 3 GO terms were common to mouse and NMR iPSCs (Figure 17C). Next, we found 151 DEGs overlapped among NMR, human and mouse iPSCs by gene symbol (Figure 17D). Except common 151 DEGs, only 91 DEGs overlapped between NMR and mouse iPSCs, whereas 218 DEGs overlapped between NMR and human iPSCs. The data suggest that the reprogramming-associated transcriptome changes in NMR cells are more like those of human cells.

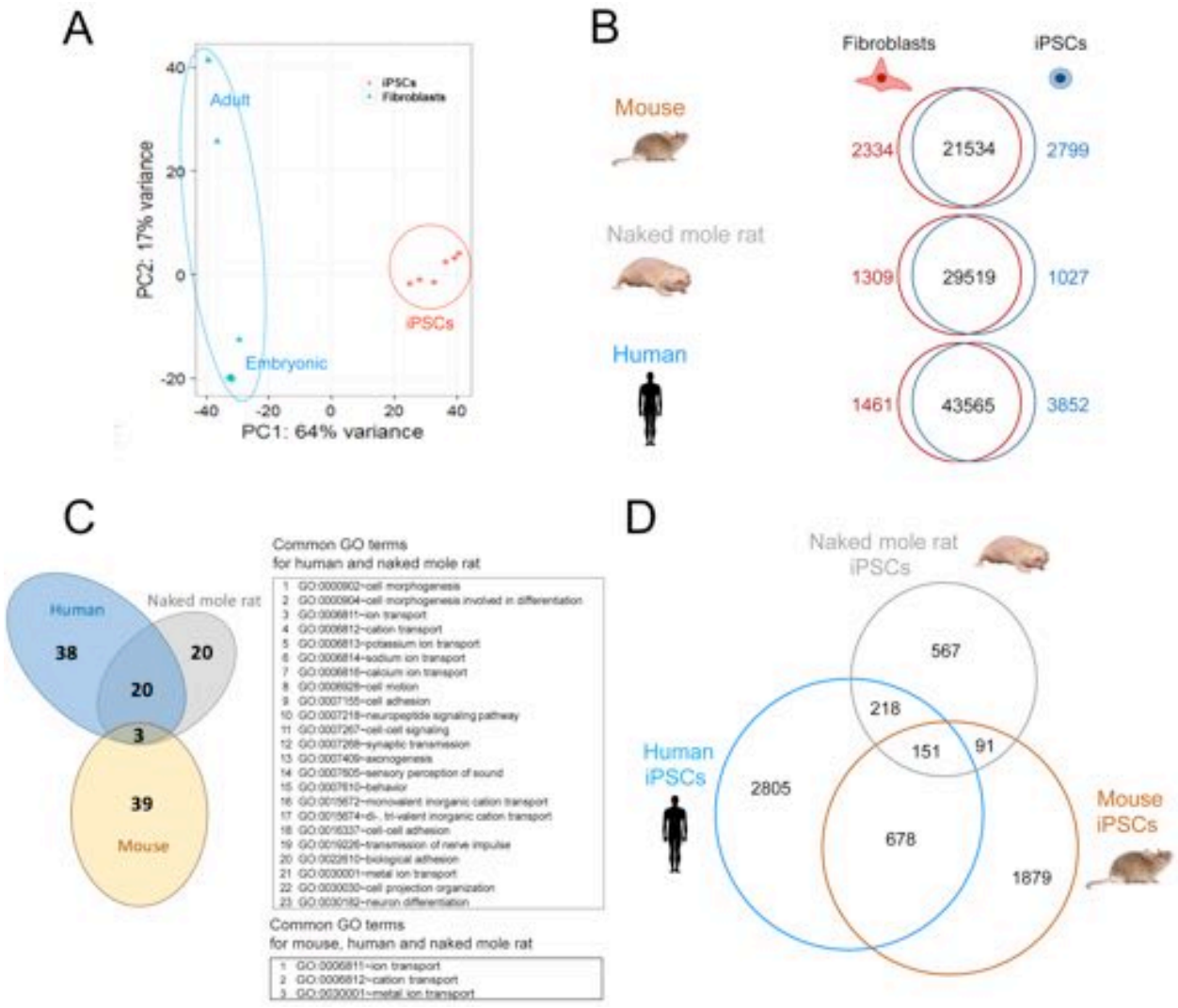

Figure 17. Gene expression analyses of mouse, NMR and human iPSCs.
(**A**) PCA of global gene expression patterns of NMR fibroblasts and iPSCs derived from them. (**B**) Venn diagrams showing pairwise comparison of gene expression. Red and blue numbers denote differentially expressed genes (FDR<0.05 and fold change>2); black numbers denote expressed genes with no significant differences between indicated samples. (**C**) Venn diagram showing common GO terms among NMR, human and mouse. The set of 23 (NMR/human) and 3 (NMR/mouse or human/mouse) GO terms is shown. See also Figures 16-18. (**D**) Venn diagrams showing unique and common differentially expressed genes among NMR, human and mouse iPSCs.

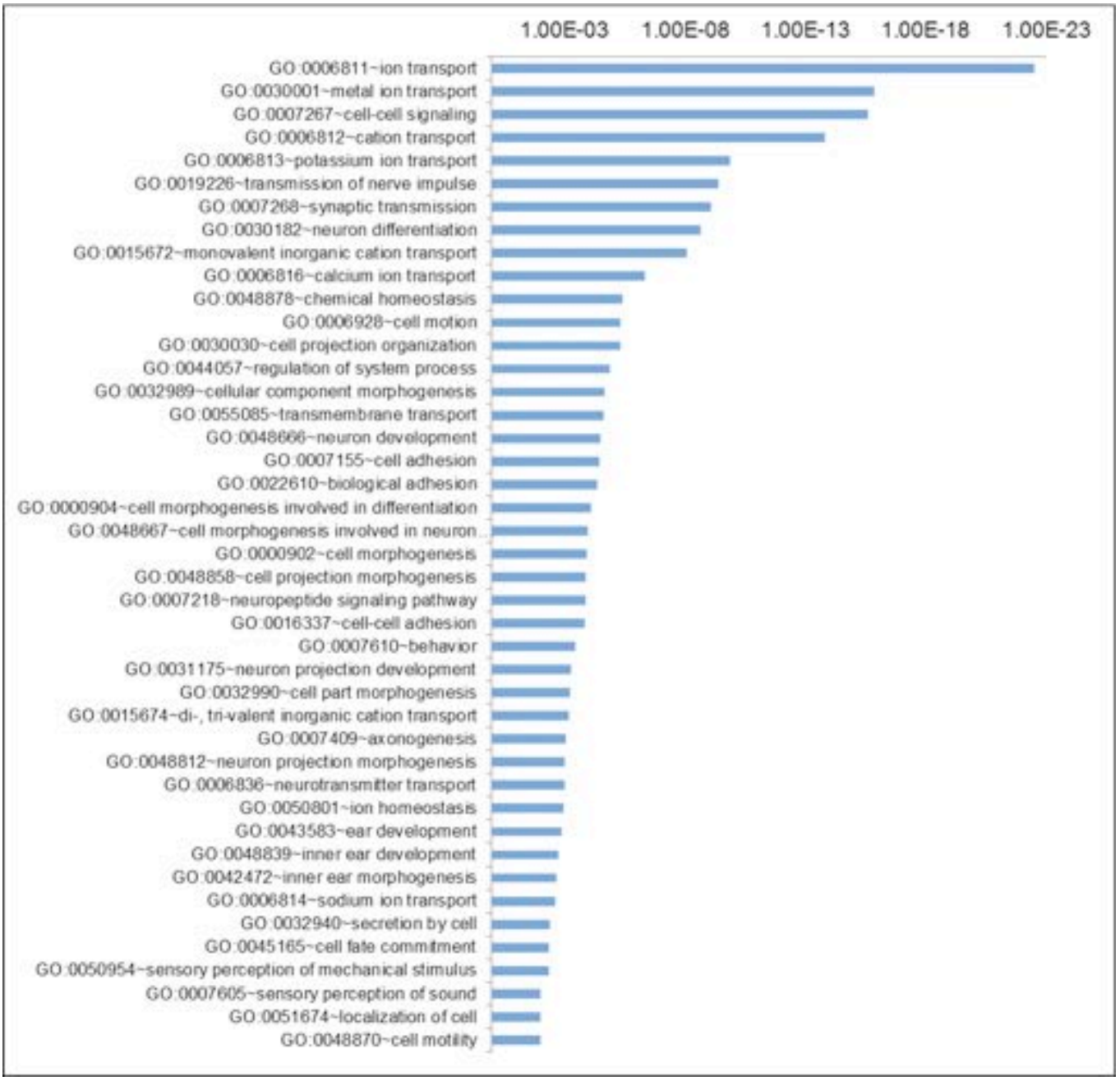

Figure 18. GO analysis of differentially expressed genes (FDR<0.05) in NMR iPSCs compared to NMR fibroblasts.

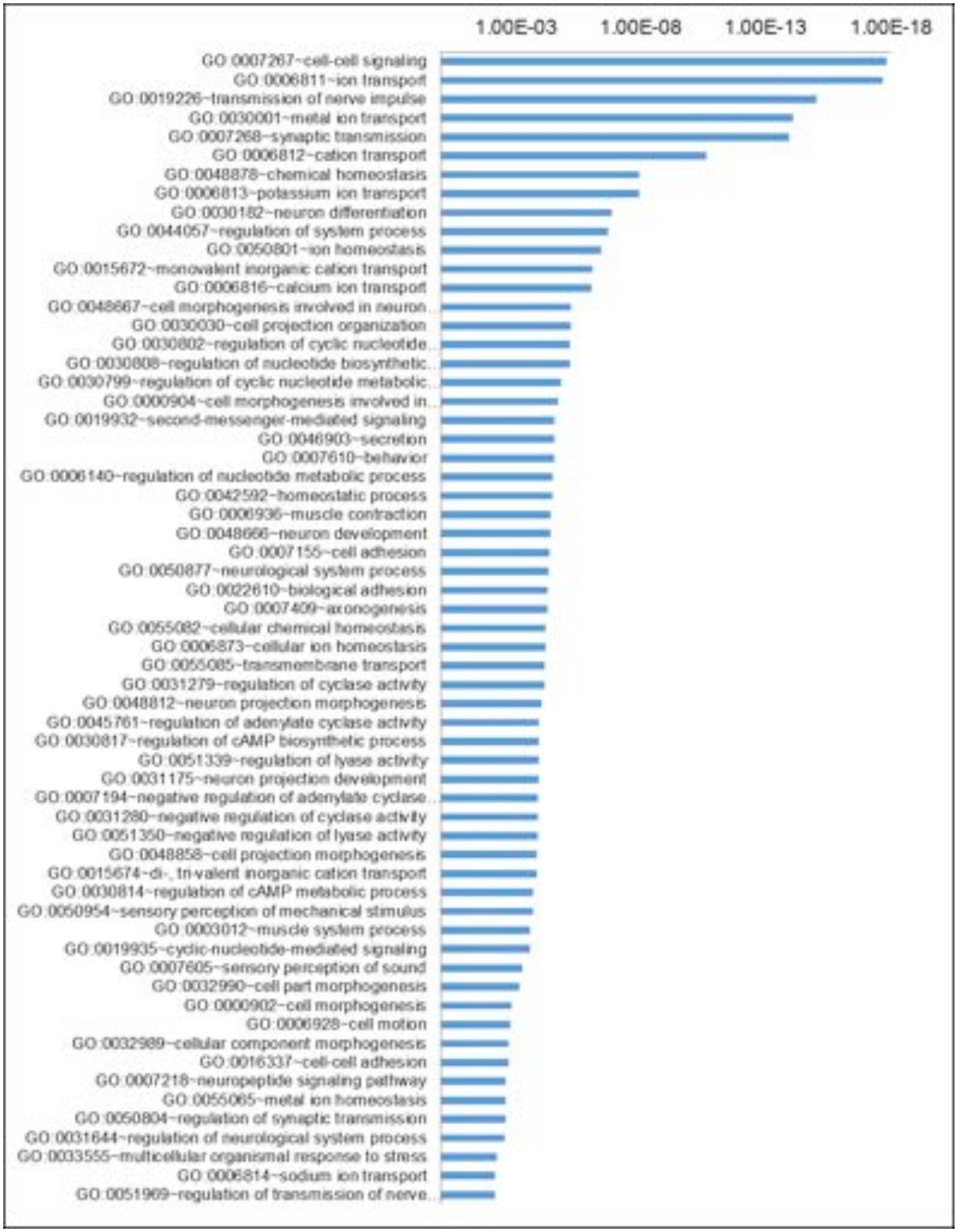

Figure 19. GO analysis of differentially expressed genes (FDR<0.05) in human iPSCs compared to human fibroblasts.

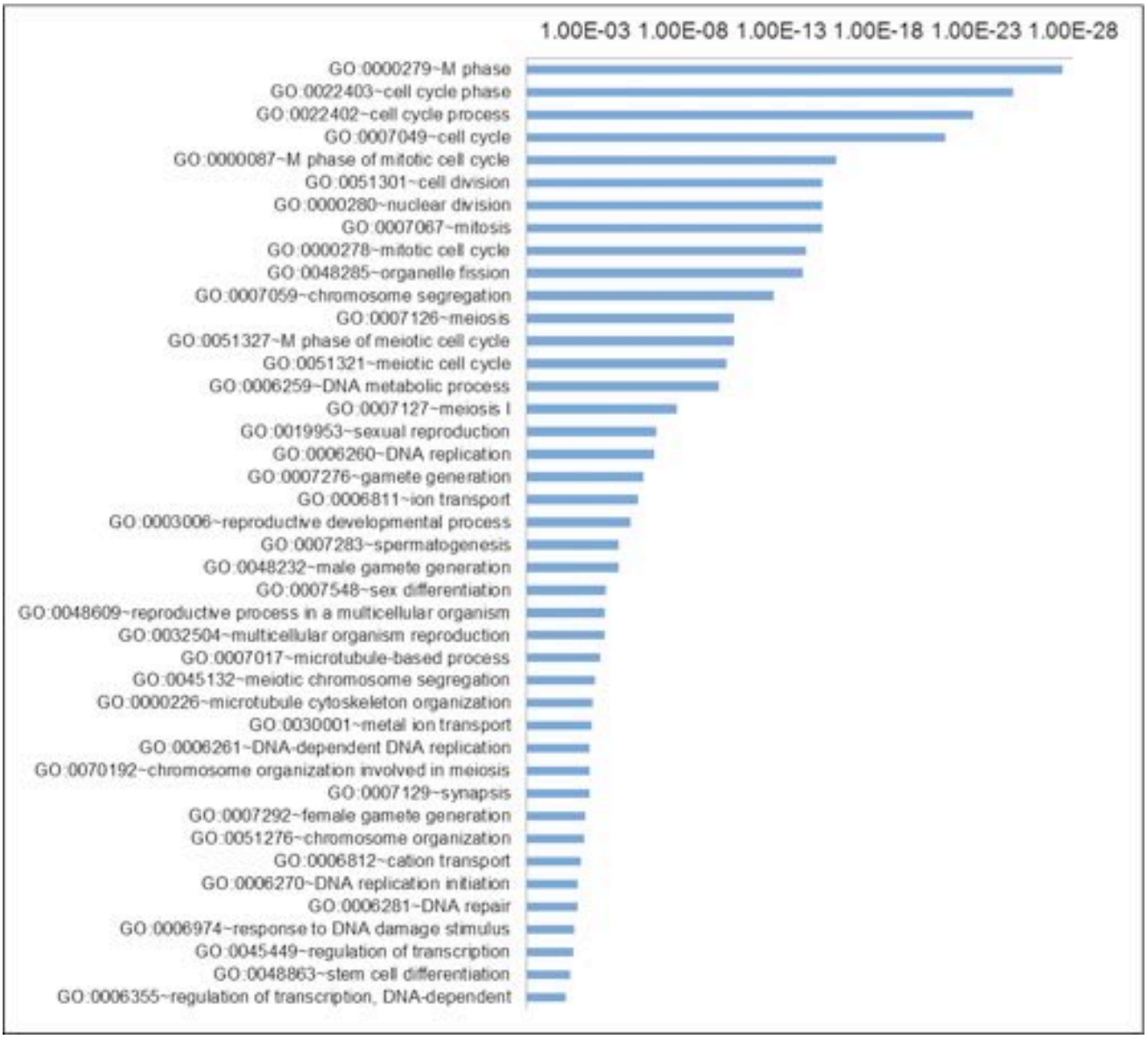

Figure 20. GO analysis of differentially expressed genes (FDR<0.05) in mouse iPSCs compared to mouse fibroblasts.

Discussion

We reported the development and characterization of NMR iPSCs and describe protocols for robust preparation of these cells. The NMR is a mouse-sized rodent, but viable NMR iPSCs could not be generated by employing a conventional system that supports mouse iPSCs derivation. Although we observed altered expression of reprogramming-associated genes (Ecad, Esrrb, Utf1 and Sox2) and detected OCT4-expressing cells, this procedure did not lead to reprogramming. However, further analyses revealed the importance of N2B27 medium for NMR iPSC derivation. We also found that LIF+2i conditions, which activate LIF/STAT3 and Wnt/β-catenin signaling, inhibit FGF/MEK, and support naıve PSCs across species (Ye et al., 2014), was necessary and sufficient for inducing and maintaining naive pluripotency in NMR cells. Also, N2B27-3i was superior to N2B27-2i, highlighting positive influence of the ALK5 inhibitor A83-01, as previously reported for rat iPSCs (Li et al., 2009). In addition, we examined appropriate conditions for feeder-free monolayer culture and found that NMR iPSCs grown on matrigel maintained AP expression. This finding opens opportunities for feeder-free iPSC culture, transfection and cell differentiation without EB formation. We further found that the expression of SV40 Large T accelerated reprogramming of NMR iPSCs. Although this factor did not seem to alter the reprogramming efficiency (0.17% vs. 0.24%), the reprogramming time was significantly reduced (16 days vs 30 days).

The resulting iPSCs could be maintained for prolonged periods of time, with no notable difference in morphology after 30 passages. These cells expressed typical markers of pluripotency and differentiated into all three germ layers. On the other hand, some phenotypes of the NMR iPSCs were different from those of iPSCs from other species. For example, we found that NMR iPSCs were resistant to forming teratomas when injected into the mouse renal tubule, instead forming nerves, consistent with tumor resistance from early development stages. It is interesting that NMR iPSCs may be able to differentiate in vivo without forming tumors. It is an attractive possibility that these approaches may lead to the development of tumor-free iPSCs for therapeutic applications. Besides, NMR iPSCs showed a propensity for tetraploidy, which was observed in various culture models and was more prevalent in embryonic cells. Although tetraploidy may be associated with abnormality in cells, in the NMR this phenotype appeared regardless of cells and conditions used. Inappropriate tetraploidization is a frequent event in early stages of cancer development (Davoli and de Lange, 2011). However, despite a high percent of tetraploid cells, NMR iPSCs contributed to interspecific chimera and did not give rise to teratoma. In the mouse, TESCs (tetraploid embryonic stem cells) possess essential pluripotency, differentiation potency to form teratomas and show contribution to the inner cell masses in aggregated chimeric blastocysts (Imai et al., 2015). Besides, the viable tetraploid mammal Tympanoctomys barrerae (Octodontidae) displays genomic imprinting and X chromosome inactivation, which is partially conserved in the tetraploid genome (Bacquet et al., 2008). Future comprehensive epigenetic or genomic analyses are necessary to elucidate these

characteristics of embryonic fibroblasts and iPSCs in NMR. These characteristics may be related to known NMR phenotypes, e.g. early contact inhibition and resistance to cancer.

When our study was prepared for publication, another group reported the development of NMR iPSCs (Miyawaki et al., 2016). They also found resistance to teratoma formation and attributed this feature to elevated ARF expression. We used a different procedure to derive iPSCs and found that they could be generated at low oxygen and with a higher (~30 fold) efficiency of reprogramming in the case of adult fibroblasts. Most importantly, we demonstrated chimeric contribution of NMR iPSCs for robust evidence of pluripotency. The availability of different iPSC reagents, especially since they differ in their characteristics, should be of great benefit to the research community.

The teratoma phenotype of our iPSCs prompted us to examine the ability of NMR iPSCs to contribute to embryonic development of mice. Interspecific chimera were generated several years ago using mouse blastocysts injected with rat iPSCs and rat blastocysts injected with mouse iPSCs (Kobayashi et al., 2010). Both mouse and rat iPSCs could contribute to various cell types of the embryos and adult animals (Kobayashi et al., 2010). More recently, chimera models were developed involving rhesus monkey and human cells (Fang et al., 2014; Mascetti et al., 2016). We found that NMR iPSCs could contribute to embryonic development when injected into mouse blastocysts, followed by implantation. Although NMRs are characterized by slower development (~70 days gestation period) compared to mouse (19-21 days), apparently, NMR cells could divide and differentiate within mouse embryos, at least until E13.5. They were also

detected in the placenta and contributed to fetus through different lineages such as ectoderm (TUJ-1) and mesoderm (a-actinin). To produce interspecific chimera, genetic diversification and evolutionary distance should be considered as they form a 'xenobarrier' (Wu et al. 2016). Interestingly, the chimeric contribution of NMR cells to the mouse embryo was successful despite the great evolutionary distance (70 million years ago). Analysis of chimeric embryos suggested a possibility of naïve pluripotency of the NMR iPSCs and an opportunity of production of fully developed interspecific chimera between mouse and NMR.

We also examined gene expression changes associated with reprogramming of NMR cells, and these were more similar to those of human than mouse iPSCs. Interestingly, despite the fact that the ancestor of mouse and NMR diverged from the ancestor of humans about 93 million years ago, NMR iPSCs share more common GO terms with human iPSCs rather than with mouse iPSCs. Although NMR is a rodent, NMRs and humans are characterized by extended lifespans and longer gestation periods, especially compared to what would is expected based on their body sizes.

Our study highlights potential uses of the developed NMR iPSCs for various types of biomedical applications. We showed that they could differentiate into various cell types, be implanted into embryos, and be manipulated genetically despite their propensity for tetraploidy. Previously, studies involving NMRs were limited to the analyses of live animals and tissue samples. Very few cell culture studies have been performed, and they were limited to adult fibroblasts. In addition, no cell lines have been reported for NMR, precluding characterization of the remarkable phenotypes associated

with this animal. With the development of NMR iPSCs, some of the major hurdles in NMR research may be overcome, accelerating studies on the phenotypes of these extraordinary animals.

Materials and methods

Animal ethics

The animal welfare, use, and care were carried out according to the protocols approved by the Institutional Animal Care and Use Committee (IACUC) of the Brigham and Women's Hospital, Harvard University and University of Illinois-Chicago.

Isolation and culture of embryonic and adult fibroblasts

NMRs used in this work were from the facility at University of Illinois in Chicago. The NMR embryos were harvested at the early stage of fetogenesis, ~45 days post-coitum. Each fetus was harvested and dissected, voided of internal organs and brain, and the remaining part was washed in sterile PBS to remove remaining blood. Each fetus was teased into fine pieces in 5 ml of 0.25% trypsin-EDTA solution, transferred into a 15 ml tube, and digested overnight at 4 °C. DMEM with 20% fetal bovine serum (FBS) was added to inactivate trypsin and tissues were pipetted vigorously and repeatedly to break up the digested tissues into a cell suspension. The cells were plated onto cell culture plates and incubated in a humidified incubator at 32 °C with 3% O2 and 5% CO2 atmosphere. Adherent cells were NMR embryonic fibroblasts. Adult fibroblasts were established from kidney, testis and skin of a 1-year-old male. Mouse embryonic and adult fibroblasts were from mouse fetus (E13.5) and lung of a 10-week-old C57BL/6 male, respectively. Both NMR and mouse fibroblasts were maintained in DMEM (DMEM high glucose + Glutamax) with 10% (mouse) and 15% (NMR) FBS, 1X

antibiotic/antimycotic, 1X non-essential amino acids, 0.1 mM β-mercaptoethanol. All NMR cells were cultured at 32 °C or 37 °C, 3% O2 and 5% CO2, while mouse cells were at 37 °C and 5% CO2. NMR fibroblasts used in this study are listed in Table 1.

Lentiviral and retroviral production and infection

To produce infectious lentiviral particles, HEK293T cells cultured on 10 cm dishes were transfected with the vectors 4F2A (mouse OSKM: tetO-FUW-OSKM; human OSKM: FUW-tetO-hOCT4, FUW-tetO- hSOX2, FUW-tetO-hKlf4, FUW-tetO-hMYC) and M2rtTA (Addgene plasmids #20321, #20726, #20724, #20723, #20725 and # 20342, respectively) together or pWPI (EGFP; Addgene plasmid # 12254) with packaging plasmids VSV-G and 8.91 (gag/pol). These plasmids were introduced into HEK293 LTV cells using the calcium phosphate precipitation method. Medium was replaced 12 h following transfection, and after an additional 48 and 72 h, supernatants containing viral particles were harvested and filtered through a 0.45 μm cellulose acetate filter. EGFP alone or equal volumes of mOSKM or hOSKM and M2rtTA lentiviral supernatants were mixed, supplemented with polybrene at the final concentration of 6 μg/ml and directly used for transduction of mouse and NMR fibroblasts. To establish immortalized embryonic fibroblasts, retrovirus was produced using plasmids derived from pBabe-puro vector in combination with the standard GAG-Pol and VSV-G vectors. The diluted viral medium was overlaid onto early stage (passage <3) of NMR primary fibroblasts and infected cells were enriched by selection with puromycin.

Reprogramming of mouse and NMR fibroblasts to iPSCs

After 1 day of lentiviral transduction, approximately 100,000 infected fibroblasts were seeded per well of 6-well plate. Three different culture conditions were used to test the ability of cells to reprogram. First, lentiviral infected mouse and NMR fibroblasts were grown onto mitomycin C inactivated or gamma-irradiated MEF feeder cells in ESC medium in the presence of 2 μg/ml doxycycline (DMEM supplemented with 15% FBS, 1000 units/ml mouse leukemia inhibitory factor or 10 ng/ml basic fibroblast growth factor, 0.1 mM β-mercaptoethanol, 1% nonessential amino acids, 2 mM glutamine and 1% antibiotic/antimycotic). The other conditions also represented the culture of infected fibroblasts grown on MEF feeder cells or Matrigel matrix, but we used N2/B27+2i medium (1:1 mixture of N2 medium (DMEM/F12 supplemented with 1x N2, 1% antibiotic/antimycotic, 0.005% BSA, 0.1 mM β-mercaptoethanol, 1% nonessential amino acids) and B27 medium (Neurobasal medium supplemented with 1x B27 (without retinoic acid), 1% antibiotic/antimycotic, 2 mM L-glutamine, 0.1 mM β-mercaptoethanol, 0.005% BSA, 1% nonessential amino acids) supplemented with 1000 U/ml mLIF, 3 μM GSK3b inhibitor (CHIR99021) and 1 μM MEK1/2 inhibitor (PD0325901). In each of two culture conditions, growth media were replaced every 24 h.

Establishment and maintenance of mouse and NMR iPSCs

ES-like colonies were observed and picked after culturing cells in N2/B27 2i medium both in feeder and feeder-free conditions. Isolated colonies were digested in

0.05% trypsin and passaged on gelatin-coated 6-well plates onto MEF feeder cells. NMR iPSCs were maintained in N2/B27 + mLIF 2i or 3i (additional 0.5 μM inhibitor ALK5; A83-01) media and were routinely subcultured every 6-7 days. In mouse, iPSC colonies were picked on day 10, dissociated by 0.05% trypsin digestion, and plated into new 6-well dishes onto mitomycin C inactivated or irradiated MEF feeder cells. Mouse iPSCs were subcultured every 2–3 days and were maintained in ESC culture medium in the presence of 1000 U/ml mLIF. Doxycycline was removed from the culture medium after passage 5. NMR iPSCs using in this study are listed in Table 1.

Alkaline phosphatase staining and immunofluorescence

AP staining was performed using the Alkaline Phosphatase Staining Kit (Stemgent) according to manufacturer's instructions. For fluorescence immunocytochemistry, iPSCs were cultured on mitotically inactivated MEFs for 2–3 days in the case of mouse iPSCs and for 6-7 days in the case of NMR iPSCs, and fixed using PBS containing 4% PFA (Sigma) for 15 min at room temperature. After rinsing with PBS, fixed cells were blocked and permeabilized for 1 h in PBS containing 10% (v/v) goat serum (Sigma) in 0.1% Triton X-100-PBS. Primary antibodies were as follows: OCT4 (Santa Cruz Biotech), SOX2 (Millipore), NANOG (Millipore) and SSEA-1 (Santa Cruz Biotech), which were diluted 1:200 in blocking solution. Fixed cells were incubated with primary antibody overnight at 4 °C. After washing out the unbound antibodies, fixed cells were incubated with secondary antibodies (labeled with Alexa-488, 1:200 dilution, Jackson ImmunoResearch) for 1 h at room temperature. Nuclei were counterstained using

1 μg/ml Hoechst 33342 (Life Technologies). All fluorescence imaging was conducted using an LSM 700 confocal microscope (Zeiss).

In vitro differentiation and immunofluorescence

Colonies growing on MEFs were detached using 0.05% trypsin and grown as a suspension culture on low adherent plates using ESC medium without dox and LIF. After 1 week of suspension growth, cells were transferred to 12- or 24-well plates coated with 0.1% gelatin and grown in DMEM supplemented with 20% FBS. EBs were grown for 1–2 weeks prior to fixation and immunofluorescence staining. Cultures were fixed and stained as described above using the following antibodies: AFP (1:200, Santa Cruz Biotech), GATA4 (1:200, Santa Cruz Biotech), OCT4 (1:200, Santa Cruz Biotech), α-actinin (1:200, Sigma), GFAP (1:500, Dako), and TUJ-1(1:500, Covance).

Teratoma formation

NMR iPSCs or EGFP expressed iPSCs grown on matrigel were collected by 0.05% trypsin treatment and injected under the kidney capsules into NOD–SCID (NOD.CB17-Prkdc/J) mice. The kidney capsules were collected 10 weeks after the injection and processed for paraffin embedding and hematoxylin and eosin staining or immunofluorescence co-staining with primary polyclonal antibodies against GFP (chicken IgY; Invitrogen) and TUJ-1(1:500, Covance). Secondary antibodies were Alexa488-conjugated anti-chicken IgY (Invitrogen) and Alexa Fluor 647 anti-rabbit IgG (1:200 dilution, Jackson ImmunoResearch). Genomic DNA of kidney capsules was

extracted using DNeasy Blood & Tissue Kit (Qiagen). PCR with GoTaq polymerase using specific primers to M2rtTA lentiviral vector was performed to confirm the origin of NMR iPSCs in the kidney capsules.

Karyotype analysis

Karyotyping was performed at the Cytogenetics Core Laboratory in Brigham and Women's Hospital using standard protocols for chromosomal G-banding.

Flow Cytometry

Flow cytometry for DNA content was performed by fixing cells in ethanol and staining with propidium iodide (PI). Cells were analyzed on the 585/42 channel with a BD Accuri C6 Analyzer (BD Biosciences).

RT-PCR and real-time PCR analysis

To perform qPCR, total RNA from individual samples was extracted using TRIzol® reagent (Invitrogen, MA) according to the manufacturer's instructions. Complementary DNA was synthesized using a High-capacity RNA-to-cDNA Kit (Applied Biosystems, CA). PCR primers are listed in Table 2. Relative gene expression was calculated by normalizing the threshold cycle (Ct) values of each gene to that of the GAPDH via the Δ–Ct method (Livak and Schmittgen, 2011).

Interspecific chimera production

To generate chimeric mouse embryos containing NMR iPSCs, C57BL/6-derived blastocysts injected with EGFP-expressed NMR iPSCs were transplanted into the uteri of foster mothers (ICR; CD1 mouse). The generated chimera features were analyzed at E13.5. They were fixed with 4% paraformaldehyde, embedded for frozen sectioning in O.C.T. compound, and co-immunostained with primary polyclonal antibodies against GFP (chicken IgY; Invitrogen) and TUJ-1(1:500, Covance) or a-actinin (1:200, Sigma). Secondary antibodies were Alexa488-conjugated anti-chicken IgY (Invitrogen) and Alexa Fluor 647 anti-rabbit or -mouse IgG (1:200 dilution, Jackson ImmunoResearch). Genomic DNA of chimeric mouse embryos was extracted using DNeasy Blood & Tissue Kit (Qiagen). PCR with GoTaq polymerase using same primers as in teratoma formation section was performed to confirm the origin of NMR iPSCs in the embryos.

RNA-seq and data analysis

Total RNA was extracted from mouse and NMR samples using RNeasy plus kit (Qiagen). Short-insert paired-end libraries were prepared using the Illumina TruSeq Sample Preparation Kit v2, and sequenced bi-directionally (101 bp in each direction) on Illumina HiSeq 2000 (Illumina, San Diego, CA). Mus musculus (GRCm38) and Heterocephalus glaber (hetGla2) reference genomes and annotation files were from NCBI. Differential gene expression analysis for RNA-seq data was performed as follows: FastQC package (version 0.11.4) was used for quality control, raw data were trimmed using Trim_Galore (version 0.4.0) and aligned to reference genome using TopHat2

(version 2.0.9); Bowtie 2.1.0.0 was used for aligning reads to genes. Transcripts were assembled using Cufflinks, and feature counts performed using a Python package HTseq. Generated simple count matrix was used for follow-up analysis based on EdgeR and DESeq. Raw sequencing data for 20 biological samples have been deposited into the Short Read Archive database under accession number SRP116326. Human fibroblast and iPSC datasets were from GSE36552 (Choi et al., 2015).

Statistical analysis

Statistical analyses were performed using a two-tailed t-test (*t-test, $P < 0.05$; **t-test, $P < 0.001$). Values are shown as the mean ± standard error of mean (s.e.m.) of multiple independent experiments, not technical replicates.

Table 1. NMR fibroblasts and iPSCs used in this study.

NMR Fibroblasts

No.	Cell line	Origin	SV40 large T	Sex	Karyotyping	No. of iPSCs Clones
1	ef1	Embryonic fibroblasts	O	female	diploid + tetraploid	11
2	ef2	Embryonic fibroblasts	O	Male	diploid	19
3	ef5	Embryonic fibroblasts	O	female	diploid + tetraploid	14
4	eLung	Embryonic fibroblasts from lung	×	Male	diploid + tetraploid	13
5	ef5N	Embryonic fibroblasts	×	female	diploid + tetraploid	5
6	K1	Adult fibroblasts from kidney	×	Male	diploid	8
7	K2	Adult fibroblasts from kidney	×	Male	diploid	3
8	Skin	Adult fibroblasts from skin	×	Male	n.a	3
9	Testis	Adult fibroblasts from testis	×	Male	n.a	3

n.a = not applicable

NMR iPSCs

No.	Cell line	Origin	Pluripotency Test	Differentiation Test	Karyotyping	Teratoma assay	RNA-seq
1	1-4	ef1	AP, ICA	EB	tetraploid	n.a	n.a
2	1-5	ef1	AP, ICA, i-1 (RT-PCR),	EB, ICA, EBi-1 (RT PCR)	tetraploid	n.a	O
3	2-6	ef2	AP, ICA	EB	tetraploid	n.a	n.a
4	2-8	ef2	AP, ICA ,i-2 (RT-PCR),	EB, ICA, EBi-2 (RT PCR)	diploid	O	n.a
5	5-2	ef5	AP, ICA	EB	tetraploid	O	n.a
6	5-7	ef5	AP, ICA	EB	tetraploid	n.a	O
7	L-2	eLung	AP, ICA, e-1 (RT PCR)	EB, ICA, EBe-1 (RT PCR)	tetraploid	O	O
8	L-4	eLung	AP, ICA	EB	tetraploid	n.a	n.a
9	5-CN	ef5N	AP, ICA, e-2 (RT PCR)	EB, ICA, EBe-2 (RT PCR)	tetraploid	O	O
10	K1-6	K1	AP, ICA	EB	tetraploid	n.a	n.a
11	K1-8	K1	AP, ICA ,a-1 (RT PCR)	EB, ICA, EBa-1 (RT PCR)	tetraploid	O	O
12	K2-1	K2	AP, ICA ,a-2 (RT PCR)	EB, ICA, EBa-2 (RT PCR)	tetraploid	O	O
13	K2-2	K2	AP, ICA	EB	tetraploid	n.a	n.a
14	SK1-1	Skin	AP, ICA	EB, ICA	tetraploid	n.a	n.a
15	Testis1-1	Testis	AP, ICA	EB, ICA	tetraploid	n.a	n.a

AP = Alkaline phosphatase positive
ICA = Immunocytochemical analysis (Oct4,Sox2 and SSEA1)
EB = Embryobody formation
n.a = not applicable

Table 2. Primer sequences used in this study.

Gene name	Forward (F) or reverse (R)	5'-3'	Used
Snail	F	CCAACCTACGTGCTCACCTG	qRT-PCR for *Snail* : reprogramming
	R	ACTCTTGGTGTTTGTGGAGCA	
Tgfb1	F	CGCTTCTGCTACCGCTACTG	qRT-PCR for *Tgbf1* : reprogramming
	R	GCGAGCCGTAATTTGGACAG	
Ecad	F	GGTGCTCTTCCAGGAACCTC	qRT-PCR for *Ecad* : reprogramming
*(*E-cadherin*)*	R	TGGCTGTGAGGCAATGTAGG	
Esrrb	F	AAGCACATCCCAGGCTTCTC	qRT-PCR for *Esrrb* : reprogramming
	R	CAGCTTGTCATCGTAGGGCA	
Utf1	F	TCTCGGGAGTCCAGCTACC	qRT-PCR for *Utf1*: reprogramming
	R	AGCAGCAATTCCGTCTCCC	RT-PCR for *Utf1* : pluripotency
Endo-Sox2	F	CATGTCCCAGCACTACCAGG	qRT-PCR for *Sox2* : reprogramming
	R	TTTCTGCCTCTCCTCGTTCG	RT-PCR for *Sox2* : pluripotency
Gapdh-1	F	AGGTCGGAGTGAACGGATTTG	qRT-PCR for control : reprogramming
	R	CCGTGGGTGGAGTCATACTG	
Nanog	F	AAGTACCTCAGCCTGCAGCAGATGC	RT-PCR for *Nanog* : pluripotency
	R	TTTTCTGCCACCGCTTACATTTCAT	Miyawaki et al (2016)
Fgf4	F	CGTGAGCATCTTTGGAGTGGCCAGC	RT-PCR for *Fgf4* : pluripotency
	R	CAGCCTGGGGAGAAAGTGGGTGAC	Miyawaki et al (2016)
Zfp42 (Rex-1)	F	CCACGGACATCTCCCCTTAC	RT-PCR for *Zfp42* : pluripotency
	R	TGGTAGTTGAATGCGGCTGG	
Tert	F	CCTGCTCAAGCTGGGTCATCACCGTG	RT-PCR for *Tert* : pluripotency
	R	TCAGTCCAGGATGGTCTTGAAGT	Miyawaki et al (2016)
β-Actin	F	ACAACGGCTCCGGCATGTGCAA	RT-PCR for *β-Actin* : pluripotency
	R	CATTGTAGAAGGTGTGGTGCCAGA	Miyawaki et al (2016)
Sox17	F	GAAGGTGAAGGGCGAGGT	RT-PCR for *Sox17* : differentiation
	R	TGCGCGTAGCTGTAGTTG	
Gata4	F	ACACCCCAACCTAGCAGACA	RT-PCR for *Gata-4* : differentiation
	R	CTGACGGGAGATGTGTAGCC	
Pdx1	F	CCACGGACATCTCCCCTTAC	RT-PCR for *Pdx1* : differentiation
	R	TGGTAGTTGAATGCGGCTGG	
Acta2	F	GGGATGGAATCTGCTGGCAT	RT-PCR for *Acta2* : differentiation
	R	GCGGTGGACAATAGAGGGTC	
Actc1	F	TACCACCGCTGAACGTGAAA	RT-PCR for *Actc1* : differentiation
	R	ATTTGCGGTGGACGATGGAT	
Kdr	F	CTGCACAGCATTTGGGAACC	RT-PCR for *Kdr* : differentiation
	R	GTTCATCCAGGGGCAGTTCA	

Gene name	Forward (F) or reverse (R)	5'-3'	Used
Sox1	F	GAAGGAGCACCCGGACTACA	RT-PCR for *Sox1* : differentiation
	R	GCCCTGTGAGTTGGAGATGGG	
Pax6	F	GAATTCTGCAGGTGTCCAACGG	RT-PCR for *Pax6* : differentiation
	R	TCCTCAGCTTCTCCTCTCGT	
Nes (Nestin)	F	GGCTACGGACCACTGAAAA	RT-PCR for *Nes* : differentiation
	R	CATCCTGGGCTCTGACCTCT	
Gapdh-2	F	AGGTCGGAGTGAACGGATTTG	RT-PCR for *Gapdh* : differentiation
	R	CCGTGGGTGGAGTCATACTG	
M2rtTA	F	GTACGCTCTGTCCGCCGTGG	Genomic PCR for *M2rtTA* :
	R	CAAGGGCATCGGCTGGGAGC	Teratoma and chimera genotyping
Oct-4 tg	F	ACATCGCCAATCAGCTTGG	qRT-PCR for *Oct4*: transgene
	R	AGAACCATACTCGAACCACATCC	Carey et al (2009)
c-Myc tg	F	GGCTGGAGATGTTGAGAGCAA	qRT-PCR for *c-Myc*: transgene
	R	AAAGGAAATCCAGTGGCGC	Carey et al (2009)

Chapter 3

Age-related changes in a rat-mouse chimeric model

Abstract

Research on interspecific chimeras is of increased interest for both basic and translational science. However, the information on the stability and survival of donor cells inside the host body over the lifetime remains unclear. Here, we report the establishment of rat iPSCs from lung fibroblasts. These iPSCs displayed pluripotency-associated markers, formed derivatives of all three germ layers *in vitro*, as well as teratoma *in vivo*. We further succeeded in generating full-term rat-mouse chimeras after injection of rat iPSCs to mouse blastocysts. The analysis of social interaction suggested that rat-mouse chimeras were not recognized by mice as distinct individuals compared to wildtype control. Interestingly, all adult chimeras showed diminished chimeric phenotype which developed as a function of age. This finding suggests that rat cells have lower capacity to compete with host stem cells for the stem-cell niche, or are characterized by lower survival with the host, over the lifetime of interspecific chimeras.

Introduction

Research on interspecific chimeras is of growing interest for both basic and translational science. Analyses of evolutionary divergence, development of matching models across species, pluripotency potential of PSCs, generation of humanized mice and rats as human disease models, and production of human organs for drug testing as well as for transplantation are some of the many possible applications of interspecific chimera (Wu *et al.*, 2016, 2017). First full-term chimeras were reported between two different mouse species – *Mus caroli* and *Mus musculus* – using ICM of former one and blastocysts of latter (Rossant and Frels, 1980). This and the follow-up study (Rossant *et al.*, 1983), when *Mus caroli* pups were born using blastocysts composed of *Mus musculus* trophectoderm and *Mus caroli* ICM, concluded that the trophectoderm and the uterus must be from the same species for embryo implantation and development. The authentic interest in generating interspecific chimeras has been reborn with the establishment of naïve pluripotency culture environment and recent rapid progress in iPSCs and gene editing techniques. Recent studies revealed several interesting insights. It was shown that utilization of genetically modified pancreogenesis-disabled mouse blastocysts and donor rat PSCs resulted in the formation of mouse-sized pancreas entirely derived from rat cells (Kobayashi *et al.*, 2010; Wu *et al.*, 2017). Moreover, chimeras born upon injection of rat PSCs into mouse blastocysts were generally mouse-sized and *vice versa*.

Establishment of iPSCs from extremely long-lived animals and development of relevant interspecific chimeric models may open new avenues for studying the exceptional traits underlying their longevity. But, first, it is important to gain enough information on the stability and survival of donor cells inside the host body over the lifetime.

Here, we report the establishment of rat iPSCs from lung fibroblasts using drug-inducible expression of OSKM in 2i/LIF culture environment. These iPSCs displayed markers associated with pluripotency, formed derivatives of all three germ layers *in vitro*, and resulted in teratoma following injection to immunodeficient mice. We further succeeded in generating full-term rat-mouse chimeras after injection of rat iPSCs to mouse blastocysts. To date, no difference in survival rate has been observed between chimeras and non-chimeric littermates. The oldest chimera reached 17 months of age and is still alive. These data suggest that rat naïve iPSCs could colonize mouse blastocysts and contribute to live-born chimeras without radically compromising lifespan of host organisms. Social interaction analysis suggests that rat-mouse chimeras are not recognized by mice as distinct individuals compared to wildtype control. Interestingly, we observed that all aged chimeras showed decreased contribution of pigmented hairs from rat cells over the lifetime. This finding suggests that rat cells have lower capacity to compete with host stem cells for the stem-cell niche, or are characterized by lower survival with the host, over the lifetime of interspecific chimeras.

Results

Generation and characterization of naïve rat iPSCs

Primary rat fibroblasts isolated from lung tissue (Fig. 21A) were used to establish donor iPSCs for further formation of rat-mouse chimeras.

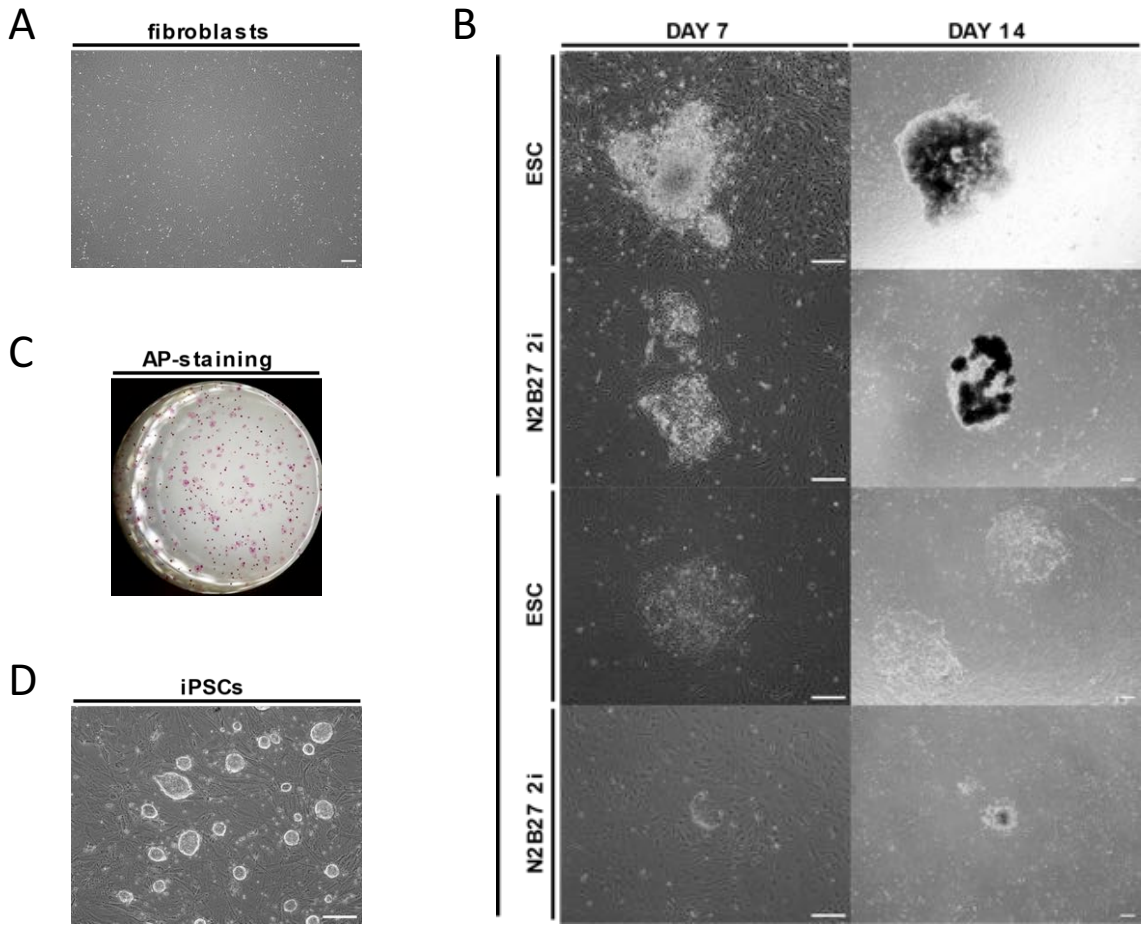

Figure 21. Reprogramming of rat fibroblasts to iPSCs
(**A**) Morphology of primary rat fibroblasts from lung tissue. (**B**) Primary ESC-like colony formation during the reprogramming process (day 7 and day 14 of Dox treatment are shown) using mouse or human OSKM factors in serum + LIF or serum-free N2B27+2i+LIF culture media. (**C**) AP-positive colonies derived from rat fibroblasts in N2B27+2i+LIF conditions. (**D**) Morphology of generated rat iPSCs. All scale bars, 100 μm.

For reprogramming, we used doxycycline-inducible lentiviral constructs encoding either mouse or human *Oct4*, *Sox2*, *Klf4*, and *c-Myc* genes downstream of a tetracycline operator to provide forced expression of pluripotency factors (Hockemeyer *et al.*, 2008; Carey *et al.*, 2009). We first employed both serum/LIF and serum-free/2i/LIF culture conditions as both were shown to promote the formation of primary ESC-like colonies in the rat (Li *et al.*, 2009). In all four combinations used (mOSKM, hOSKM, serum/LIF, N2B27/2i/LIF), first colonies were observed by day 7 of doxycycline treatment and continued to propagate (Fig. 21B). However, successful capturing and culturing of authentic rat PSCs is associated with 2i conditions (Buehr *et al.*, 2008; Li *et al.*, 2008). The same conditions are known for their ability to reveal and sustain the ground state of pluripotency, a germline- and chimeric-competent naïve state that resemble to developmental time point of preimplantation epiblast (Ying *et al.*, 2008; Nichols and Smith, 2009, 2011). For these reasons, we chose to pick dome-shaped ESC-like colonies that appeared in 2i conditions for further characterization. More precisely, we applied decreased concentration of GSK3 inhibitor, as it was shown that rat ESCs are more sensitive to GSK inhibition which favors the activation of differentiation genes due to the relative abundance of LEF1 (Chen, Blair and Smith, 2013). The resulting cells exhibited positive staining for alkaline phosphatase (Fig. 21C).

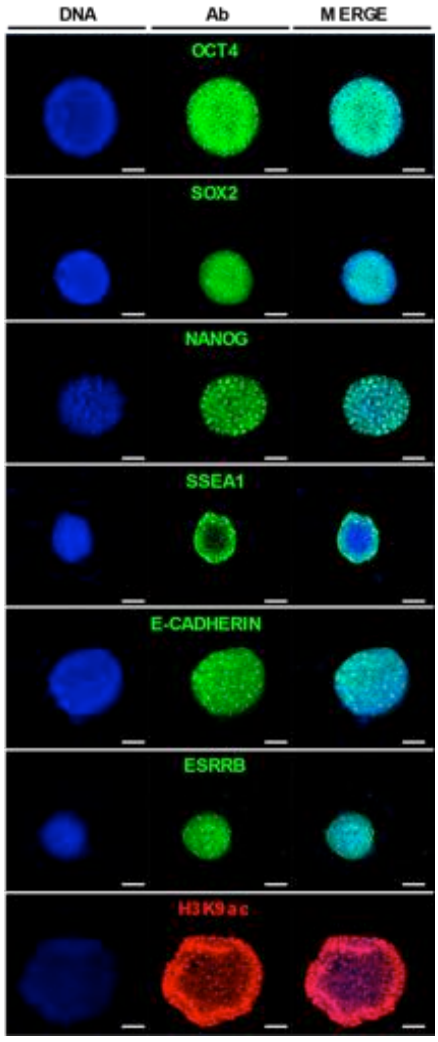

Figure 22. Characterization of rat iPSCs: pluripotency associated markers
Representative images of rat iPSC colonies following immunostaining for OCT4, SOX2, NANOG, SSEA-1, e-cadherin, ESRRB, and acetylated H3 lysine 23. All scale bars, 100 μm.

Using immunofluorescent cytochemistry, we examined and confirmed the expression of pluripotency associated markers Oct4, Sox2, Nanog, SSEA1, e-cadherin, ESRRB, H3K23ac (Fig. 22). We maintained established cells in culture for over 40 passages replating every 3-4 days with no differentiation observed (Fig. 21D).

To evaluate *in vitro* differentiation propensity of generated iPSCs, we applied an assay to monitor embryoid body formation. For this, cells were cultured in suspension for 6-7 days until large aggregates were formed. After being transferred to gelatin-coated culture dishes, EBs underwent massive spontaneous differentiation. Immunostaining with antibodies specific for three germ lineages revealed cells with the expression of TUJ1, GFAP (ectoderm), desmin, a-actinin (mesoderm), and vimentin, FOXA2 (endoderm) (Fig. 23). After two weeks in culture, we also observed spontaneously beating cell structures suggesting derivation of cardiomyocytes.

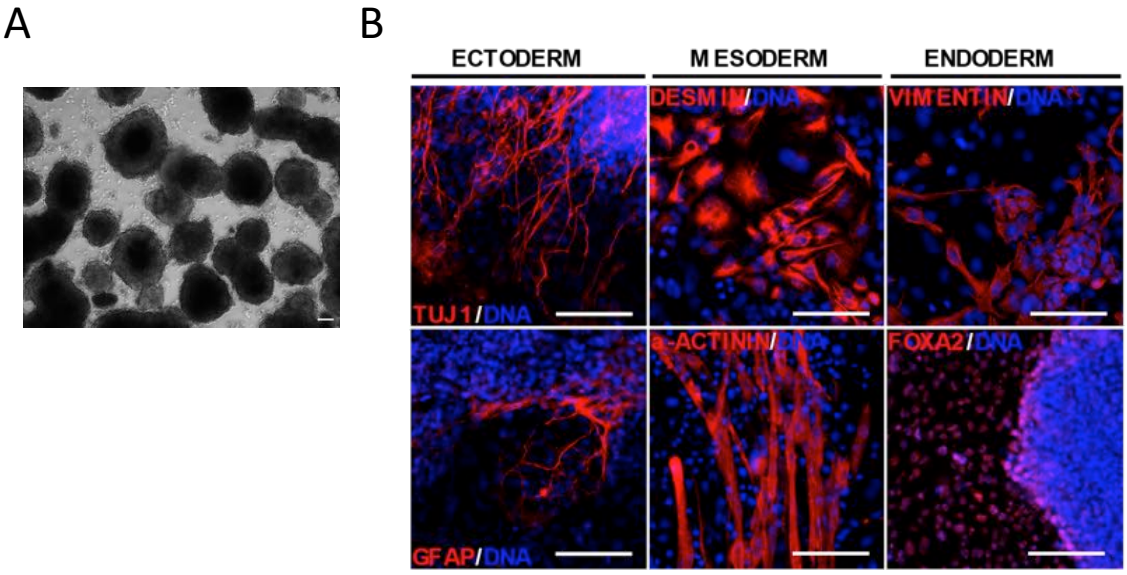

Figure 23. Characterization of rat iPSCs: *in vitro* differentiation
(A) EB formation. (**B**) Immunocytochemical analyses of EB derivatives: ectoderm (TUJ1 and GFAP), mesoderm (desmin and a-actinin) and endoderm (vimentin and FOXA2) markers. All scale bars, 100 μm.

To assess the full differentiation potential of derived iPSCs *in vivo*, we prepared an enhanced green fluorescent protein (EGFP)-expressed cell line that was injected under kidney capsules of 3 severe combined immunodeficient (SCID) mice. Seven weeks after

the injection, the animals were sacrificed. All three mice showed tumor formation. We first examined the size and mass of isolated teratoma (Fig. 24A and B). Macroscopic observation revealed that all three teratomas were almost entirely EGFP-expressing (Fig. 24C). Histological analyses revealed differentiated cell types and structures of all three germ layers (Fig. 24D). These results indicated that generated rat iPSCs were competent for mature multilineage differentiation.

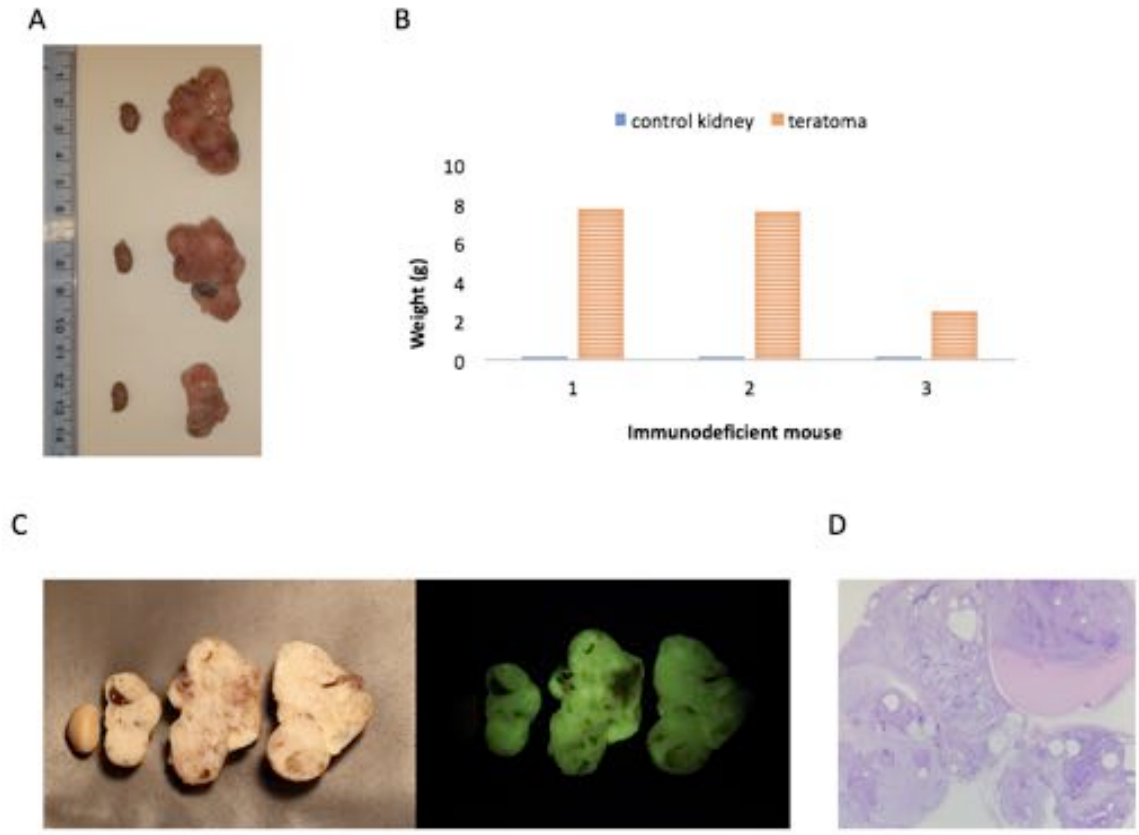

Figure 24. Characterization of rat iPSCs: teratoma formation assay
(A) Teratomas and control kidneys 7 weeks after iPSCs transplantation to renal capsules of 3 SCID mice. (**B**) Weight (grams) of teratomas and control kidneys. (**C**) The presence of fluorescent protein signal from teratomas derived from EGFP-expressing rat iPSCs (right). (**D**) Histology of the teratoma stained with hematoxylin and eosin.

Rat-mouse chimera formation

To characterize naïve pluripotency of iPSCs and generate interspecific chimeras *in vivo*, EGFP-labeled rat iPSCs were microinjected into embryonic day 3.5 (E3.5) blastocysts of B6-albino mice (Fig. 25A). Approximately 60 injected blastocysts were evenly transferred to the uteri of four pseudopregnant female mice. Blastocysts from one surrogate mouse mother were allowed to develop to the E13.5. After dissection, 4 embryos appeared to be aborted while 11 were normally developed (Fig. 25B). Among these 11, the evaluation of EGFP expression by fluorescence microscopy revealed chimerism in 4 embryos (Fig. 25C), thereby suggesting chimera forming efficiencies of ~27% at E13.5, consistent with previous reports (Kobayashi *et al.*, 2010; Wu *et al.*, 2017).

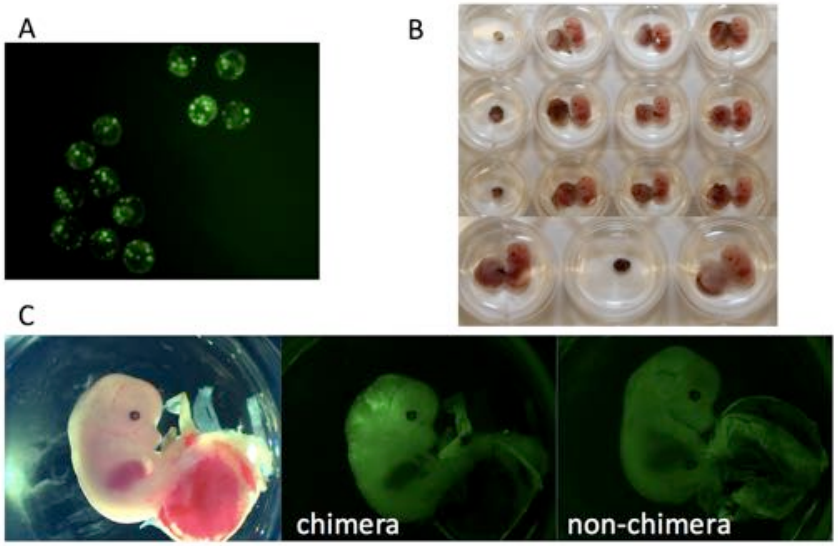

Figure 25. Generation of rat-mouse interspecific chimeras
(A) B6-albino mouse blastocyst stage embryos soon after the injection of EGFP-expressing rat iPSCs. (**B**) Aborted and normal fetuses obtained from one surrogate mother 11 days after embryo transfer into uteri of 2.5 dpc pseudopregnant mice (E13.5). (**C**) Interspecific chimera fetus (left: phase, middle: EGFP) and non-chimeric fetus (right) at E13.5.

Three other surrogate mothers were allowed to develop to full term, giving birth to 15 pups. When fur growth was completed, chimerism was judged by coat color because rat iPSCs were derived from pigmented rat while mouse blastocysts were from albino hosts (B6(Cg)-Tyr^{c-2J}/J) that carried a mutation in the tyrosinase (Tyr) gene and thus exhibited the absence of pigmentation in skin, hair and eyes. DNA analysis of hair follicles (chimeras #1, #3, and #4) and skin biopsy (chimera #1) from pigmented patches using rat-specific primers confirmed the presence of rat DNA (Fig. 26B). We further derived primary cells from pigmented skin biopsy of chimera #1. Although EGFP expression might be lost upon chromatin remodeling during differentiation of rat iPSCs and establishment of lineage specific cell identity, we were able to detect EGFP-positive cells among cultured primary cells (Fig. 26C), further supporting their rat origin.

Full term development rate of live-born interspecific chimeras was the same ~27% as for fetal chimeras at E13.5, a frequency that is similar to previously published data (Kobayashi *et al.*, 2010). At day 17 after birth, one of perinatal chimeras, which had a black head patch, was found dead. All other chimeras developed into adulthood. To date, no difference in survival rate has been observed between chimeras and non-chimeric littermates. The oldest chimera reached 17 months of age and remains alive. These data suggest that rat naïve iPSCs could colonize mouse blastocysts and contribute to live-born chimeras without radically affecting the lifespan of host organisms, consistent with published reports (Kobayashi *et al.*, 2010; Wu *et al.*, 2017).

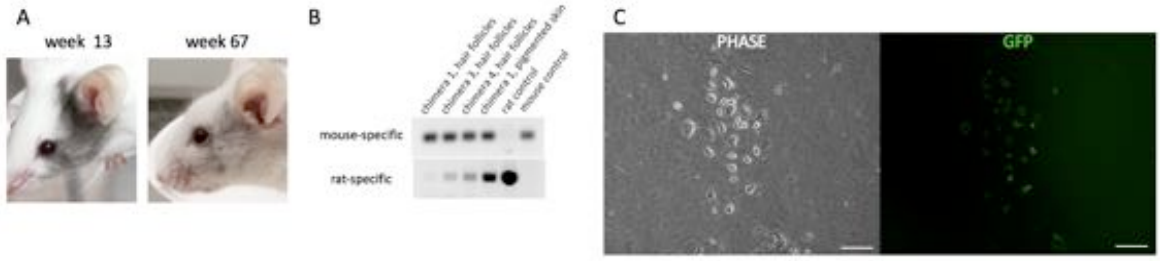

Figure 26. Contribution of rat cells to pigmented coat of albino mice.
(A) Coat color contribution of rat cells in chimera #1 at two indicated ages. (**B**) PCR confirmation of the rat origin of pigmented hair follicles and skin. (**C**) GFP fluorescence of primary cells isolated from pigmented skin biopsy of chimera 1.

Social interaction analysis of rat-mouse chimeras

To assess whether the rat-mouse chimeras might exhibit some distinctive behavioral features, we used confirmed (based on their coat coloring) chimeras as a target in a social preference study by giving age-matched C57BL/6J mice a choice to socialize more with a control B6-albino mouse, or with the chimera. Mice typically avoid predators and predator odors so we hypothesized that a mouse would avoid the chimera and prefer to socialize with another mouse if the test mouse detected any rat qualities in the chimera. A variation of standard three-chamber social interaction test (Moy *et al.*, 2004), where a known chimera and a control mouse are placed under the cups into the opposite chambers, was used for this purpose. When access to both compartments was opened for wild type C57BL/6J test mouse located in the center chamber, the mouse was given a chance to explore for ten minutes. Evaluation of the time spent by six test mice interacting with either confirmed chimeras or control mice showed that the test mice did not avoid rat-mouse chimeras, indicating no significant difference in social preference for chimera vs. control mouse (Fig. 27).

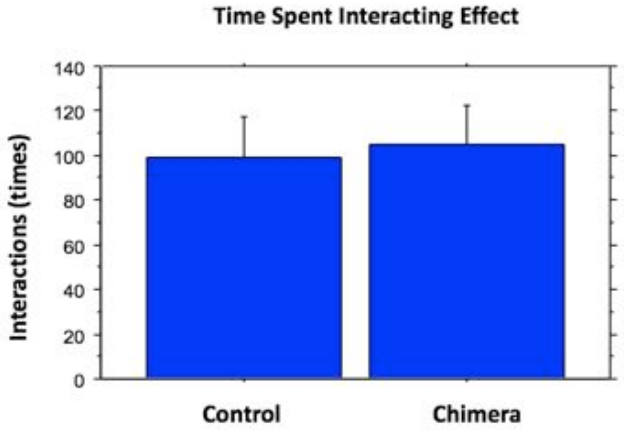

Figure 27. Test of social preference between B6-albino control and rat-mouse chimeras. Values are mean ± 1 standard error from six tested wildtype C57BL/6J mice.

These results suggest that rat-mouse chimeras are not recognized by mice as distinct individuals compared to wildtype controls, although more advanced behavioral studies using rats as a positive control are desired to confirm this hypothesis.

Diminished chimeric phenotype in older chimeras

Although melanocytes in B6-albino mice are unable to produce melanin responsible for pigmentation, they do develop and thereby, a competition for melanoblasts takes place between mouse host and rat donor cells resulting in a various extent of visible chimerism. All 27% of animals, which were determined to be chimeric by coat pigmentation, had a black spot on one side of the face (Fig. 28). In addition to this, in chimera #1 one eye was red colored, which is typical for albino mice, while the second eye was black, indicating respective color of retinal pigmented epithelium. The highest chimeric contribution was observed in chimera #4, which has an additional black

hair stripe on the left side of the back, together with one fully black and one dark-red eyes (Fig. 28C).

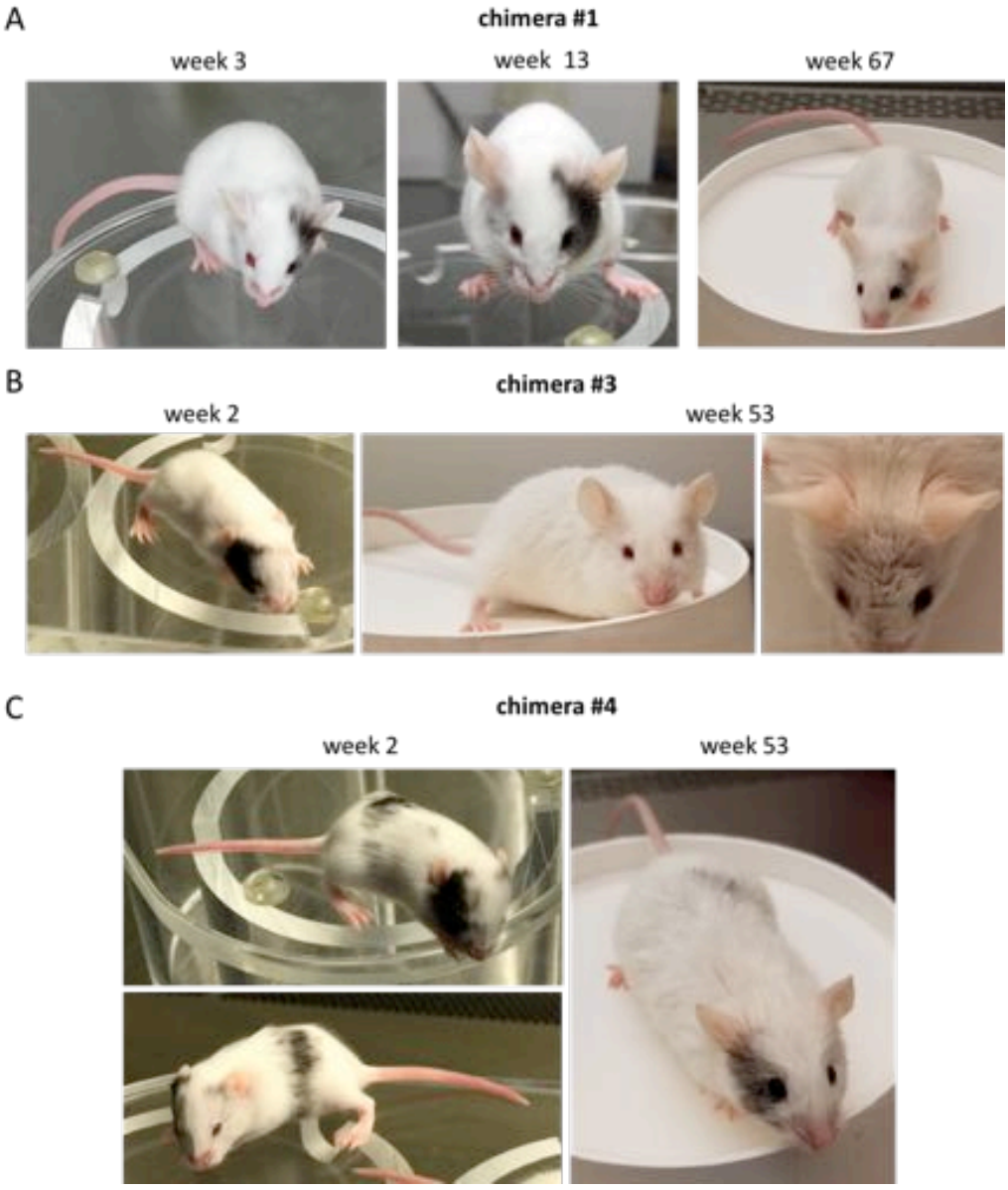

Figure 28. Diminished chimeric phenotype of rat-mouse chimeras at indicated ages. (**A**) Face spotting pattern of chimera #1 at week 3, week 13, and week 67 of age. (**B**) Vanishing hair pigmentation of chimera #3 at week 2 vs. week 53 of age. (**C**) Pigmented spotting pattern of chimera #1 at week 2 vs. week 53 of age.

We consistently monitored chimeras as they were growing older. Inspection of the coat phenotype in aged individuals revealed that pigmented hair contribution from rat cells decreased over time. This striking observation applied to all chimeric animals that we developed. Specifically, the face spotting area in chimera #1 reduced dramatically by week 67 of age though was still visible (Fig. 28A). The black spot on the face of chimera #3 completely disappeared by week 53 (Fig. 28B). In chimera #4, both pigmented spots retained by week 53 although their density was clearly reduced (Fig. 28C).

Overall, all adult chimeras showed diminished chimeric phenotype which developed as a function of age. This finding suggests that rat cells exhibit lower capacity to compete with host stem cells for the stem-cell niche over the lifetime of interspecific chimeras, or that rat cells show lower survival with the host.

Materials and methods

Animal ethics

The animal welfare, use, and care were carried out according to the protocols approved by the Institutional Animal Care and Use Committee (IACUC) of the Brigham and Women's Hospital, Harvard Medical School.

Materials

Chemicals were purchased from Sigma-Aldrich (St Louis, MO, USA) and all culture reagents were acquired from Thermo Fisher Scientific (Waltham, MA, USA), unless otherwise specified.

Culture of rat fibroblasts

Rat fibroblasts were cultured at 37 °C in humidified atmosphere containing 3% O2 and 5% CO2. Cultivation was in DMEM (DMEM high glucose + Glutamax) with 10% FBS, 1X antibiotic/antimycotic, 1X non-essential amino acids, 0.1 mM β-mercaptoethanol.

Lentiviral production and infection

For production of lentiviral particles, Lenti-X 293T cells (Clontech) at 70-80% confluency, cultured on 10 cm dishes were transfected with following vectors: polycistronic mouse OSKM (tetO-FUW-OSKM; Addgene plasmid #20321), human Oct4

(FUW-tetO-hOCT4; Addgene plasmid #20726), human Sox2 (FUW-tetO-hSOX2; Addgene plasmid #20724), human Klf4 (FUW-tetO-hKlf4; Addgene plasmid #20723), human c-Myc (FUW-tetO-hMYC; Addgene plasmid #20725), and M2rtTA (Addgene plasmid #20342), as well as pWPI (EGFP; Addgene plasmid #12254) together with packaging plasmids VSV-G and 8.91 (gag/pol). Transfection was performed using the calcium phosphate precipitation method. Medium was replaced 12 hours following transfection. After additional 24 and 48 hours, supernatants containing viral particles were harvested and filtered through a 0.45 μm cellulose acetate filter. EGFP alone or equal volumes of mOSKM or hOSKM with M2rtTA lentiviral supernatants were mixed, supplemented with polybrene at the final concentration of 4 μg/ml and directly used for transduction of rat fibroblasts.

Establishment and maintenance of rat iPSCs

Three days after lentiviral transduction, approximately 100,000 infected fibroblasts were seeded per well of 6-well plate on mitomycin C inactivated or gamma-irradiated mouse embryonic fibroblasts (MEFs). Two different culture conditions were used for reprogramming: (1) DMEM supplemented with 10% FBS, 1000 units/ml mouse leukemia inhibitory factor, 0.1 mM β-mercaptoethanol, 1% nonessential amino acids, 2 mM glutamine and 1% antibiotic/antimycotic, 2 μg/ml Dox and (2) N2/B27+2i medium (1:1 mixture of N2 medium (DMEM/F12 supplemented with 1x N2, 1% antibiotic/antimycotic, 0.005% BSA, 0.1 mM β-mercaptoethanol, 1% nonessential amino acids) and B27 medium (Neurobasal medium supplemented with 1x B27 (without

retinoic acid), 1% antibiotic/antimycotic, 2 mM L-glutamine, 0.1 mM β-mercaptoethanol, 0.005% BSA, 1% nonessential amino acids supplemented with 1000 U/ml mLIF, 1 μM GSK3b inhibitor (CHIR99021), 1 μM MEK1/2 inhibitor (PD0325901) and 2 μg/ml Dox. Culture media was changed every 24 h.

The ESC-like colonies were formed, picked, and further maintained on feeder in N2B27+2i+LIF medium. The ESC-like colonies were formed, picked, digested in 0.05% trypsin and passaged on gelatin-coated 6-well plates onto MEF feeder cells for further maintenance in N2B27+2i+LIF medium. iPSCs were split every 3-4 days, and Dox was withdrawn after passage 3.

Three days after transduction, infected cells were seeded on mitomycin C inactivated MEFs. N2B27+2i reprogramming medium containing 2 μg/ml Dox was used. Culture media was changed every 24 h. The ESC-like colonies were formed, picked, and further maintained on feeder in N2B27+2i+LIF medium. Cells were split every 3-4 days, and Dox was withdrawn after passage 3.

Alkaline phosphatase staining and immunofluorescence

AP staining was performed according to the manufacturer's protocol using the Alkaline Phosphatase Staining Kit (Stemgent). For fluorescence immunocytochemistry, iPSCs were cultured 2-3 days on mitotically inactivated MEFs and fixed using PBS containing 4% PFA for 15 min at room temperature. After rinsing with PBS, fixed cells were blocked and permeabilized for 1 h in PBS containing 10% (v/v) goat serum in 0.1% Triton X-100-PBS. Primary antibodies were as follows: OCT4 (Santa Cruz Biotech),

SOX2 (Millipore), NANOG (Millipore), SSEA-1 (Santa Cruz Biotech), e-cadherin (Abcam), ESRRB (Abcam), and acetylated H3K9 (Abcam), which were diluted 1:200 in blocking solution. Fixed cells were incubated with primary antibody overnight at 4 °C. After washing out the unbound antibodies, fixed cells were incubated with secondary antibodies (labeled with Alexa-488 or Alexa-647, 1:1000 dilution, Jackson ImmunoResearch) for 1 h at room temperature. Nuclei were counterstained using 1 μg/ml Hoechst 33342 (Life Technologies). All fluorescence imaging was conducted using an LSM 700 confocal microscope (Zeiss).

In vitro differentiation and immunofluorescence

iPSCs were detached using 0.05% trypsin and were grown in suspension for 6-7 days in low-attachment plates in DMEM with 10% FBS, 1X antibiotic/antimycotic, 1X non-essential amino acids, 0.1 mM β-mercaptoethanol without 2i and LIF. Formed EBs were then seeded on 0.1% gelatin-coated plates for subsequent spontaneous differentiation. After 1-2 weeks, cells were fixed and immunoassayed using following antibodies: TUJ-1(1:500, Covance), GFAP (1:500, Dako), desmin (1:200, Abcam), α-actinin (1:200, Sigma), vimentin (1:200, Abcam), FOXA2 (1:200, Abnova).

Teratoma formation

EGFP-expressing iPSCs were collected by 0.05% trypsin treatment and injected beneath the kidney capsule of NOD–SCID (NOD.CB17-Prkdc/J) mice. Seven weeks

after injection, kidney capsules were collected, sectioned and processed for paraffin embedding and hematoxylin and eosin staining.

Rat-mouse chimera formation

Approximately 10-12 EGFP-expressing iPSCs were injected in B6-albino (B6(Cg)-Tyr^{c-2J}/J) mouse blastocysts at embryonic day 3.5 (E3.5). Injected blastocysts were transplanted into the uteri of foster mothers (ICR; CD1 mice). For fetal chimeras, pregnancy was aborted at E13.5, and the embryos were harvested. They were fixed with 4% paraformaldehyde and analyzed by fluorescence microscopy. For neonatal chimera production, surrogate mothers were allowed to develop to full term to give a birth.

Social preference test

Testing was performed in a three-chamber sociability apparatus with openings between the compartments. Each chamber was 20 cm x 40 cm and the walls were made from clear Plexiglas. The walls of the middle section had a small opening (4 cm w x 6 cm h) to allow free access to each chamber. During the test phase, the B6 albino and chimera were enclosed in a small, round wire cup (Galaxy Cup, Spectrum Diversified Designs, Inc., Streetsboro, OH), which allowed nose contact between the bars, but prevented fighting. The cups were placed on opposite end of the apparatus, one on each side of the end chambers. Six wildtype age-matched C57BL/6J mice were used as a test group. First, test mouse was given a habituation trial in which it was placed in the middle chamber and allowed to explore the entire chamber for 10 min with 2 empty cups. For the test trial, the

B6 albino was placed under one cup and a chimera under the second cup, and the test mouse was allowed to explore the chamber for 10 min. Two separate chimeras were alternated and the side of the chamber that housed the B6 albino and chimeras were counterbalanced. Sessions were video recorded and analyzed with software (Topscan, CleverSys, Reston, VA). Time spent near the cup as a measure of social interaction was analyzed for each mouse.

Chapter 4

Mechanisms of Naked Mole Rat Thermogenesis

Abstract

The naked mole rat (NMR; *Heterocephalus glaber*) is an exceptionally long-lived subterranean rodent that is thought to have lost the ability to effectively regulate body temperature. It is regarded as the only known poikilothermic mammal. The central role in heat production in small mammals is played by non-shivering thermogenesis, mediated by uncoupling protein 1 (UCP1) in the brown adipose tissue (BAT). Despite being conserved across mammals, NMR UCP1 harbors unique amino acid changes within a proposed regulatory site. In this study, we examined the role of UCP1 *in vitro* and *in vivo* and characterized thermogenesis in NMRs and mice. Bioenergetic profiles of NMR UCP1-expressing cells and isolated mitochondria revealed functional UCP1, but its lower uncoupling activity compared to the mouse ortholog. Likewise, NMR and mouse BAT mitochondria showed similar uncoupling characteristics, but lower UCP1 activity in the case of the NMR. Anatomical inspection revealed three large functional BAT depots in NMRs, which were not visible after 24 h exposure to room temperature. However, in response to short-term β3-adrenergic stimulation, NMRs robustly increased body surface temperature, core body temperature and energy expenditure. Continuous monitoring of NMR core body temperature in response to exposure to various ambient temperatures revealed clear yet limited capacity for its upregulation. Overall, our data reveal a functional UCP1 in NMRs as well as the use of BAT by these animals to buffer body temperature changes through non-shivering thermogenesis, indicating intact thermogenic

machinery. Exhaustion of BAT lipid content, heat loss and failure to access conventional white adipose energy stores may be among the factors that contribute to a highly variable and poikilothermic pattern of body temperature in these animals.

Introduction

The naked mole rat (NMR; *Heterocephalus glaber*) is one of most unusual mammals. These mouse-sized animals live 10 times longer than mice (~30 years vs. ~3 years) and despite their small size are recognized as the longest-living rodents (Edrey *et al.*, 2011). NMRs are also highly resistant to both spontaneous and experimentally induced cancer (Seluanov *et al.*, 2009; Liang *et al.*, 2010). These hairless eusocial subterranean rodents reside in warm and humid burrows in tropical North East Africa, living in large colonies with single breeding females (Jarvis, 1981). The temperature in the NMR's underground niche reaches 29-32 °C and is stable over the course of the whole year (Bennett, Jarvis and Davies, 1988). It was proposed that, having exploited these thermally buffered conditions, NMRs lost the ability to effectively regulate body temperature, thus becoming thermoconforming to ambient environment (Buffenstein and Yahav, 1991). In their natural habitat, where there is no need to be cold-tolerant for prolonged periods of time, NMRs may huddle in groups when temperature changes, which helps them to maintain body temperature. Being housed in laboratories at the temperatures imitating their natural environment, NMRs were shown to exhibit a poikilothermic response to ambient temperature variation; however, they may also employ endothermy in the narrow temperature range 29-34 °C as well as in response to noradrenaline intervention, thus proving themselves as the only known endothermic poikilothermic mammals (Buffenstein and Yahav, 1991; Hislop and Buffenstein, 1994).

While all mammals exposed to cold will initially shiver in order to elevate heat production (Griggio, 1982), the central role of heat production in small mammals is driven by non-shivering thermogenesis (NST), which is regulated by the sympathetic nervous system through noradrenergic innervation of brown adipose tissue (BAT) in response to cold exposure (Carneheim, Nedergaard and Cannon, 1984; Cannon and Nedergaard, 2011). The balance between implementation of shivering and NST depends heavily on an animal's history of cold exposure. Thus, while animals exposed to the cold for the first time may respond mainly by shivering, in those with prior exposure to cold the response would be facultative and adaptive NST in the BAT (Carneheim, Nedergaard and Cannon, 1984; Cannon and Nedergaard, 2011; Speakman, 2013).

The principal mechanism driving production of heat in the BAT is mediated through uncoupling protein 1 (UCP1), which resides in the inner mitochondrial membrane and dissipates the mitochondrial proton gradient to generate heat rather than ATP production (Cannon, 2004). UCP1 was found in all examined mammals except pigs and dolphins, and is thought to be the only true thermogenic uncoupling protein (Cannon and Nedergaard, 2011; McGaugh and Schwartz, 2017). However, the exact molecular mechanism of its uncoupling remains unclear, and the mechanism of UCP1 activation in response to norepinephrine stimulus remains a subject of debate (Cannon and Nedergaard, 2017; Crichton, Lee and Kunji, 2017; Schreiber *et al.*, 2017; Shin *et al.*, 2017). Analysis of the NMR genome revealed that its UCP1, despite being highly conserved across mammals, harbors unique amino acid changes (Gln146, Arg263, Trp264 and Thr303) that occur within the site that supports regulation of the protein by

fatty acids and nucleotides (Fig. 29). As such, it was proposed that these changes may influence the function of UCP1 through the loss of tight regulation by purine nucleotides as inhibitors and fatty acids as activators, in turn leading to ineffective thermogenesis (Kim *et al.*, 2011; Gorbunova *et al.*, 2014).

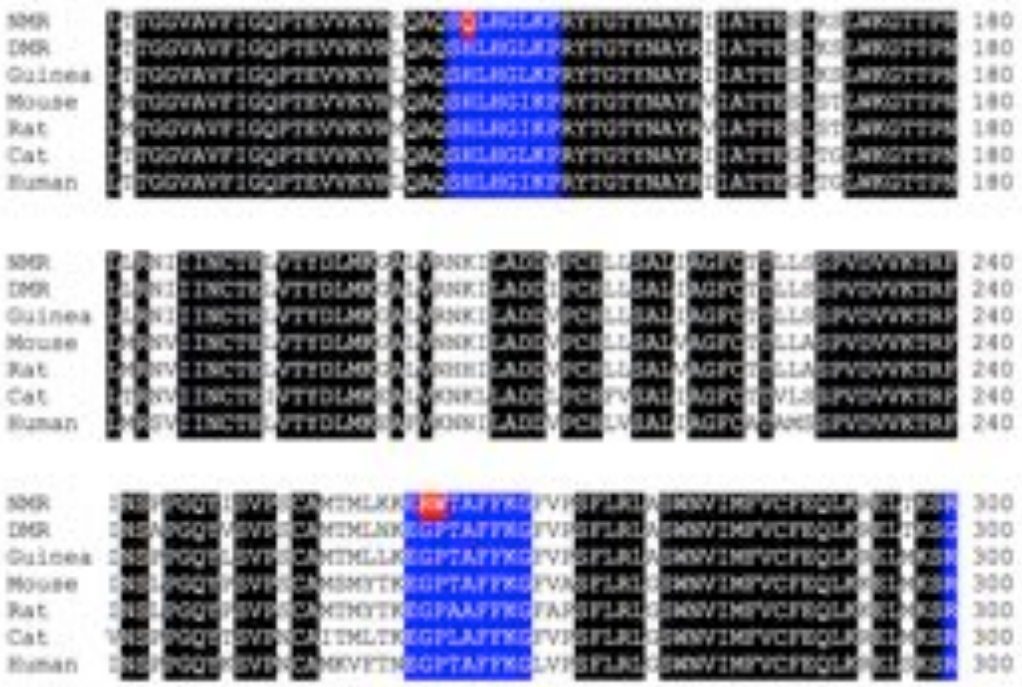

Figure 29. Unique sequence changes in NMR UCP1.
Alignment of mammalian UCP1 sequences. Amino acids unique to the NMR are highlighted in red, and conserved motifs in blue. Identical residues are shaded in black.

In this study, we first characterized the function of NMR UCP1 and the role of its unique amino acid changes. We further specifically compared the thermogenic responses of NMR and C57Bl/6J mice in response to cold exposure and a specific β3-adrenergic agonist. We found that NMRs are capable of acute and robust UCP1 mediated thermogenesis.

Results

NMR UCP1 is functional when expressed in mammalian cells

To examine UCP1 function in the NMR, we first characterized its activity *in vitro* by examining uncoupling properties of the protein in comparison with the mouse ortholog. For this, we generated tetracycline-inducible Flp-In 293 T-Rex cell lines with stably integrated NMR and mouse UCP1 forms with an HA-tag at the N-terminus. Immunoblot analyses confirmed the expression of nmrUCP1-HA and mUCP1-HA in generated cell lines (Fig. 30A). As expected, mouse and NMR UCP1 proteins resided in mitochondria (Fig. 30B). To examine the uncoupling properties of ectopically expressed proteins, we analyzed the respiration profiles and uncoupling efficiencies of cell lines using a Seahorse analyzer. Activation of both mouse and NMR UCP1 proteins was observed in response to the retinoic acid analog TTNPB, which specifically activates UCP1 but is not metabolized (Rial *et al.*, 1999), whereas there was no TTNPD activator effect in the control HEK 293 cells. The bioenergetics profile of cell lines with both NMR and mouse UCP1-containing mitochondria revealed similar oxygen consumption rates (OCR), as well as the common pattern and dose dependency for modulators of cellular respiration (Fig. 30C), supporting the active status of both NMR and mouse UCP1 forms.

NMR UCP1 is functional in isolated mitochondria

Despite similar respiration profiles of mouse and NMR UCP1-expressing HEK 293 cells, the question remained whether the unique amino acid changes at the conserved

regulatory site affected its function. To examine this, we developed three additional HEK 293 cell lines, each stably expressing mutant versions of mouse UCP1, in which the respective residues were replaced with those of the NMR UCP1, including H146Q, Arg263Gly/Trp264Pro, and all three residues. We then isolated mitochondria from the 5 generated cell lines and measured the activity of various UCP1 forms in response to TTNPB activation and GDP inhibition. We observed a lower activity of NMR UCP1 than that of the mouse protein (Fig. 30D). However, it was not due to the unique mutations in the NMR protein. Mitochondria from all three cell lines expressing the mutant mouse UCP1 containing NMR residues showed a similar activity to those from cells expressing WT mouse UCP1 (Fig. 30E). We also found that all mouse, NMR and mutant UCP1 proteins showed similar responses to GDP inhibition (Fig. 30F). Taken together, the data suggest that NMR UCP1 was functional despite its mutations. It also responded to activators and inhibitors, although had a lower uncoupling activity compared to that of the mouse ortholog.

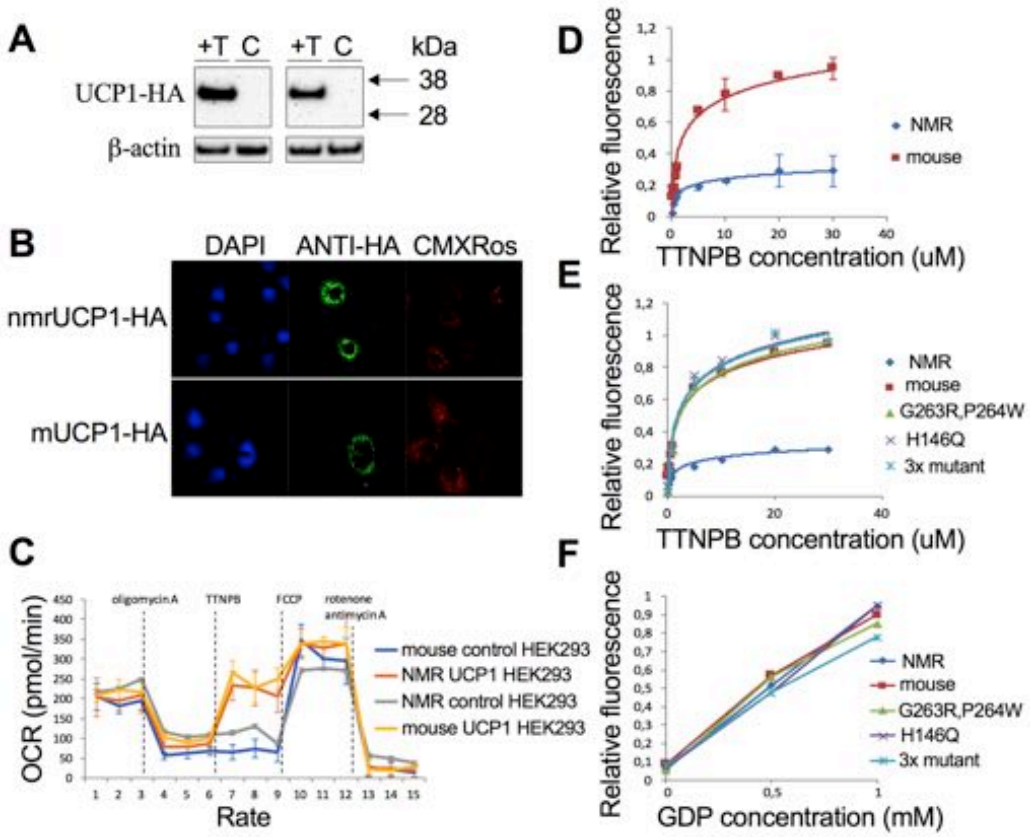

Figure 30. Characterization of NMR UCP1 function *in vitro*.

(**A**) Western blotting of nmrUCP1-HA and mUCP1-HA proteins stably expressed in HEK 293 cells. (**B**) Localization of transiently expressed NMR and mouse UCP1 forms. UCP1 proteins were immunostained based on their HA tags, and mitochondria were stained with Mito-Tracker Red. (**C**) Oxygen consumption rates (OCR) measured by Seahorse assays in HEK 293 cells expressing mouse and NMR UCP1, demonstrating specific activation of stably expressed proteins in comparison with control cells. Normalization was by cell number. The figure shows basal respiration, proton leak respiration (after oligomycin treatment), specific UCP1 respiration (TTNPB), maximal substrate oxidation (FCCP) and non-mitochondrial respiration (antimycin A/rotenone). All values are mean ± SEM from three independent experiments. (**D**) Relative fluorescence tracings of safranin O uptake by mitochondria from HEK 293 cells expressing mouse or NMR UCP1 respiring on succinate in response to sequential addition of TTNPB during safranin O measurement. The relative changes in fluorescent signal are proportional to the membrane potential; larger changes in relative fluorescence units indicate lower membrane potentials. Upon activation by TTNPB, UCP1 increases the conductance of the inner mitochondrial membrane. All values are mean ± SEM from three independent experiments. (**E**) Relative fluorescence tracings of safranin O uptake by mitochondria from HEK 293 cells expressing NMR, mouse, and mutant mouse UCP1 forms respiring on succinate in response to sequential addition of TTNPB during safranin

O measurement. All values are mean ± SEM from three independent experiments. (**F**) Relative fluorescence tracings of safranin O uptake by mitochondria from HEK 293 expressing NMR, mouse, and mutant mouse UCP1s respiring on succinate in response to sequential addition of GDP during safranin O measurement. Upon inhibition by GDP, UCP1 reduces the conductance of the inner mitochondrial membrane. All values are mean ± SEM from three independent experiments.

Abundant functional BAT in the NMR

Next, we examined the UCP1 function in NMR tissues. Post-mortem anatomical inspection of NMRs revealed three large BAT depots, which were classified as superficial (spf) (directly adjacent to the skin), mid (around the superficial muscles of the neck and upper back), and deep (around the deep neck muscles even on the ventral side of the animal). As expected, similar inspection of mice revealed a relatively low amount of BAT, mainly between the scapulas. All examined NMR BAT depots expressed UCP1 (Figure 31). Safranin O was used to evaluate the mitochondrial membrane potential in isolated mitochondria from NMR and mouse BAT tissues. The decrease in safranin O fluorescence is caused by an increase in mitochondrial membrane potential (Akerman and Wikstrom, 1976). Mitochondria isolated from the NMR BAT showed an TTNPB-activated, GDP-inhibited uncoupling activity (Fig. 32A). Comparison of NMR and mouse UCP1 activities in isolated mitochondria from the BAT showed their similar uncoupling characteristics; however, the mouse tissue was more active, consistent with the data in isolated mitochondria from HEK 293 cells (Fig. 32B). Thus, the NMR BAT in all three detected depots in animals at thermoneutral conditions is active and has functional UCP1. This raised the question whether the NMR BAT is capable of NST in thermocomfort conditions or in response to cold exposure.

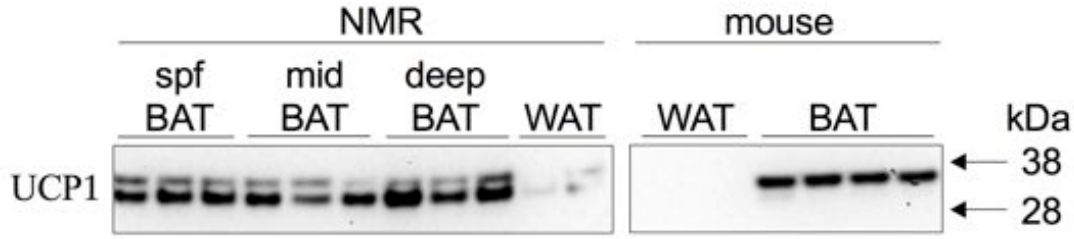

Figure 31. Western blot analysis of NMR and mouse UCP1 proteins from brown and white adipose tissues of these animals.

Activation of the BAT by cold exposure

To examine how the NMR BAT reacts to acute cold exposure, six animals were divided in two groups, three individuals per group. One group continued to be kept in euthermic conditions (30-32 °C), while the second group was kept at 24-25 °C for the next 24 h. Afterwards, animals from both groups were dissected and BAT mass examined. The BAT mass in cold-exposed animals was dramatically reduced compared to the euthermic animals (Fig. 32C), suggesting that cold exposed NMRs utilized lipid stored in BAT for heat production. Together, these experiments demonstrate the functional UCP1 as well as the functional BAT in the NMR, implying the capacity for active thermogenesis in these animals.

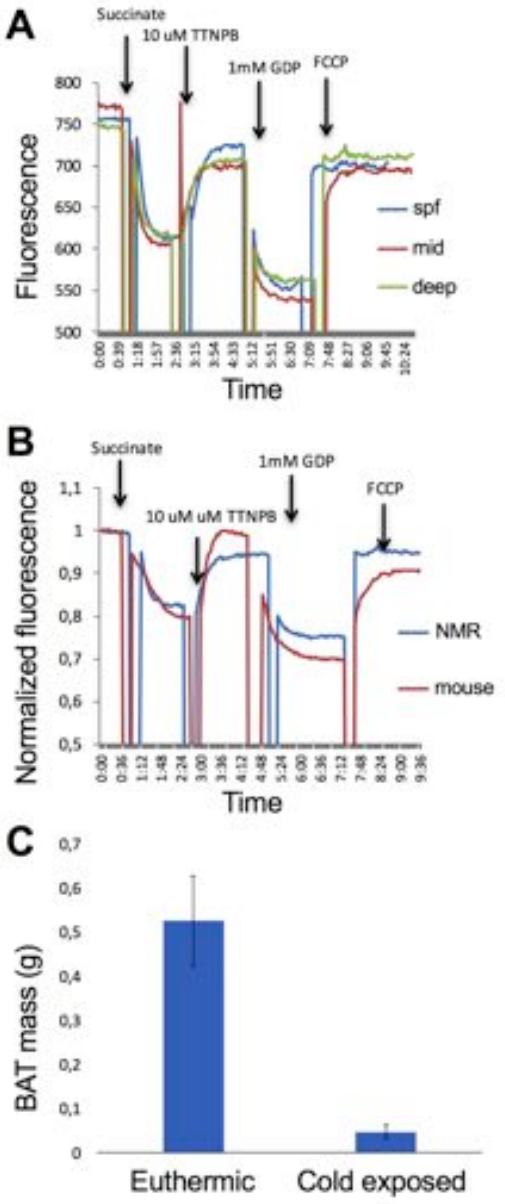

Figure 32. Characterization of the naked mole rat brown adipose tissue.

(**A**) Representative fluorescence tracings of safranin O uptake by mitochondria isolated from indicated NMR BAT depots (superficial (spf), mid and deep), respiring on succinate in response to sequential addition of TTNPB (specific UCP1 respiration), GDP (UCP1 inhibition) and FCCP (maximal substrate oxidation) during safranin O measurement. (**B**) Representative fluorescence tracings of safranin O uptake by mitochondria isolated from NMR and mouse BAT. (**C**) The mass of NMR BAT from 3 euthermic animals and 3 animals exposed to room temperature for 24 h. Values represent means ± standard SEM for three independent experiments.

Active thermogenic response in NMRs

We further investigated the ability of NMRs to elevate body temperature *in vivo* through stimulation of β3-adrenergic receptors, the signaling pathway that is normally activated in mice in response to cold exposure by noradrenaline. Thermal imaging can non-invasively measure surface temperature and by extension, heat loss. Imaging of un-anesthetized freely moving NMR demonstrated more than 2 °C increase in surface temperature (both interscapular and total body), following b3AR agonist. In contrast, the corresponding increase for mice was approximately 2 °C. The increase in both species was statistically significant ($p<0.05$) (Fig. 33A-C). We found roughly similar body compositions by nuclear magnetic resonance of mice and NMR, despite the large difference in age (Fig. 34).

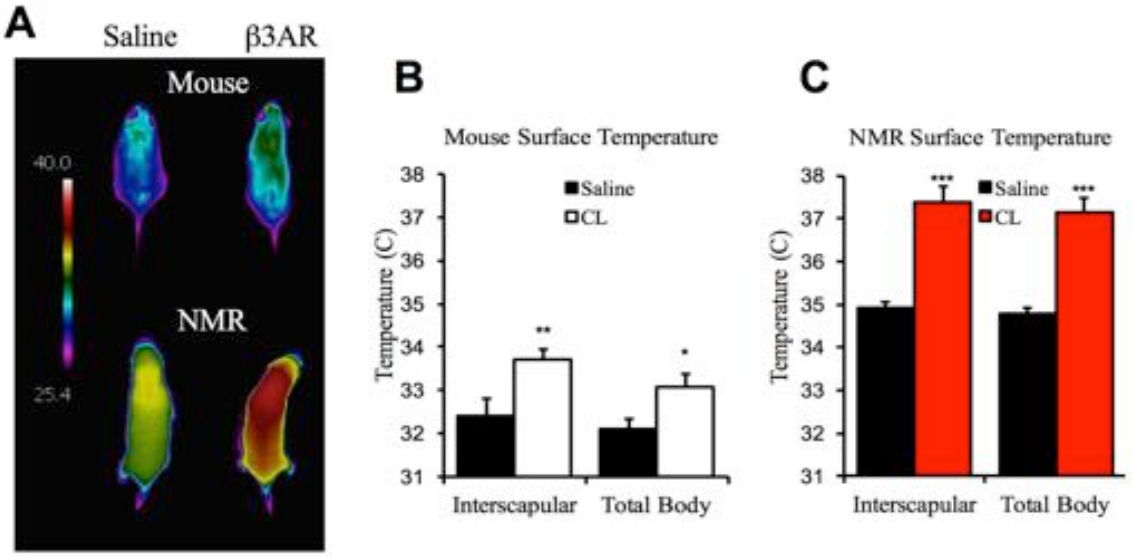

Figure 33. Surface temperature of NMRs and mice in response to saline and β3-adrenergic agonist CL-316,243 interventions.
(**A**) Thermal images of NMRs and mice after saline and CL-316,243 injections. (**B**) mouse and (**C**) NMR average surface temperature. * $p<0.05$, ** $p<0.01$, *** $p< 0.001$

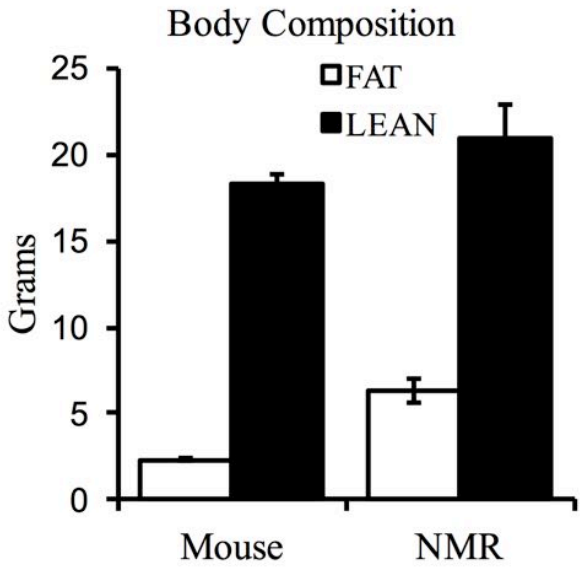

Figure 34. Body composition of NMRs and mice as measured by nuclear magnetic resonance.

To more precisely characterize BAT thermogenic activity and its activation following β3-adrenergic stimulation, we monitored body composition, metabolic rate, and core body temperature in 5 mice and 4 NMRs implanted with wireless thermal sensors and housed in a temperature controlled Comprehensive Lab Animal Monitoring System (CLAMS). Prior to measurements, all animals were housed at 30 °C (mice were housed for one week and NMR for the entirety of housing at our facility). To test for a non-specific stress response caused by injection, all animals were initially monitored during an intraperitoneal injection of normal saline. We observed a small increase in body temperature and metabolic rate in mice, but no change in respiratory exchange ratio (RER). However, there was no apparent physiological response to saline injection in the NMR (Fig. 35A and E). In response to high-affinity β3-adrenergic stimulation, both mice and NMRs treated with 1 mg/kg CL316,243 (CL) showed a thermogenic response as

defined by increased body temperature, increased metabolic rate, and increased lipid oxidation as observed with a lower RER (Fig. 35). All measurements shown (Fig. 35 C, D, G, H, K, and L) were statistically significant ($p<0.05$). Strikingly, NMRs exhibited a greater absolute- and fold-increase in core and surface temperature compared to mice (Fig. 33B-C and 35C-D).

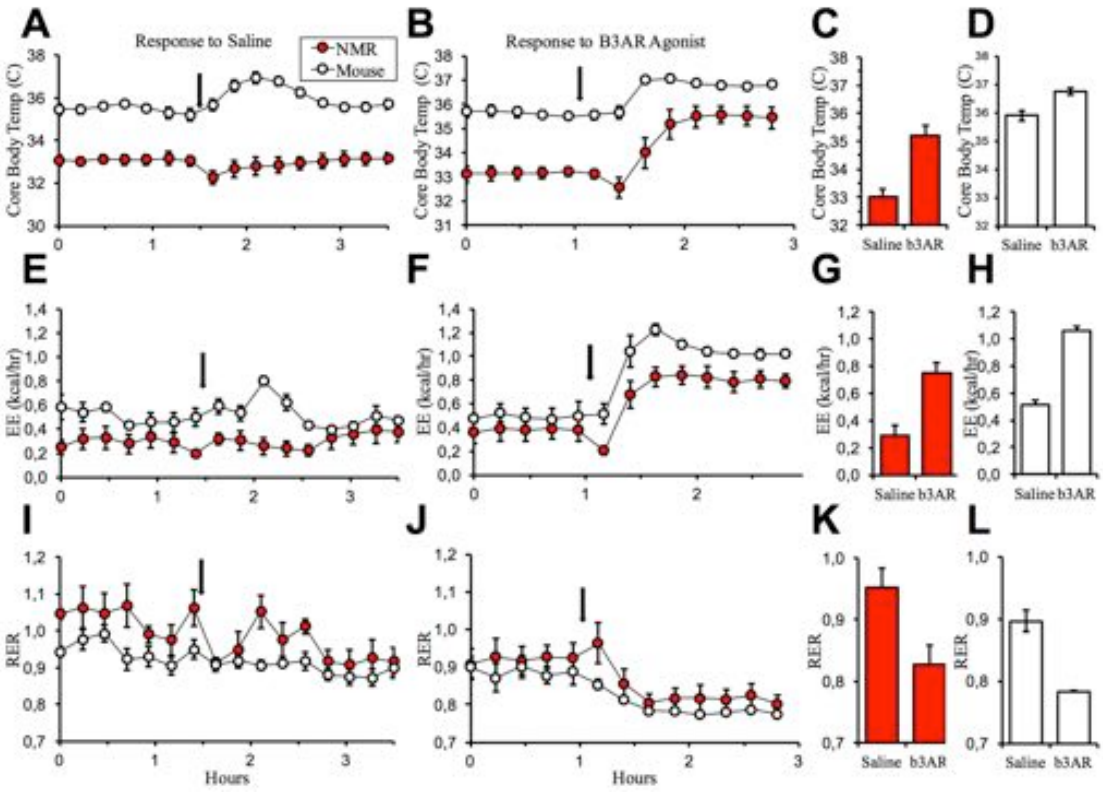

Figure 35. Comprehensive monitoring of NMRs and mice in response to saline and β3- adrenergic agonist CL-316,243 interventions.
(A-D) NMR and mouse average core body temperature. (**E-H**) NMR and mouse average energy expenditure. (**I-L**) NMR and mouse respiratory exchange ratio. All values are mean ± SEM from five mice and four NMRs. All bar plots (C, D, G, H, K, and L) reach statistical significance.

Overall, the NMR produced a response which was qualitatively similar to mice in response to a thermogenic stimulus.

Changes in body temperature in response to cold exposure

After confirming the ability of NMRs to generate heat and elevate body temperature in response to chemical stimulation of β3-adrenergic receptors, we decided to reinvestigate regulation of body temperature in response to exposure to a series of temperature conditions below NMR thermoneutrality. To do this, five NMRs with implanted wireless thermal sensors were individually housed in a temperature controlled CLAMS for ten days. After the first two days of acclimatization at 32 °C, we gradually decreased the ambient temperature exposing them to 28 °C, 25 °C, 22 °C, and 18 °C, one day at each (12 hour exposure in the case of 18 °C). The cold-exposure periods were alternated by returning the animals back to 32 °C for 24 hours. The data obtained by continuous monitoring of NMR core body temperature during this period revealed a clear yet limited capacity of all animals to upregulate the body temperature while exposed to all tested ambient temperatures below thermoneutrality (Fig. 36).

At the thermoneutral (for NMRs) 32 °C, their average body temperature was approximately 33-33.5 °C. At 28 °C, the average core body temperature of NMRs changed within the range of 30-32 °C. Being exposed to 25 °C, they exhibited variable average body temperature of 27-30 °C. When ambient temperature dropped to 22 °C, the NMR T_b was within 23.5-27.5 °C range. Finally, at the lowest tested ambient temperature of 18 °C, the NMRs were able to maintain their body temperature at the level of 20-23.5 °C (Fig. 36B). With these data, we confirmed the poikilothermic behavior of NMRs

despite their apparent thermogenic response and body temperature upregulation during cold exposure.

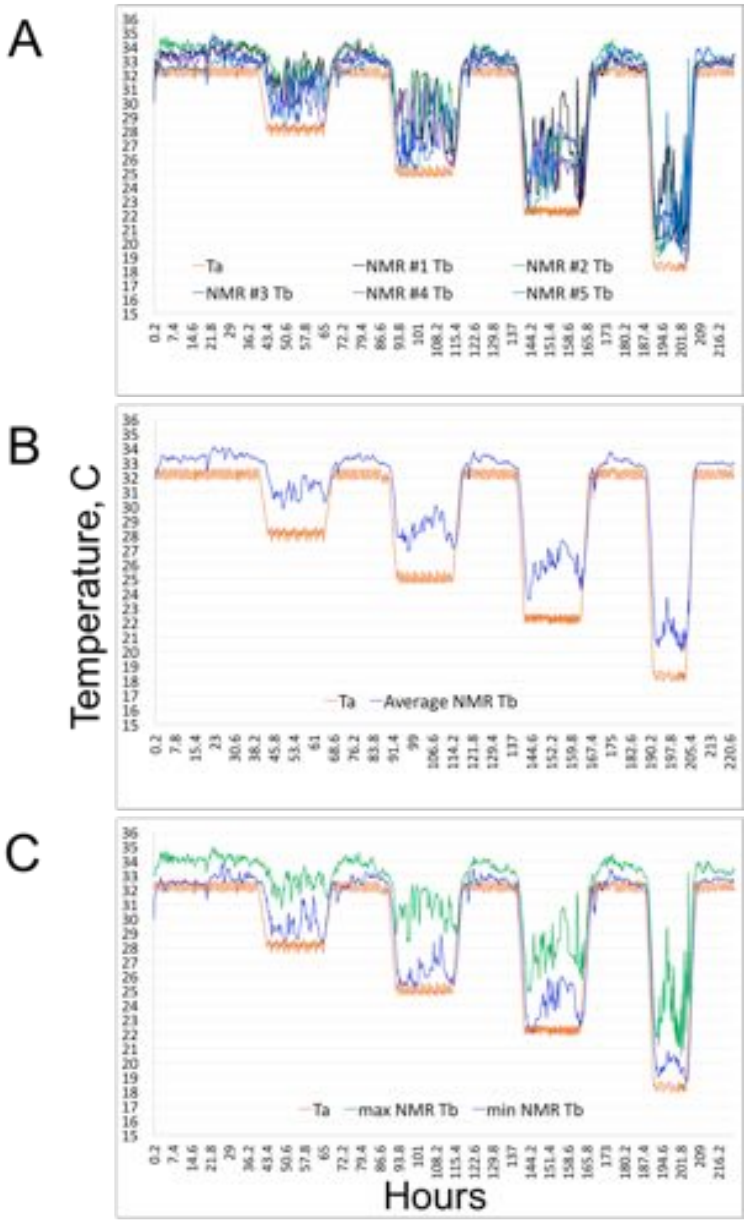

Figure 36. Effect of ambient temperature on NMR core body temperature.
(A) Core body temperature changes of five monitored NMRs in response to various ambient temperature (orange). (**B**) Average NMR core body temperature (blue) at various ambient temperatures (orange). (**C**) Maximum (green) and minimum (blue) values of NMR core body temperature at various ambient temperatures (orange). Ta – ambient temperature; Tb – core body temperature.

Our findings indicate that, bellow thermoneutrality, the average core body temperature of NMRs is at least 1.5-2 °C above the ambient temperature, in contrast to ~ 0.5 °C, previously reported (Buffenstein and Yahav, 1991). In addition, at these conditions, we observed dramatic (on the order of 4 degrees) body temperature changes in individual animals. Interestingly, the Tb of animals fluctuated significantly when animals were below thermoneutrality, whereas it was almost constant at 32 °C. It appears that NMRs regulate thermogenesis, switching it on and off on the scale of hours. At the colder temperatures utilized, the core body temperature fluctuated from above the ambient temperature to below thermoneutrality. The findings suggest the limited capacity of NMRs for thermogenesis, which is exacerbated by heat loss due to the lack of fur.

Discussion

It was shown more than 25 years ago that the NMR exhibits a poikilothermic response to ambient temperature, closely tracking one over the entire range (12-37 °C) measured (Buffenstein and Yahav, 1991). This surprising finding makes the NMR the only mammal known to be unable to maintain stable body temperature while in active state. However, it was also reported that these rodents show an endothermic response, increasing body temperature and oxygen consumption in response to noradrenaline intervention, suggesting that they are in fact endothermic poikilotherms (Hislop and Buffenstein, 1994). These puzzling observations were consistent with the idea that the endogenous heat production through an NST response in NMRs may be inefficient, but if and how NMRs thermoregulate remained not fully clear.

NST is a major heat production mechanism in mammals that relies on the function of UCP1 (Cannon, 2004). However, analysis of the NMR genome revealed unique amino acid changes in this protein (Gln146, Arg263, Trp264 and Thr303) within the site regulated by fatty acids and nucleotides (Kim *et al.*, 2011). It was then of interest to examine how these unusual characteristics of UCP1 impact the function of this thermogenic protein. To address this question, we characterized the functional state of NMR UCP1 *in vitro* and *in vivo* as well as the response of BAT to cold exposure and β3-adrenergic receptor activation.

In the *in vitro* experiments involving expression of NMR and mouse UCP1 forms in HEK 293 cells, the NMR and mouse UCP1-expressing cells showed similar oxygen consumption rate and pattern and dose dependency of the response to a specific UCP1 activator TTNPB. These results immediately suggested that NMR UCP1 may be functional. Analyses of oxygen consumption rate by isolated mitochondria further supported this idea; however, we found that the activity of NMR UCP1 was lower than that of the mouse ortholog. Surprisingly, the higher activity of mouse protein was not due to differences in the regulatory site, as mitochondria with the WT and mutant versions of mouse UCP1 showed a similar uncoupling activity. All UCP1 forms could also be inhibited by GDP. Perhaps, the lower activity of NMR UCP1 was due to some other mechanisms. Nevertheless, NMR UCP1 was clearly functional and could be both activated and inhibited, as expected for UCP1 proteins in other organisms.

Anatomical identification of three large depots of the BAT in the NMR under thermoneutral conditions was also surprising, considering the poikilothermic characteristics of these animals and their exploitation of thermally stable subterranean burrows with temperatures around 31–32 °C. While BAT hyperplasia is usually caused by adaptation to prolonged cold exposure in small mammals (Bukowiecki *et al.*, 1982), this might not be a case for the NMR. Instead the data suggest that the BAT may be used in an effort to maintain constant body temperature despite the inability maintain it for a prolonged period of time. Since the NMR is unable to increase its maximum NST capacity in response to prolonged cold exposure (Woodley and Buffenstein, 2002), it may lack some other features inherent to homoeothermic rodents. The presence of large NMR

BAT depots may be due to disuse and accumulation of lipid stores under laboratory housing conditions, similar to that in mice housed at thermoneutrality. In contrast, their presence might be explained if assumed that even in controlled laboratory conditions animals were exposed to temperatures slightly lower than 31 °C, which would be enough for employment of NST and thus for BAT accumulation. The NMR BAT depots expressed UCP1 and the isolated BAT mitochondria confirmed the TTNPB-activated and GDP-inhibited uncoupling activity, revealing their active state of the BAT and UCP1. However, the uncoupling activity of mouse BAT mitochondria was higher, consistent with the data in isolated mitochondria from HEK 293 cells. Cold-exposed NMRs lost most of their BAT mass. This is likely the result of NST-mediated heat production that further suggests an active effort to maintain constant body temperature. Once the BAT energy content is exhausted, the NMRs may not be able to summon energy from other depots and fail to buffer further temperature changes. There may also be more rapid heat-loss kinetics due to the lack of fur.

Our data on the ability to upregulate body temperature *in vivo* pharmacologically by stimulating β3-adrenergic receptors revealed that NMRs could strongly elevate temperature and metabolic rate in response to β3-adrenergic agonist injection. This finding is consistent with the results of the response to noradrenaline, which induces a wider thermogenic response (Hislop and Buffenstein, 1994; Cannon and Nedergaard, 2011). Although NMRs increased body temperature in both cases, there were differences. In our hands, NMRs showed no response to saline injection, whereas in the previous work there was a 0.8 ± 0.5 °C elevation in body temperature. It is possible that the

difference was due to exploitation of modern CLAMS, which subjects animals to lower stress and achieves more accurate measurements. The failure of the NMR to mount a modest stress response to saline administration appears to agree with a relative pain insensitivity reported in this species (Park *et al.*, 2008).

An interesting finding was also that NMRs increased body temperature and metabolic rate more than mice. This could probably be explained by the large amount of the BAT in the NMR, which could produce more heat per unit time even despite a lower UCP1 activity. It could also be that NMRs require lower agonist levels to induce the thermogenic response. In addition, it may be that for the NMRs, which were never housed outside their thermoneutral zone (31-34 °C) (Woodley, 2000), there could be a bigger stress that to the mouse (Gordon, 1995; Gordon, Becker and Ali, 1998; Cannon and Nedergaard, 2011). Alternatively, it might be explained by initially very low basal metabolic rate of NMRs, amongst the lowest recorded as a function of body size for all mammals (McNab, 1966; Woodley and Buffenstein, 2002), and thus a higher capacity for its elevation.

When we reinvestigated the regulation of NMR body temperature in response to exposure to a series of temperature conditions below NMR thermoneutrality (28 °C, 25 °C, 22 °C, and 18 °C), we confirmed the poikilothermic behavior of NMRs despite their apparent thermogenic response and body temperature upregulation during cold exposure. However, our data indicate that, bellow thermoneutrality, the average core body temperature of NMRs is at least 1.5-2 °C above the ambient temperature, in contrast to ~ 0.5 °C, previously reported (Buffenstein and Yahav, 1991). We suggest that longer

duration of our experiment compared to the original study, as well as greater accuracy of our data due to implantable temperature probes may explain the observed difference. Also, we found interesting that the body temperature of the NMRs fluctuated significantly when animals were below thermoneutrality, whereas it was almost constant at 32 °C. It seems that that NMRs regulate thermogenesis by switching it on and off on the scale of hours.

Overall, the inability of the NMR to maintain constant body temperature, together with its intact BAT thermogenesis machinery and functional UCP1, suggest a possible explanation for the poikilothermic behavior that involves a high level of heat loss due to the lack of fur and thus poor insulation of these rodents (Tucker, 1981).

Materials and methods

Animal ethics

The animal welfare, use, and care were carried out according to the protocols approved by the Institutional Animal Care and Use Committee (IACUC) of the Brigham and Women's Hospital, Harvard University, University of Illinois-Chicago and University of Rochester.

Stable expression of nmrUCP1 in HEK293 cells

For the analysis of NMR and mouse UCP1 in HEK 293 cells, mouse UCP1 CDS (GenBank: BC012701.1) and NMR UCP1 mRNA isolated from frozen tissues of these animals were transcribed to cDNA, cloned and used for stable transfection of Flp-In™ 293 T-REx cells (Invitrogen; R78007). Generation of stable cell lines exhibiting tetracycline-inducible expression of UCP1, and their growth and maintenance were performed in accordance with the manufacturer's instructions.

Western blotting

The expression of UCP1 was verified by immunoblot detection. Cells were lysed in ice-cold lysis buffer (20 mM Tris-HCl, pH 8.0, 137 mM NaCl, 10% (v/v) glycerol, 1% (v/v) Nonidet P-40, and 2 mM EDTA containing protease inhibitors (Roche Applied Science)), and the protein concentration of the homogenates was determined with the

Bradford assay (Bio-Rad). Cell homogenates were fractionated by SDS-PAGE using NuPAGE Novex gels (Invitrogen), and the separated proteins were transferred onto a PVDF membrane (Invitrogen), followed by blocking with 5% skim milk for 1 h, and an incubation with primary antibodies overnight at 4 °C. The membrane was washed with TBST (25 mM Tris, pH 7.4, 150 mM NaCl, 2 mM KCl and 0.01% Tween 20), incubated for 1 h at room temperature with secondary antibodies and then washed with TBST buffer again. Immunoreactive proteins were visualized using an enhanced chemiluminescence detection system (Pierce Biotechnology, Rockford, IL, USA).

UCP1 localization in HEK 293 cells

Cells expressing NMR or mouse UCP1 proteins were fixed using PBS containing 4% paraformaldehyde (Sigma) for 15 min at room temperature. After rinsing with PBS, fixed cells were blocked and permeabilized for 1 h in PBS containing 10% (v/v) goat serum (Sigma) in 0.1% Triton X-100-PBS. Fixed cells were incubated with primary anti-HA tag antibodies (Abcam) overnight at 4 °C. After washing out the unbound antibodies, fixed cells were incubated with secondary antibodies (labeled with Alexa 488, 1:200 dilution, Jackson ImmunoResearch) for 1 h at room temperature. Nuclei were counterstained using 1 mg/mL DAPI solution (Life Technologies; 62248). Mitochondrial localization was observed by staining with Mito-Tracker Red (Invitrogen, M7512) according to manufacturer's instructions. Fluorescence imaging was conducted using an LSM 700 confocal microscope (Zeiss).

Cellular oxygen consumption

Cells expressing mouse and NMR UCP1 were seeded into gelatin-coated XF24 culture microplates (Seahorse Bioscience) and cultured in DMEM (DMEM high glucose + GlutaMAX) with 10% FBS, 1X antibiotic/antimycotic overnight at 37 °C in an atmosphere of 5% CO_2. The XF24 plates were then transferred to a temperature-controlled (37 °C) XF24 Extracellular Flux analyzer (Seahorse Bioscience). Leak respiration was induced by addition of 1 μM oligomycin (inhibiting ATP synthase) by automatic pneumatic injection. Next, 10 μM of TTNPB (4-[(E)-2-(5,6,7,8- tetrahydro-5,5,8,8-tetramethyl-2-naphthalenyl)-1 propenyl]benzoic acid) diluted in dimethylsulphoxide was injected to specifically activate UCP1, followed by an injection of 0.5 μM FCCP (carbonyl cyanide p trifluoromethoxyphenylhydrazone) to completely uncouple mitochondria. Finally, injection of 2 μM rotenone with 1 μM antimycin A (respiratory chain inhibitors) was performed to measure basal non-mitochondrial respiration.

Isolation of mitochondria

Mitochondria were isolated from HEK 293T cells and BAT by homogenization and subsequent differential centrifugation. Homogenization was performed with Dounce homogenizer in extraction buffer (10 mM HEPES, pH 7.5, 200 mM mannitol, 70 mM sucrose, 1 mM EGTA, and 2 mg/ml BSA) containing protease inhibitor (Roche) and 20 mM N-ethylmaleimide. The homogenate was centrifuged at 600 g for 10 min and the supernatant was filtered through 250 μm diameter gauze. It was further centrifuged at

11,000 g for 10 min. The supernatant was the cytosolic fraction. The pellet was resuspended in extraction buffer without BSA and centrifuged at 600 g for 10 min. Then, the supernatant was re-centrifuged at 11,000 g for 10 min. Finally, the pellet was the mitochondrial fraction. Total mitochondrial protein concentration was quantified using the Bradford method. All steps were performed on ice or at 4 °C.

Mitochondrial respiration and membrane potential

Membrane potential of isolated mitochondria was measured by safranin O fluorescence (Sigma-Aldrich). Measurements were conducted in a XF24 microplates (Seahorse Bioscience). Fluorescence signal intensity was recorded at an excitation of 495 nm and an emission wavelength of 586 nm at 37 °C using a Seahorse XF96 Flux Analyzer (Seahorse Bioscience). Succinate was used to initiate mitochondrial respiration. TTNPB was used to specifically activate UCP1 and GDP for UCP1 inhibition. At the end, FCCP was injected to dissipate the membrane potential.

Comprehensive monitoring and thermal imaging of NMRs and mice

A total of 6 mice and 6 naked mole rats were placed on separate days into open-circuit Oxymax chambers, a component of the Comprehensive Lab Animal Monitoring System (CLAMS; Columbus Instruments) and maintained for a total of 9 h at thermoneutrality, within which saline injection and intraperitoneal injection of the selective β3-adrenergic receptor agonist CL316,243 (0.5 mg/kg) (Sigma Chemical) were performed for each animal. For body temperature monitoring during exposure to various

ambient temperatures, 5 NMRs were individually housed in the CLAMS for a total of 10 days. Mice were on Picolab Rodent Diet 5053 Chow and NMRs were on fresh yams (Star Market) upon entering the CLAMS. Post-mortem body compositions of mice were determined via EchoMRI after removing temperature probes. Body compositions of NMRs were determined via EchoMRI before the temperature probe implantation surgery. NMRs had one week recovery following surgery before entering the CLAMS. Thermal imaging of the dorsal side of the mouse and NMR were taken without anesthetizing with isoflurane and quantitated as described (Crane *et al.*, 2014). Body weights were obtained at the beginning and end of the experiment. Mice were acclimated for one day prior to the experiment. NMRs were not acclimated to maintain their group housing for as long as possible to avoid undue stress. Rates (ml/h) of O_2 consumption (V_{O2}) and CO_2 production (V_{CO2}), as well as core body temperatures were determined at 18 min intervals. Respiratory exchange ratio (RER) values were calculated as VCO2/VO2. Rates of energy expenditure (kcal/h) were calculated from gas exchange. Activity was determined according to beam breaks and food intake was measured gravimetrically. One mouse and 2 NMRs did not respond to beta 3-agonist and were excluded from data analysis.

Statistical analysis

All data are presented as mean values ± SEM. For statistical comparison, two-way ANOVA or two-tailed Student t test were performed. $p < 0.05$ was considered statistically significant.

Chapter 5

Conclusions

This dissertation is dedicated to comparative biology of aging with focus on the exceptionally long-lived species, the naked mole rat, interspecific models, and development and application of induced pluripotent stem cells as a new tool for comparative aging studies. iPSCs may help address many of the challenges related to the limited availability of biological samples from non-traditional model animals and serve as means of creating interspecific chimeras involving long- and short-lived species.

Using drug-inducible expression of Oct4, Sox2, Klf4, and c-Myc pluripotency-associated transcriptional factors, we generated iPSCs from fibroblasts of mouse, rat, and the longest-lived, cancer-resistant rodent, the naked mole rat. The established iPSCs were shown to display markers associated with pluripotency and form derivatives of all three germ layers *in vitro*. Interestingly, while rat and mouse iPSCs readily formed teratomas following injection to immunodeficient mice, naked mole rat iPSCs showed resistance to teratoma formation. They also showed other features such as propensity for a tetraploid karyotype. These naked mole rat iPSCs and the associated protocols should pave the way for generation of gene-targeted naked mole rat models for biomedical research and provide much needed cell culture systems to facilitate aging and cancer research at the cellular and molecular levels.

Remarkably, upon injection to mouse blastocysts, not only rat but also naked mole rat iPSCs contributed to interspecific embryonic chimeras, consistent with naïve pluripotency. The fact that naked mole rat iPSCs cells can divide and differentiate within mouse embryo despite faster gestation period (19-21 vs. ~70 days) and great evolutionary distance (70 million years) indicates that such paradigm-shifting models as chimeric

models between long- and short-lived species may be prepared and used for comparative aging studies and research on lifespan control and cancer prevention.

Analysis of age-related changes in full-term rat-mouse chimeric model revealed a striking loss of chimerism over time, suggesting lower survival of rat cells within the mouse host. These and other findings reveal a novel insight into chimerism and bring us closer to understanding the biology of interspecific mammalian chimeras.

Finally, as thermogenesis is an established regulator of lifespan and the naked mole is the only known poikilothermic mammal, we examined the link between thermoregulation and aging by performing comparative studies on thermogenesis between mice and naked mole rats. We showed that naked mole rat brown adipose tissue thermogenic machinery was intact and that mitochondrial protein UCP1 was functional despite the unique amino acid changes in the regulatory site. Continuous monitoring of NMR core body temperature in response to exposure to various ambient temperatures revealed clear yet limited capacity for its upregulation. With these data, we showed the poikilothermic behavior of NMRs despite their apparent thermogenic response and body temperature upregulation during cold exposure. Thereby, exhaustion of brown adipose tissue lipid content, heat loss and failure to access conventional white adipose energy stores may be among the factors contributing to a highly variable and poikilothermic pattern of body temperature in naked mole rats.

Overall, establishment of iPSCs from extremely long-lived animals and development of relevant interspecific chimeric models and new whole organism

thermogenic models open new avenues for studying the traits underlying exceptional longevity.

Bibliography

Akerman, K. E. O. and Wikstrom, M. K. F. (1976) 'Safranine as a Probe of Mitochondrial-Membrane Potential', *Febs Letters*, 68(2), pp. 191–197.

Andziak, B., Connor, T. P. O. and Buffenstein, R. (2005) 'Antioxidants do not explain the disparate longevity between mice and the longest-living rodent , the naked mole-rat', 126, pp. 1206–1212. doi: 10.1016/j.mad.2005.06.009.

Austad, S. N. (2001) 'An experimental paradigm for the study of slowly aging organisms', *Experimental Gerontology*, 36(4–6), pp. 599–605. doi: 10.1016/S0531-5565(00)00229-1.

Austad, S. N. (2009) 'Comparative biology of aging', *Journals of Gerontology - Series A Biological Sciences and Medical Sciences*, 64(2), pp. 199–201. doi: 10.1093/gerona/gln060.

Avilion, A. A. *et al.* (2003) 'Multipotent cell lineages in early mouse development depend on SOX2 function', *Genes and Development*, 17(1), pp. 126–140. doi: 10.1101/gad.224503.

Banito, A. *et al.* (2009) 'Senescence impairs successful reprogramming to pluripotent stem cells', *Genes and Development*. doi: 10.1101/gad.1811609.

Bedzhov, I. *et al.* (2014) 'Correction to: "Developmental plasticity, cell fate specification and morphogenesis in the early mouse embryo"', *Philosophical Transactions of the Royal Society B: Biological Sciences*, 370(1661), pp. 20140339–20140339. doi:

10.1098/rstb.2014.0339.

Bennett, N. C., Jarvis, J. U. M. and Davies, K. C. (1988) 'Daily and seasonal temperatures in the burrows of African rodent moles', *South African Journal of Zoology*, 3(3), pp. 189–195. doi: 10.1080/02541858.1988.11448101.

Blakeley, P. *et al.* (2015) 'Defining the three cell lineages of the human blastocyst by single-cell RNA-seq', *Development*, 142(18), pp. 3151–3165. doi: 10.1242/dev.123547.

Bongso, A. *et al.* (1994) 'Isolation and culture of inner cell mass cells from human blastocysts', *Human Reproduction*, 9(11), pp. 2110–2117.

Boroviak, T. *et al.* (2014) 'The ability of inner-cell-mass cells to self-renew as embryonic stem cells is acquired following epiblast specification', *Nature Cell Biology*, 16(6), pp. 513–525. doi: 10.1038/ncb2965.

Boyer, L. A. *et al.* (2005) 'Core transcriptional regulatory circuitry in human embryonic stem cells', *Cell*, 122(6), pp. 947–956. doi: 10.1016/j.cell.2005.08.020.

Brambrink, T. *et al.* (2008) 'Sequential Expression of Pluripotency Markers during Direct Reprogramming of Mouse Somatic Cells', *Cell Stem Cell*, 2(2), pp. 151–159. doi: 10.1016/j.stem.2008.01.004.

Brons, I. G. M. *et al.* (2007) 'Derivation of pluripotent epiblast stem cells from mammalian embryos', *Nature*, 448(7150), pp. 191–195. doi: 10.1038/nature05950.

Buehr, M. *et al.* (2008) 'Capture of Authentic Embryonic Stem Cells from Rat Blastocysts', *Cell*. Elsevier Ltd, 135(7), pp. 1287–1298. doi: 10.1016/j.cell.2008.12.007.

Buffenstein, R. (2005) 'The Naked Mole-Rat : A New Long-Living Model for Human Aging Research', *Journal of gerontology*, 60(11), pp. 1369–1377. doi:

10.1093/gerona/60.11.1369.

Buffenstein, R. *et al.* (2012) 'Naked Mole Rat', *The Laboratory Rabbit, Guinea Pig, Hamster, and Other Rodents*, pp. 1055–1074. doi: 10.1016/B978-0-12-380920-9.00045-6.

Buffenstein, R. and Yahav, S. (1991) 'Is the naked mole-rat Hererocephalus glaber an endothermic yet poikilothermic mammal?', *Journal of Thermal Biology*, 16(4), pp. 227–232. doi: 10.1016/0306-4565(91)90030-6.

Buganim, Y. *et al.* (2012) 'Single-cell expression analyses during cellular reprogramming reveal an early stochastic and a late hierarchic phase', *Cell*. Elsevier Inc., 150(6), pp. 1209–1222. doi: 10.1016/j.cell.2012.08.023.

Buganim, Y., Faddah, D. A. and Jaenisch, R. (2013) 'Mechanisms and models of somatic cell reprogramming', *Nature Reviews Genetics*, 14(6), pp. 427–439. doi: 10.1038/nrg3473.

Bukowiecki, L. *et al.* (1982) 'Brown adipose tissue hyperplasia: a fundamental mechanism of adaptation to cold and hyperphagia.', *The American journal of physiology*, 242(6), pp. E353–E359. Available at: http://www.ncbi.nlm.nih.gov/pubmed/6953766.

Cannon, B. (2004) 'Brown Adipose Tissue: Function and Physiological Significance', *Physiological Reviews*, 84(1), pp. 277–359. doi: 10.1152/physrev.00015.2003.

Cannon, B. and Nedergaard, J. (2011) 'Nonshivering thermogenesis and its adequate measurement in metabolic studies', *Journal of Experimental Biology*, 214(2), pp. 242–253. doi: 10.1242/jeb.050989.

Cannon, B. and Nedergaard, J. (2017) 'What Ignites UCP1?', *Cell Metabolism*. Elsevier

Inc., 26(5), pp. 697–698. doi: 10.1016/j.cmet.2017.10.012.

Capecchi, M. R. (2005) 'Gene targeting in mice: functional analysis of the mammalian genome for the twenty-first century', *Nature Reviews Genetics*, 6(6), pp. 507–512. doi: 10.1038/nrg1619.

Carey, B. W. *et al.* (2009) 'Reprogramming of murine and human somatic cells using a single polycistronic vector.', *Proceedings of the National Academy of Sciences of the United States of America*, 106(1), pp. 157–62. doi: 10.1073/pnas.0811426106.

Carneheim, C., Nedergaard, J. and Cannon, B. (1984) 'Beta-adrenergic stimulation of lipoprotein lipase in rat brown adipose tissue during acclimation to cold.', *The American journal of physiology*, 246(4 Pt 1), pp. E327-33. Available at: http://www.ncbi.nlm.nih.gov/pubmed/6372506.

Chen, Y., Blair, K. and Smith, A. (2013) 'Robust self-renewal of rat embryonic stem cells requires fine-tuning of glycogen synthase kinase-3 inhibition', *Stem Cell Reports*. The Authors, 1(3), pp. 209–217. doi: 10.1016/j.stemcr.2013.07.003.

Crane, J. D. *et al.* (2014) 'A standardized infrared imaging technique that specifically detects UCP1-mediated thermogenesis invivo', *Molecular Metabolism*. Elsevier GmbH, 3(4), pp. 490–494. doi: 10.1016/j.molmet.2014.04.007.

Crichton, P. G., Lee, Y. and Kunji, E. R. S. (2017) 'The molecular features of uncoupling protein 1 support a conventional mitochondrial carrier-like mechanism', *Biochimie*. Elsevier B.V, 134, pp. 35–50. doi: 10.1016/j.biochi.2016.12.016.

Daly, T. J., Williams, L. A. and Buffenstein, R. (1997) 'Catecholaminergic innervation of interscapular brown adipose tissue in the naked mole-rat (Heterocephalus glaber)', *J*

Anat, 190 (Pt 3, pp. 321–326. doi: 10.1046/j.1469-7580.1997.19030321.x.

Davidson, K. C., Mason, E. A. and Pera, M. F. (2015) 'The pluripotent state in mouse and human', *Development*, 142(18), pp. 3090–3099. doi: 10.1242/dev.116061.

Deweerdt, S. (2012) 'Comparative biology: Looking for a master switch', *Nature*, 492(7427), pp. S10–S11. doi: 10.1038/492S10a.

Dietrich, J.-E. and Hiiragi, T. (2007) 'Stochastic patterning in the mouse pre-implantation embryo', *Development*, 134(23), pp. 4219–4231. doi: 10.1242/dev.003798.

Dorman, J. B. *et al.* (1995) 'The age-1 and daf-2 genes function in a common pathway to control the lifespan of Caenorhabditis elegans', *Genetics*, 141(4), pp. 1399–1406.

Edrey, Y. H. *et al.* (2011) 'Endocrine function and neurobiology of the longest-living rodent, the naked mole-rat', *Experimental Gerontology*. Elsevier Inc., 46(2–3), pp. 116–123. doi: 10.1016/j.exger.2010.09.005.

Endo, H. *et al.* (2002) 'Localization of the cytochrome p450 side-chain cleavage enzyme in the inactive testis of the naked mole-rat.', *Zoological science*, 19(6), pp. 673–8. doi: 10.2108/zsj.19.673.

Esteban, M. A. *et al.* (2009) 'Generation of induced pluripotent stem cell lines from Tibetan miniature pig', *Journal of Biological Chemistry*, 284(26), pp. 17634–17640. doi: 10.1074/jbc.M109.008938.

Evans, M. J. and Kaufman, M. H. (1981) *Establishment in culture of pluripotential cells from mouse embryos*, *Nature*. doi: 10.1038/292154a0.

Faulkes, C. G. and Abbott, D. H. (1991) 'Social control of reproduction in breeding and non-breeding male naked mole-rats (Heterocephalus glaber).', *Journal of reproduction*

and fertility, 93, pp. 427–435. doi: 10.1530/jrf.0.0930427.

Faulkes, C. G. and Abbott, D. H. (1993) 'Evidence that primer pheromones do not cause social suppression of reproduction in male and female naked mole-rats (Heterocephalus glaber).', *Journal of reproduction and fertility*, 99(December), pp. 225–230. doi: 10.1530/jrf.0.0990225.

Faulkes, C. G., Abbott, D. H. and Jarvis, J. U. M. (1990) 'Social suppression of ovarian cyclicity in captive and wild colonies of naked mole-rats, Heterocephalus glaber.', *Journal of reproduction and fertility*, 88(2), pp. 559–568. doi: 10.1530/jrf.0.0910593.

Fehilly, C. B., Willadsen, S. M. and Tucker, E. M. (1984) 'Interspecific chimaerism between sheep and goat', *Nature*, 307(5952), pp. 634–636. doi: 10.1038/307634a0.

Gardner, R. L. and Johnson, M. H. (1973) 'Investigation of early mammalian development using interspecific chimaeras between rat and mouse', *Nature New Biology*, 246(151), pp. 86–89. doi: 10.1038/newbio246086a0.

Golipour, A. *et al.* (2012) 'A late transition in somatic cell reprogramming requires regulators distinct from the pluripotency network', *Cell Stem Cell*. Elsevier Inc., 11(6), pp. 769–782. doi: 10.1016/j.stem.2012.11.008.

Gorbunova, V. *et al.* (2014) 'Comparative genetics of longevity and cancer: insights from long-lived rodents.', *Nature reviews. Genetics*. Nature Publishing Group, 15(8), pp. 531–40. doi: 10.1038/nrg3728.

Gorbunova, V., Bozzella, M. J. and Seluanov, A. (2008) 'Rodents for comparative aging studies: From mice to beavers', *Age*, 30(2–3), pp. 111–119. doi: 10.1007/s11357-008-9053-4.

Gordon, C. J. (1995) *Temperature Regulation in Laboratory Rodents*, *Journal of anatomy*. doi: 10.1017/CBO9780511565595.

Gordon, C. J., Becker, P. and Ali, J. S. (1998) 'Behavioral thermoregulatory responses of single- and group-housed mice', *Physiology and Behavior*, 65(2), pp. 255–262. doi: 10.1016/S0031-9384(98)00148-6.

Griggio, M. A. (1982) 'the Participation of Shivering and Cold-Acclimated Rats', 73(3), pp. 0–3. doi: https://doi.org/10.1016/0300-9629(82)90189-X.

Guo, G. *et al.* (2009) 'Klf4 reverts developmentally programmed restriction of ground state pluripotency', *Development*, 136(7), pp. 1063–1069. doi: 10.1242/dev.030957.

Gurdon, J. B. (1962) 'The developmental capacity of nuclei taken from intestinal epithelium cells of feeding tadpoles.', *Journal of embryology and experimental morphology*, 10(4), pp. 622–40. doi: 10.1002/stem.684.

Hanna, J. *et al.* (2009) 'Direct cell reprogramming is a stochastic process amenable to acceleration', *Nature*. Nature Publishing Group, 462(7273), pp. 595–601. doi: 10.1038/nature08592.

Hansson, J. *et al.* (2012) 'Highly Coordinated Proteome Dynamics during Reprogramming of Somatic Cells to Pluripotency', *Cell Reports*. The Authors, 2(6), pp. 1579–1592. doi: 10.1016/j.celrep.2012.10.014.

Hayashi, K. *et al.* (2008) 'Dynamic Equilibrium and Heterogeneity of Mouse Pluripotent Stem Cells with Distinct Functional and Epigenetic States', *Cell Stem Cell*, 3(4), pp. 391–401. doi: 10.1016/j.stem.2008.07.027.

Hetling, J. R. *et al.* (2005) 'Features of visual function in the naked mole-rat

Heterocephalus glaber', *Journal of Comparative Physiology A: Neuroethology, Sensory, Neural, and Behavioral Physiology*, 191(4), pp. 317–330. doi: 10.1007/s00359-004-0584-6.

Hislop, M. S. and Buffenstein, R. (1994) 'Noradrenaline induces nonshivering thermogenesis in both the naked mole-rat (Heterocephalus glaber) and the Damara mole-rat (Cryptomys damarensis) despite very different modes of thermoregulation', *Journal of Thermal Biology*, 19(1), pp. 25–32. doi: 10.1016/0306-4565(94)90006-X.

Hockemeyer, D. *et al.* (2008) 'A Drug-Inducible System for Direct Reprogramming of Human Somatic Cells to Pluripotency', *Cell Stem Cell*, 3(3), pp. 346–353. doi: 10.1016/j.stem.2008.08.014.

Holmes, M. M. *et al.* (2007) 'Social control of brain morphology in a eusocial mammal.', *Pnas*, 104(25), pp. 10548–52. doi: 10.1073/pnas.0610344104.

Holmes, M. M. *et al.* (2009) 'Frontiers in Neuroendocrinology Neuroendocrinology and sexual differentiation in eusocial mammals', *Frontiers in Neuroendocrinology*. Elsevier Inc., 30(4), pp. 519–533. doi: 10.1016/j.yfrne.2009.04.010.

Huang, Y. *et al.* (2012) 'In Vivo Differentiation Potential of Epiblast Stem Cells Revealed by Chimeric Embryo Formation', *Cell Reports*. The Authors, 2(6), pp. 1571–1578. doi: 10.1016/j.celrep.2012.10.022.

Husson, Z. and Smith, E. S. J. (2018) 'Naked mole-rat cortical neurons are resistant to acid-induced cell death', *Molecular Brain*. Molecular Brain, 11(1), pp. 1–10. doi: 10.1186/s13041-018-0369-4.

Jarvis, J. U. (1981) 'Eusociality in a mammal: cooperative breeding in naked mole-rat

colonies.', *Science*, 212(4494), pp. 571–573. doi: 10.1126/science.7209555.

Johansen, K. *et al.* (1976) 'Blood respiratory properties in the naked mole rat Heterocephalus glaber, a mammal of low body temperature', *Respiration Physiology*, 28(3), pp. 303–314. doi: 10.1016/0034-5687(76)90025-6.

Judd, T. M. and Sherman, P. W. (1996) 'Naked mole-rats recruit colony mates to food sources', *Animal Behaviour*, pp. 957–969. doi: 10.1006/anbe.1996.0244.

Kapahi, P. *et al.* (2004) 'Regulation of lifespan in Drosophila by modulation of genes in the TOR signaling pathway', *Current Biology*, 14(10), pp. 885–890. doi: 10.1016/j.cub.2004.03.059.

Kenyon, C. J. (2010) 'The genetics of ageing', *Nature*, 464(7288), pp. 504–512. doi: 10.1038/nature08980.

Kim, E. B. *et al.* (2011) 'Genome sequencing reveals insights into physiology and longevity of the naked mole rat', *Nature*. Nature Publishing Group, 479(7372), pp. 223–227. doi: 10.1038/nature10533.

Knoepfler, P. S. (2008) 'Why Myc? An Unexpected Ingredient in the Stem Cell Cocktail', *Cell Stem Cell*, 2(1), pp. 18–21. doi: 10.1016/j.stem.2007.12.004.

Kobayashi, T. *et al.* (2010) 'Generation of Rat Pancreas in Mouse by Interspecific Blastocyst Injection of Pluripotent Stem Cells', *Cell*. Elsevier Ltd, 142(5), pp. 787–799. doi: 10.1016/j.cell.2010.07.039.

Kock, D. *et al.* (2006) 'On the nomenclature of Bathyergidae and Fukomys n. gen. (Mammalia: Rodentia)', *Zootaxa*, 55(1142), pp. 51–55. doi: print.

Kojima, Y. *et al.* (2014) 'The transcriptional and functional properties of mouse epiblast

stem cells resemble the anterior primitive streak', *Cell Stem Cell*. Elsevier Inc., 14(1), pp. 107–120. doi: 10.1016/j.stem.2013.09.014.

Koopman, P. and Cotton, R. G. (1984) 'A factor produced by feeder cells which inhibits embryonal carcinoma cell differentiation. Characterization and partial purification', *Exp Cell Res*, 154(1), pp. 233–242.

Larson, J. and Park, T. J. (2009) 'Extreme hypoxia tolerance of naked mole-rat brain', *NeuroReport*, 20(18), pp. 1634–1637. doi: 10.1097/WNR.0b013e32833370cf.

LaVinka, P. C. and Park, T. J. (2012) 'Blunted Behavioral and C Fos Responses to Acidic Fumes in the African Naked Mole-Rat', *PLoS ONE*, 7(9). doi: 10.1371/journal.pone.0045060.

Lewis, K. N. *et al.* (2012) 'Stress resistance in the naked mole-rat: The bare essentials - A mini-review', *Gerontology*, 58(5), pp. 453–462. doi: 10.1159/000335966.

Lewis, K. N. *et al.* (2016) 'Unraveling the message: insights into comparative genomics of the naked mole-rat', *Mammalian Genome*. Springer US, pp. 259–278. doi: 10.1007/s00335-016-9648-5.

Lewis, K. N. and Buffenstein, R. (2015) 'The Naked Mole-Rat: A Resilient Rodent Model of Aging, Longevity, and Healthspan. A Resilient Rodent Model of Aging, Longevity, and Healthspan', *Handbook of the Biology of Aging: Eighth Edition*, pp. 179–204. doi: 10.1016/B978-0-12-411596-5.00006-X.

Li, P. *et al.* (2008) 'Germline Competent Embryonic Stem Cells Derived from Rat Blastocysts', *Cell*. Cell Press, 135(7), pp. 1299–1310. doi: 10.1016/j.cell.2008.12.006.

Li, R. *et al.* (2010) 'A mesenchymal-to-Epithelial transition initiates and is required for

the nuclear reprogramming of mouse fibroblasts', *Cell Stem Cell*, 7(1), pp. 51–63. doi: 10.1016/j.stem.2010.04.014.

Li, W. *et al.* (2009) *Generation of Rat and Human Induced Pluripotent Stem Cells by Combining Genetic Reprogramming and Chemical Inhibitors (DOI:10.1016/j.stem.2008.11.014)*, *Cell Stem Cell*. Cell Press. doi: 10.1016/j.stem.2009.03.002.

Liang, S. *et al.* (2010) 'Resistance to experimental tumorigenesis in cells of a long-lived mammal, the naked mole-rat (Heterocephalus glaber)', *Aging Cell*, 9(4), pp. 626–635. doi: 10.1111/j.1474-9726.2010.00588.x.

Liao, J. *et al.* (2009) 'Generation of Induced Pluripotent Stem Cell Lines from Adult Rat Cells', *Cell Stem Cell*. Elsevier Inc., 4(1), pp. 11–15. doi: 10.1016/j.stem.2008.11.013.

Lin, L., Hale, S. P. and Schimmel, P. (1996) 'Aminoacylation error correction', *Nature*, 384(6604), pp. 33–34. doi: 10.1038/384033b0.

Lin, S. J., Defossez, P. A. and Guarente, L. (2000) 'Requirement of NAD and SIR2 for life-span extension by calorie restriction in saccharomyces cerevisiae', *Science*, 289(5487), pp. 2126–2128. doi: 10.1126/science.289.5487.2126.

Liu, H. *et al.* (2008) 'Generation of Induced Pluripotent Stem Cells from Adult Rhesus Monkey Fibroblasts', *Cell Stem Cell*, pp. 587–590. doi: 10.1016/j.stem.2008.10.014.

De Los Angeles, A. *et al.* (2015) 'Hallmarks of pluripotency', *Nature*, 525(7570), pp. 469–478. doi: 10.1038/nature15515.

Ludwig, T. E. *et al.* (2006) 'Derivation of human embryonic stem cells in defined conditions', *Nature Biotechnology*, 24(2), pp. 185–187. doi: 10.1038/nbt1177.

Magalhaes, J. P. d., Costa, J. and Church, G. M. (2007) 'An Analysis of the Relationship Between Metabolism, Developmental Schedules, and Longevity Using Phylogenetic Independent Contrasts', *The Journals of Gerontology Series A: Biological Sciences and Medical Sciences*, 62(2), pp. 149–160. doi: 10.1093/gerona/62.2.149.

Maherali, N. *et al.* (2007) 'Directly Reprogrammed Fibroblasts
Show Global Epigenetic Remodeling and Widespread Tissue Contribution', *Cell Stem Cell*, 1(1), pp. 55–70. doi: 10.1016/j.stem.2007.05.014.

Maherali, N. and Hochedlinger, K. (2009) 'Tgfβ Signal Inhibition Cooperates in the Induction of iPSCs and Replaces Sox2 and cMyc', *Current Biology*. Elsevier, 19(20), pp. 1718–1723. doi: 10.1016/j.cub.2009.08.025.

Mansour, A. A. *et al.* (2012) 'The H3K27 demethylase Utx regulates somatic and germ cell epigenetic reprogramming', *Nature*. Nature Publishing Group, 488(7411), pp. 409–413. doi: 10.1038/nature11272.

Marion, R. M. *et al.* (2009) 'Telomeres Acquire Embryonic Stem Cell Characteristics in Induced Pluripotent Stem Cells', *Cell Stem Cell*. Elsevier Inc., 4(2), pp. 141–154. doi: 10.1016/j.stem.2008.12.010.

Martí, M. *et al.* (2013) 'Characterization of pluripotent stem cells', *Nature Protocols*, 8(2), pp. 223–253. doi: 10.1038/nprot.2012.154.

Martin, G. R. (1981) 'Isolation of a pluripotent cell line from early mouse embryos cultured in medium conditioned by teratocarcinoma stem cells.', *Proceedings of the National Academy of Sciences*, 78(12), pp. 7634–7638. doi: 10.1073/pnas.78.12.7634.

Masaki, H. *et al.* (2016) 'Inhibition of Apoptosis Overcomes Stage-Related Compatibility

Barriers to Chimera Formation in Mouse Embryos', *Cell Stem Cell*. Elsevier Inc., 19(5), pp. 587–592. doi: 10.1016/j.stem.2016.10.013.

Mascetti, V. L. and Pedersen, R. A. (2016) 'Human-Mouse Chimerism Validates Human Stem Cell Pluripotency', *Cell Stem Cell*. The Authors, 18(1), pp. 67–72. doi: 10.1016/j.stem.2015.11.017.

McGaugh, S. and Schwartz, T. S. (2017) 'Here and there, but not everywhere: repeated loss of *uncoupling protein 1* in amniotes', *Biology Letters*, 13(1), p. 20160749. doi: 10.1098/rsbl.2016.0749.

McNab, B. K. (1966) 'The Metabolism of Fossorial Rodents: A Study of Convergence', *Ecology*, 47(5), pp. 712–733. doi: 10.2307/1934259.

McNab, B. K. (1979) 'The Influence of Body Size on the Energetics and Distribution of Fossorial and Burrowing Mammals', *Ecology*, 60(5), pp. 1010–1021. doi: 10.2307/1936869.

Meissner, A., Wernig, M. and Jaenisch, R. (2007) 'Direct reprogramming of genetically unmodified fibroblasts into pluripotent stem cells', *Nature Biotechnology*, 25(10), pp. 1177–1181. doi: 10.1038/nbt1335.

Messerschmidt, D. M. and Kemler, R. (2010) 'Nanog is required for primitive endoderm formation through a non-cell autonomous mechanism', *Developmental Biology*. Elsevier Inc., 344(1), pp. 129–137. doi: 10.1016/j.ydbio.2010.04.020.

Mitsui, K. *et al.* (2003) 'The Homeoprotein Nanog Is Required for Maintenance of Pluripotency in Mouse Epiblast and ES Cells', *Cell*, 113(5), pp. 631–642. doi: 10.1016/S0092-8674(03)00393-3.

Moy, S. S. *et al.* (2004) 'Sociability and preference for social novelty in five inbred strains: An approach to assess autistic-like behavior in mice', *Genes, Brain and Behavior*, 3(5), pp. 287–302. doi: 10.1111/j.1601-1848.2004.00076.x.

Nichols, J. *et al.* (1998) 'Formation of Pluripotent Stem Cells in the Mammalian Embryo Depends on the POU Transcription Factor Oct4', *Cell*, 95(3), pp. 379–391. doi: 10.1016/S0092-8674(00)81769-9.

Nichols, J. and Smith, A. (2009) 'Naive and Primed Pluripotent States', *Cell Stem Cell*. Elsevier Inc., 4(6), pp. 487–492. doi: 10.1016/j.stem.2009.05.015.

Nichols, J. and Smith, A. (2011) 'The origin and identity of embryonic stem cells', *Development*, 138(1), pp. 3–8. doi: 10.1242/dev.050831.

Niwa, H. *et al.* (1998) 'Self-renewal of pluripotent embryonic stem cells is mediated via activation of STAT3', *Genes & Development*, 12(13), pp. 2048–2060. doi: 10.1101/gad.12.13.2048.

Ohtsuka, S., Nishikawa-Torikai, S. and Niwa, H. (2012) 'E-Cadherin Promotes Incorporation of Mouse Epiblast Stem Cells into Normal Development', *PLoS ONE*, 7(9). doi: 10.1371/journal.pone.0045220.

Omerbašić, D. *et al.* (2016) 'Hypofunctional TrkA Accounts for the Absence of Pain Sensitization in the African Naked Mole-Rat', *Cell Reports*, 17(3), pp. 748–758. doi: 10.1016/j.celrep.2016.09.035.

Orr, M. E. *et al.* (2016) 'Extended postnatal brain development in the longest-lived rodent: Prolonged maintenance of neotenous traits in the naked mole-rat brain', *Frontiers in Neuroscience*, 10(NOV), pp. 1–17. doi: 10.3389/fnins.2016.00504.

Osorno, R. *et al.* (2012) 'The developmental dismantling of pluripotency is reversed by ectopic Oct4 expression', *Development*, 139(13), pp. 2288–2298. doi: 10.1242/dev.078071.

Pan, H. and Finkel, T. (2017) 'Key proteins and pathways that regulate lifespan', *Journal of Biological Chemistry*, 292(16), pp. 6452–6460. doi: 10.1074/jbc.R116.771915.

Park, I. H. *et al.* (2008) 'Disease-Specific Induced Pluripotent Stem Cells', *Cell*, 134(5), pp. 877–886. doi: 10.1016/j.cell.2008.07.041.

Park, T. J. *et al.* (2008) 'Selective inflammatory pain insensitivity in the African naked mole-rat (Heterocephalus glaber)', *PLoS Biology*, 6(1), pp. 0156–0170. doi: 10.1371/journal.pbio.0060013.

Park, T. J. *et al.* (2017) 'Fructose-driven glycolysis supports anoxia resistance in the naked mole-rat', *Science*, 356(6335), pp. 307–311. doi: 10.1126/science.aab3896.

Penz, O. K. *et al.* (2015) 'Protracted brain development in a rodent model of extreme longevity', *Scientific Reports*. Nature Publishing Group, 5, pp. 1–17. doi: 10.1038/srep11592.

Peroulakis, M. E., Goldman, B. and Forger, N. G. (2002) 'Perineal muscles and motoneurons are sexually monomorphic in the naked mole-rat (Heterocephalus glaber)', *Journal of Neurobiology*, 51(1), pp. 33–42. doi: 10.1002/neu.10039.

Pinto, M. *et al.* (2010) 'Lack of sexual dimorphism in femora of the eusocial and hypogonadic naked mole-rat : A novel animal model for the study of delayed puberty on the skeletal system', *Bone*. Elsevier Inc., 46(1), pp. 112–120. doi: 10.1016/j.bone.2009.08.060.

Plath, K. and Lowry, W. E. (2011) 'Progress in understanding reprogramming to the induced pluripotent state', *Nature Reviews Genetics*. Nature Publishing Group, 12(4), pp. 253–265. doi: 10.1038/nrg2955.

Polo, J. M. *et al.* (2010) 'Cell type of origin influences the molecular and functional properties of mouse induced pluripotent stem cells', *Nature Biotechnology*. Nature Publishing Group, 28(8), pp. 848–855. doi: 10.1038/nbt.1667.

Polo, J. M. *et al.* (2012) 'A molecular roadmap of reprogramming somatic cells into iPS cells', *Cell*. Elsevier Inc., 151(7), pp. 1617–1632. doi: 10.1016/j.cell.2012.11.039.

Polo, J. M. and Hochedlinger, K. (2010) 'When fibroblasts MET iPSCs', *Cell Stem Cell*. Elsevier Inc., 7(1), pp. 5–6. doi: 10.1016/j.stem.2010.05.018.

Pride, H. *et al.* (2015) 'Long-lived species have improved proteostasis compared to phylogenetically-related shorter-lived species', *Biochemical and Biophysical Research Communications*, 457(4), pp. 669–675. doi: 10.1016/j.bbrc.2015.01.046.

Rial, E. *et al.* (1999) 'Retinoids activate proton transport by the uncoupling proteins UCP1 and UCP2', *EMBO Journal*, 18(21), pp. 5827–5833. doi: 10.1093/emboj/18.21.5827.

Rodriguez, K. A. *et al.* (2016) 'Mechanisms regulating proteostasis are involved in sympatric speciation of the blind mole rat, Spalax galili', *Autophagy*. Taylor & Francis, 12(4), pp. 703–704. doi: 10.1080/15548627.2016.1143592.

Rossant, J. *et al.* (1983) 'Interspecific hybrids and chimeras in mice', *Journal of Experimental Zoology*, 228(2), pp. 223–233. doi: 10.1002/jez.1402280208.

Rossant, J. (2008) 'Stem Cells and Early Lineage Development', *Cell*, 132(4), pp. 527–

531. doi: 10.1016/j.cell.2008.01.039.

Rossant, J. (2015) 'Mouse and human blastocyst-derived stem cells: vive les differences', *Development*, 142(1), pp. 9–12. doi: 10.1242/dev.115451.

Rossant, J. and Frels, W. I. (1980) 'Interspecific chimeras in mammals: successful production of live chimeras between Mus musculus and Mus caroli', *Science (New York, N.Y.)*, 208(4442), pp. 419–421. doi: 10.1126/science.7367871.

Samavarchi-Tehrani, P. *et al.* (2010) 'Functional genomics reveals a BMP-Driven mesenchymal-to-Epithelial transition in the initiation of somatic cell reprogramming', *Cell Stem Cell*. Elsevier Inc., 7(1), pp. 64–77. doi: 10.1016/j.stem.2010.04.015.

Schnerch, A., Cerdan, C. and Bhatia, M. (2010) 'Distinguishing between mouse and human pluripotent stem cell regulation: The best laid plans of mice and men', *Stem Cells*, 28(3), pp. 419–430. doi: 10.1002/stem.298.

Schreiber, R. *et al.* (2017) 'Cold-Induced Thermogenesis Depends on ATGL-Mediated Lipolysis in Cardiac Muscle, but Not Brown Adipose Tissue', *Cell Metabolism*. Elsevier Inc., 26(5), p. 753–763.e7. doi: 10.1016/j.cmet.2017.09.004.

Seluanov, A. *et al.* (2009) 'Hypersensitivity to contact inhibition provides a clue to cancer resistance of naked mole-rat', *Proceedings of the National Academy of Sciences*, 106(46), pp. 19352–19357. doi: 10.1073/pnas.0905252106.

Shin, H. *et al.* (2017) 'Lipolysis in Brown Adipocytes Is Not Essential for Cold-Induced Thermogenesis in Mice', *Cell Metabolism*. Elsevier Inc., 26(5), p. 764–777.e5. doi: 10.1016/j.cmet.2017.09.002.

Silva, J. *et al.* (2009) 'Nanog Is the Gateway to the Pluripotent Ground State', *Cell*.

Elsevier Ltd, 138(4), pp. 722–737. doi: 10.1016/j.cell.2009.07.039.

Smith, A. (2017) 'Formative pluripotency: the executive phase in a developmental continuum', *Development*, 144(3), pp. 365–373. doi: 10.1242/dev.142679.

Smith, A. G. *et al.* (1988) 'Inhibition of pluripotential embryonic stem cell differentiation by purified polypeptides', *Nature*, 336(6200), pp. 688–690. doi: 10.1038/336688a0.

Smith, E. S. J. *et al.* (2011) 'The molecular basis of acid insensitivity in the African naked mole-rat', *Science*, 334(6062), pp. 1557–1560. doi: 10.1126/science.1213760.

Smith, R. E. *et al.* (1969) 'Brown fat and thermogenesis.', *Physiological reviews*, 49(2), pp. 330–425. doi: 10.1152/physrev.1969.49.2.330.

Smith, T. A. and Hooper, M. L. (1983) 'Medium conditioned by feeder cells inhibits the differentiation of embryonal carcinoma cultures', *Experimental Cell Research*, 145(2), pp. 458–462. doi: 10.1016/0014-4827(83)90025-3.

Smith, T. E., Faulkes, C. G. and Abbott, D. H. (1997) 'Combined Olfactory Contact with the Parent Colony and Direct Contact with Nonbreeding Animals Does Not Maintain Suppression of Ovulation in Female Naked Mole-Rats (Heterocephalus glaber)', 288, pp. 277–288.

Smith, Z. D. *et al.* (2010) 'Dynamic single-cell imaging of direct reprogramming reveals an early specifying event', *Nature Biotechnology*. Nature Publishing Group, 28(5), pp. 521–526. doi: 10.1038/nbt.1632.

Speakman, J. R. (2013) 'Measuring energy metabolism in the mouse - theoretical, practical, and analytical considerations', *Frontiers in Physiology*, 4 MAR(March), pp. 1–23. doi: 10.3389/fphys.2013.00034.

Sridharan, R. *et al.* (2009) 'Role of the Murine Reprogramming Factors in the Induction of Pluripotency', *Cell*, 136(2), pp. 364–377. doi: 10.1016/j.cell.2009.01.001.

Stadtfeld, M. *et al.* (2008) 'Defining Molecular Cornerstones during Fibroblast to iPS Cell Reprogramming in Mouse', *Cell Stem Cell*, 2(3), pp. 230–240. doi: 10.1016/j.stem.2008.02.001.

Stevens, L. C. (1970) 'The development of transplantable teratocarcinomas from intratesticular grafts of pre- and postimplantation mouse embryos', *Developmental Biology*, 21(3), pp. 364–382. doi: 10.1016/0012-1606(70)90130-2.

Stevens, L. C. and Little, C. C. (1954) 'Spontaneous Testicular Teratomas in an Inbred Strain of Mice', *Proceedings of the National Academy of Sciences*, 40(11), pp. 1080–1087. doi: 10.1073/pnas.40.11.1080.

Suchy, F. and Nakauchi, H. (2017) 'Lessons from Interspecies Mammalian Chimeras', *Annu. Rev. Cell Dev. Biol. The Annual Review of Cell and Developmental Biology*, 332215, pp. 1–22. doi: 10.1146/annurev-cellbio-100616.

Tacutu, R. *et al.* (2013) 'Human Ageing Genomic Resources: Integrated databases and tools for the biology and genetics of ageing', *Nucleic Acids Research*, 41(D1), pp. 1027–1033. doi: 10.1093/nar/gks1155.

Tada, M. *et al.* (2001) 'Nuclear reprogramming of somatic cells by in vitro hybridization with ES cells.', *Current biology : CB*, 11(19), pp. 1553–8. doi: 10.1016/S0960-9822(01)00459-6.

Takahashi, K. *et al.* (2007) 'Induction of Pluripotent Stem Cells from Adult Human Fibroblasts by Defined Factors', *Cell*, 131(5), pp. 861–872. doi:

10.1016/j.cell.2007.11.019.

Takahashi, K. and Yamanaka, S. (2006) 'Induction of Pluripotent Stem Cells from Mouse Embryonic and Adult Fibroblast Cultures by Defined Factors', *Cell*, 126(4), pp. 663–676. doi: 10.1016/j.cell.2006.07.024.

Takashima, Y. *et al.* (2014) 'Resetting Transcription Factor Control Circuitry toward Ground-State Pluripotency in Human', *Cell*, 158(6), pp. 1254–1269. doi: 10.1016/j.cell.2014.08.029.

Tesar, P. J. *et al.* (2007) 'New cell lines from mouse epiblast share defining features with human embryonic stem cells', *Nature*, 448(7150), pp. 196–199. doi: 10.1038/nature05972.

Theunissen, T. W. *et al.* (2014) 'Systematic Identification of Culture Conditions for Induction and Maintenance of Naive Human Pluripotency', *Cell Stem Cell*, 15(4), pp. 471–487. doi: 10.1016/j.stem.2014.07.002.

Theunissen, T. W. *et al.* (2016) 'Molecular Criteria for Defining the Naive Human Pluripotent State', *Cell Stem Cell*, 19(4), pp. 502–515. doi: 10.1016/j.stem.2016.06.011.

Thomson, J. A. (1998) 'Embryonic Stem Cell Lines Derived from Human Blastocysts', *Science*, 282(5391), pp. 1145–1147. doi: 10.1126/science.282.5391.1145.

Tian, X. *et al.* (2013) 'High-molecular-mass hyaluronan mediates the cancer resistance of the naked mole rat', *Nature*. Nature Publishing Group, 499(7458), pp. 346–349. doi: 10.1038/nature12234.

Tian, X. *et al.* (2015) '*INK4* locus of the tumor-resistant rodent, the naked mole rat, expresses a functional p15/p16 hybrid isoform', *Proceedings of the National Academy of*

Sciences, 112(4), pp. 1053–1058. doi: 10.1073/pnas.1418203112.

Tucker, R. (1981) 'The digging behavior and skin differentiations in Heterocephalus glaber', *Journal of Morphology*, 168(1), pp. 51–71. doi: 10.1002/jmor.1051680107.

Vallier, L. (2005) 'Activin/Nodal and FGF pathways cooperate to maintain pluripotency of human embryonic stem cells', *Journal of Cell Science*, 118(19), pp. 4495–4509. doi: 10.1242/jcs.02553.

Wakayama, T. *et al.* (1998) 'Full-term development of mice from enucleated oocytes injected with cumulus cell nuclei', *Nature*, 394(6691), pp. 369–374. doi: 10.1038/28615.

Woodley, R. (2000) 'Cold-Acclimation in an Endothermic Poikilotherm, the Naked Mole-Rat (Heterocephalus Glaber); Effects on Thermoregulation and Reproduction'.

Woodley, R. and Buffenstein, R. (2002) 'Thermogenic changes with chronic cold exposure in the naked mole-rat (Heterocephalus glaber)', *Comparative Biochemistry and Physiology - A Molecular and Integrative Physiology*, 133(3), pp. 827–834. doi: 10.1016/S1095-6433(02)00199-X.

Wu, J. *et al.* (2015) 'An alternative pluripotent state confers interspecies chimaeric competency', *Nature*, 521(7552), pp. 316–321. doi: 10.1038/nature14413.

Wu, J. *et al.* (2016) 'Stem cells and interspecies chimaeras', *Nature*. Nature Publishing Group, 540(7631), pp. 51–59. doi: 10.1038/nature20573.

Wu, J. *et al.* (2017) 'Interspecies Chimerism with Mammalian Pluripotent Stem Cells', *Cell*, 168(3), p. 473–486.e15. doi: 10.1016/j.cell.2016.12.036.

Wu, J., Yamauchi, T. and Izpisua Belmonte, J. C. (2016) 'An overview of mammalian pluripotency', *Development*, 143(10), pp. 1644–1648. doi: 10.1242/dev.132928.

Yahav, S. and Buffenstein, R. (1991) 'Huddling Behavior Facilitates Homeothermy in the Naked Mole Rat Heterocephalus-Glaber', *Physiological Zoology*, 64(3), pp. 871–884. doi: 10.1086/physzool.64.3.30158212.

Yamanaka, S. (2009) 'Elite and stochastic models for induced pluripotent stem cell generation', *Nature*. Nature Publishing Group, 460(7251), pp. 49–52. doi: 10.1038/nature08180.

Yang, Y. *et al.* (2017) 'Derivation of Pluripotent Stem Cells with In Vivo Embryonic and Extraembryonic Potency', *Cell*. Elsevier, 169(2), p. 243–257.e25. doi: 10.1016/j.cell.2017.02.005.

Ying, Q.-L. *et al.* (2003) 'BMP Induction of Id Proteins Suppresses Differentiation and Sustains Embryonic Stem Cell Self-Renewal in Collaboration with STAT3', *Cell*, 115(3), pp. 281–292. doi: 10.1016/S0092-8674(03)00847-X.

Ying, Q.-L. L. *et al.* (2008) 'The ground state of embryonic stem cell self-renewal', *Nature*, 453(7194), pp. 519–523. doi: 10.1038/nature06968.

Ying, Q. L. *et al.* (2002) 'Changing potency by spontaneous fusion', *Nature*, 416(6880), pp. 545–548. doi: 10.1038/nature729.

Ying, Q. L. and Smith, A. (2017) 'The Art of Capturing Pluripotency: Creating the Right Culture', *Stem Cell Reports*. ElsevierCompany., 8(6), pp. 1457–1464. doi: 10.1016/j.stemcr.2017.05.020.

Yu, J. *et al.* (2007) 'Induced Pluripotent Stem Cell Lines Derived from Human Somatic Cells', *Science*, 318(5858), pp. 1917–1920. doi: 10.1126/science.1151526.

Zhang, H. *et al.* (2016) 'MLL1 Inhibition Reprograms Epiblast Stem Cells to Naive

Pluripotency', *Cell Stem Cell*. Elsevier Inc., 18(4), pp. 481–494. doi: 10.1016/j.stem.2016.02.004.

Zhang, J. *et al.* (2012) 'Metabolic regulation in pluripotent stem cells during reprogramming and self-renewal', *Cell Stem Cell*. Elsevier Inc., 11(5), pp. 589–595. doi: 10.1016/j.stem.2012.10.005.